ISSN 1007-9327 (print)
ISSN 2219-2840 (online)

World Journal of *Gastroenterology*

World J Gastroenterol 2023 September 14; 29(34): 5020-5093

Published by Baishideng Publishing Group Inc

World Journal of Gastroenterology

Contents

Weekly Volume 29 Number 34 September 14, 2023

REVIEW

5020 Perioperative immunotherapy for esophageal squamous cell carcinoma: Now and future

Liu Y

ORIGINAL ARTICLE

Basic Study

5038 Suberoylanilide hydroxamic acid upregulates reticulophagy receptor expression and promotes cell death in hepatocellular carcinoma cells

Li JY, Tian T, Han B, Yang T, Guo YX, Wu JY, Chen YS, Yang Q, Xie RJ

5054 Green tea polyphenols alleviate di-(2-ethylhexyl) phthalate-induced liver injury in mice

Shi H, Zhao XH, Peng Q, Zhou XL, Liu SS, Sun CC, Cao QY, Zhu SP, Sun SY

Retrospective Study

5075 Role of biochemical markers and autoantibodies in diagnosis of early-stage primary biliary cholangitis

Zhu YJ, Li J, Liu YG, Jiang Y, Cheng XJ, Han X, Wang CY, Li J

CASE REPORT

5082 Simultaneous rectal neuroendocrine tumors and pituitary adenoma: A case report and review of literature

Li JY, Chen J, Liu J, Zhang SZ

LETTER TO THE EDITOR

5091 Gastrointestinal microbiome and cholelithiasis: Prospect in the nervous system

Mancha Chahuara M, Lopez Tufino LDM, Mugruza-Vassallo CA

World Journal of Gastroenterology

Weekly Volume 29 Number 34 September 14, 2023

Contents

ABOUT COVER

Editorial Board of *World Journal of Gastroenterology*, Takeshi Suda, MD, PhD, Professor, Department of Gastroenterology and Hepatology, Uonuma Institute of Community Medicine, Niigata University Medical and Dental Hospital, Minami Uonuma 949-7302, Niigata, Japan. tspitt@med.niigata-u.ac.jp

AIMS AND SCOPE

The primary aim of *World Journal of Gastroenterology* (*WJG*, *World J Gastroenterol*) is to provide scholars and readers from various fields of gastroenterology and hepatology with a platform to publish high-quality basic and clinical research articles and communicate their research findings online. *WJG* mainly publishes articles reporting research results and findings obtained in the field of gastroenterology and hepatology and covering a wide range of topics including gastroenterology, hepatology, gastrointestinal endoscopy, gastrointestinal surgery, gastrointestinal oncology, and pediatric gastroenterology.

INDEXING/ABSTRACTING

The *WJG* is now abstracted and indexed in Science Citation Index Expanded (SCIE, also known as SciSearch®), Current Contents/Clinical Medicine, Journal Citation Reports, Index Medicus, MEDLINE, PubMed, PubMed Central, Scopus, Reference Citation Analysis, China Science and Technology Journal Database, and Superstar Journals Database. The 2023 edition of Journal Citation Reports® cites the 2022 impact factor (IF) for *WJG* as 4.3; Quartile category: Q2. The *WJG*'s CiteScore for 2021 is 8.3.

RESPONSIBLE EDITORS FOR THIS ISSUE

NAME OF JOURNAL
World Journal of Gastroenterology

ISSN
ISSN 1007-9327 (print) ISSN 2219-2840 (online)

LAUNCH DATE
October 1, 1995

FREQUENCY
Weekly

EDITORS-IN-CHIEF
Andrzej S Tarnawski

EXECUTIVE ASSOCIATE EDITORS-IN-CHIEF
Xian-Jun Yu (Pancreatic Oncology), Jian-Gao Fan (Chronic Liver Disease), Hou-Bao Liu (Biliary Tract Disease), Naohisa Yoshida (Gastrointestinal Endoscopy)

EDITORIAL BOARD MEMBERS
http://www.wjgnet.com/1007-9327/editorialboard.htm

PUBLICATION DATE
September 14, 2023

PUBLISHING PARTNER
Pancreatic Cancer Institute, Fudan University
Biliary Tract Disease Institute, Fudan University

INSTRUCTIONS TO AUTHORS
https://www.wjgnet.com/bpg/gerinfo/204

GUIDELINES FOR ETHICS DOCUMENTS
https://www.wjgnet.com/bpg/GerInfo/287

GUIDELINES FOR NON-NATIVE SPEAKERS OF ENGLISH
https://www.wjgnet.com/bpg/gerinfo/240

PUBLICATION ETHICS
https://www.wjgnet.com/bpg/GerInfo/288

PUBLICATION MISCONDUCT
https://www.wjgnet.com/bpg/gerinfo/208

POLICY OF CO-AUTHORS
https://www.wjgnet.com/bpg/GerInfo/310

ARTICLE PROCESSING CHARGE
https://www.wjgnet.com/bpg/gerinfo/242

STEPS FOR SUBMITTING MANUSCRIPTS
https://www.wjgnet.com/bpg/GerInfo/239

ONLINE SUBMISSION
https://www.f6publishing.com

PUBLISHING PARTNER's OFFICIAL WEBSITE
https://www.shca.org.cn
https://www.zs-hospital.sh.cn

E-mail: bpgoffice@wjgnet.com https://www.wjgnet.com

World Journal of Gastroenterology

Submit a Manuscript: https://www.f6publishing.com

World J Gastroenterol 2023 September 14; 29(34): 5020-5037

DOI: 10.3748/wjg.v29.i34.5020

ISSN 1007-9327 (print) ISSN 2219-2840 (online)

REVIEW

Perioperative immunotherapy for esophageal squamous cell carcinoma: Now and future

Yong Liu

Specialty type: Gastroenterology and hepatology

Provenance and peer review: Invited article; Externally peer reviewed.

Peer-review model: Single blind

Peer-review report's scientific quality classification

Grade A (Excellent): A
Grade B (Very good): B
Grade C (Good): C
Grade D (Fair): 0
Grade E (Poor): 0

P-Reviewer: Matsuo Y, Japan; Nakano H, Japan; Viswanath Y, United Kingdom

Received: April 23, 2023
Peer-review started: April 23, 2023
First decision: July 9, 2023
Revised: July 19, 2023
Accepted: August 15, 2023
Article in press: August 15, 2023
Published online: September 14, 2023

Yong Liu, Department of Thoracic Surgery, The Central Hospital of Wuhan, Tongji Medical College, Huazhong University of Science and Technology, Wuhan 430011, Hubei Province, China

Corresponding author: Yong Liu, Doctor, MD, Chief Doctor, Surgeon, Surgical Oncologist, Department of Thoracic Surgery, The Central Hospital of Wuhan, Tongji Medical College, Huazhong University of Science and Technology, No. 26 Shengli Street, Wuhan 430011, Hubei Province, China. liuyong7575@163.com

Abstract

Esophageal cancer (EC) ranks among the most prevalent malignant tumors affecting the digestive tract. Esophageal squamous cell carcinoma (ESCC) stands as the prevailing pathological subtype, encompassing approximately 90% of all EC patients. In clinical stage II-IVA locally advanced ESCC cases, the primary approach to treatment involves a combination of neoadjuvant therapy and surgical resection. Despite concerted efforts, the long-term outcomes for ESCC patients remain unsatisfactory, with dismal prognoses. However, recent years have witnessed remarkable strides in immunotherapy, particularly in the second- and first-line treatment of advanced or metastatic ESCC, with the development of monoclonal antibodies that inhibit programmed death 1 or programmed death ligand 1 demonstrating encouraging responses and perioperative clinical benefits for various malignancies, including ESCC. This comprehensive review aims to present the current landscape of perioperative immunotherapy for resectable ESCC, focusing specifically on the role of immune checkpoint inhibitors during the perioperative period. Additionally, the review will explore promising biomarkers and offer insights into future prospects.

Key Words: Esophageal squamous cell carcinoma; Immune checkpoint inhibitors; Immunotherapy; Neoadjuvant; Randomized clinical trial

Core Tip: Esophageal cancer ranks among the most prevalent malignant tumors affecting the digestive tract. In locally advanced esophageal squamous cell carcinoma (ESCC), the mainstay of treatment involves neoadjuvant therapy in conjunction with surgical resection. Notably, immunotherapy has achieved significant breakthroughs in the second- and first-line treatment of advanced or metastatic ESCC. This review focuses on the current landscape of perioperative immunotherapy for resectable ESCC and discusses promising biomarkers and future perspectives.

Citation: Liu Y. Perioperative immunotherapy for esophageal squamous cell carcinoma: Now and future. *World J Gastroenterol* 2023; 29(34): 5020-5037
URL: https://www.wjgnet.com/1007-9327/full/v29/i34/5020.htm
DOI: https://dx.doi.org/10.3748/wjg.v29.i34.5020

INTRODUCTION

Esophageal cancer (EC), one of the most prevalent malignancies affecting the digestive tract, originates from the epithelial lining of the esophagus. According to the International Agency for Research on Cancer's latest update on the global cancer burden, based on the GLOBOCAN 2020 projections of cancer incidence and mortality, EC ranks seventh in terms of cancer incidence worldwide and sixth in cancer-related mortality[1]. The incidence of EC varies significantly across countries and regions, with East Asia having the highest disease occurrence, being twice the global average (12.2/1000). EC can be classified into two histological subtypes: Esophageal squamous cell carcinoma (ESCC) and esophageal adenocarcinoma (EAC). EAC is the predominant pathological type in relatively low-incidence areas such as Europe and America. However, globally, ESCC accounts for approximately 90% of all EC cases[2], and more than half of the ESCC cases occur in China[3].

For many years, surgery has served as the primary treatment for early-stage ESCC. High-grade dysplasia and very early-stage tumors are amenable to local therapies such as endoscopic resection, ablation, or surgery. Surgery can improve the 5-year survival rate to 60%-85% in patients with early-stage disease[4]. However, due to the subtle nature of early symptoms, many patients present with advanced or metastatic disease at the time of diagnosis. For locally advanced disease, surgery alone has not yielded satisfactory results, with a median survival time of 12 to 18 mo and a 5-year survival rate of 15%-39%[5,6]. Furthermore, local or systemic recurrence is common, with recurrence reported in 35%-50% of patients who had underwent surgery alone[7].

Neoadjuvant therapy combined with surgery stands as a cornerstone in the treatment of locally advanced ESCC, typically encompassing clinical stages II to IVA[8]. The medical community widely acknowledges the value of neoadjuvant therapy due to its efficiency compared to postoperative adjuvant therapy. Moreover, it leads to reductions in tumor and lymph node (LN) volumes, improves the R0 resection rate, and enhances long-term survival rates[9-11]. Additionally, neoadjuvant therapy allows for the evaluation of patient response using resected specimens[12]. Numerous randomized controlled trials (RCTs) have indicated that preoperative or neoadjuvant chemoradiotherapy (nCRT) may result in longer overall survival (OS) compared to surgery alone[13-15]. The CROSS trial established nCRT as the first-line therapeutic choice for resectable locally advanced ESCC, combining radiotherapy with a chemotherapy regimen containing carboplatin and paclitaxel[16]. The NEOCRTEC5010 phase III, multi-center, open-label RCT confirmed the findings of the CROSS trial for ESCC[9]. However, the optimal neoadjuvant therapy for resectable locally advanced ESCC remains a topic of debate. Neoadjuvant chemotherapy showed improved OS over surgery alone only for EAC, whereas nCRT demonstrated considerably better OS than surgery alone for both EAC and ESCC, according to the NewEC study [17]. Several subsequent meta-analyses also supported the utility of preoperative nCRT, showing improved OS compared to other treatment modalities, including surgery alone, neoadjuvant chemotherapy, and neoadjuvant radiotherapy, albeit with increased postoperative mortality[18,19]. Postoperative morbidity was similar between the nCRT and S (surgery) groups (55.6% *vs* 52.8%; $P = 0.720$), while in-hospital postoperative mortality was significantly higher in the CRT group (11.1% *vs* 3.4%; $P = 0.049$)[20]. A Japanese study[21] examined late complications, revealing grade 2 anastomotic stricture as the most common event, occurring in 30% of the 33 patients. A total of 12 events of grade 3 or worse complications were observed in ten patients, including gastric tube ulcer, cardiac complications, and pulmonary complications. The 5-year incidence rate was 22%, and three patients succumbed to the late complications. A clear advantage of nCRT over neoadjuvant chemotherapy was not established.

Presently, both the National Comprehensive Cancer Network and the Chinese Society of Clinical Oncology guidelines recommend chemoradiotherapy (CRT) as the standard approach for locally advanced ESCC[22-24]. Despite significant efforts made by the medical community, the expected long-term outcomes for ESCC patients have seen limited improvement, remaining poor. The 5-year OS in patients undergoing nCRT and surgery is approximately 50%, and the incidence of local recurrence or distant metastasis remains high[25]. Relapse after nCRT is common and constitutes a major hurdle to overcome[26].

Immunotherapy is a therapeutic approach that involves the use of substances to stimulate or suppress the immune system, aiding the body in combating cancer, infections, and other diseases. It encompasses biologic/targeted agents that aim to enhance and restore the immune system's ability to recognize and eliminate cancer cells by modifying and/or blocking costimulatory signals[27,28]. Over the past few years, immunotherapy has achieved remarkable progress in cancer treatment, particularly with the advent of immune checkpoint inhibitors (ICIs)[29]. The development of ICIs,

which inhibit programmed death 1 (PD-1) or programmed death ligand 1 (PD-L1), has shown convincing responses and clinical benefits across various malignancies, including ESCC[30,31].

In the study "KEYNOTE-181", Pembrolizumab demonstrated superior OS, a higher objective response rate, and a lower incidence of grades 3-5 treatment-related adverse events (trAEs) compared to chemotherapy in the second-line setting [32]. Grades 3-5 trAEs occurred in 18.2% of patients treated with Pembrolizumab *vs* 40.9% in the chemotherapy group. Other trials such as "RATIONALE-302"[33], "ATTRACTION-3"[34], and "ESCORT"[35] have also reported positive outcomes. In these trials, immunotherapy showed lower rates of grades 3-5 trAEs compared to chemotherapy, with percentages of 18.8% *vs* 55.8% in "RATIONALE-302"[33], 18% *vs* 63% in "ATTRACTION-3"[34], and 19% *vs* 39% in "ESCORT"[35].

It is important to note that in studies like "JUPITER-06"[36], "CheckMate-648"[37], "ORIENT-15"[38], "ESCORT-1st"[39], and "KEYNOTE-590"[40], treating patients with advanced EC using PD-1 inhibitors in combination with chemotherapy as first-line therapy resulted in significantly longer OS and progression-free survival (PFS) compared to chemotherapy alone. The occurrence rates of grades 3-5 trAEs in these trials were relatively comparable.

Neoadjuvant immunotherapy has been explored in various other malignancies, such as lung cancer[41,42], melanoma [43], bladder cancer[44], colon cancer[45], and glioblastoma[46]. In a clinical trial (NCT02259621) investigating neoadjuvant Nivolumab, surgery was not delayed, and 45% of resected tumors showed a major pathological response (MPR). In the NADIM trial[42], patients were treated with a neoadjuvant regimen consisting of paclitaxel and carboplatin in combination with Nivolumab. Out of the initial 51 patients deemed eligible, 46 patients received neoadjuvant treatment and subsequently underwent surgery. At the 24-mo mark, the PFS rate was observed to be 77.1%. Among the 27 patients who had melanoma, eight experienced either a complete response or an MPR after receiving a single dose of the anti-PD-1 drug, Pembrolizumab. Importantly, all eight of these patients remained free from the disease[43]. In a single-arm phase II study exploring Atezolizumab before cystectomy in 95 patients with muscle-invasive urothelial cancer (NCT02662309), the pathological complete response (pCR) rate was 31%[44]. In the exploratory NICHE study (NCT03026140)[45], patients with early-stage colon cancers, categorized as mismatch repair-deficient (dMMR) or mismatch repair-proficient (pMMR) tumors, received a single dose of Ipilimumab and two doses of Nivolumab before surgery. Among dMMR tumors, 20 out of 20 displayed a pathological response, with 19 cases of MPR and 12 cases of pCR. In pMMR tumors, 4 out of 15 showed pathological responses, with three cases of MPR and one case of partial response. In a single-arm phase II clinical trial (NCT02550249)[46], a presurgical dose of Nivolumab followed by postsurgical Nivolumab until disease progression or unacceptable toxicity was tested in 30 patients. However, no significant clinical benefit was observed following salvage surgery, although two out of the three patients treated with Nivolumab before and after primary surgery remained alive 33 and 28 mo later.

Based on this background, this review aims to depict the current scenario in the field of perioperative immunotherapy for resectable ESCC, focusing in particular on an overview of the role of ICIs in this field, alongside a discussion of the promising biomarkers and forecast of future perspectives.

PERIOPERATIVE IMMUNOTHERAPY OF ESCC

Drugs for immunotherapy of ESCC

Cancer cells have the ability to evade immune surveillance by disrupting the balance of the tumor microenvironment (TME). This disruption can lead to tumor development by blocking apoptosis, promoting angiogenesis, proliferation, and distant metastasis, and evading immune detection[47]. CD8(+) T cells, also known as cytotoxic T lymphocytes, play a crucial role in killing tumor cells, and their presence in the TME is associated with improved cancer prognosis[48]. For CD8(+) T cells to effectively kill tumor cells, two signals are essential: The recognition of antigens presented by major histocompatibility complexes[49] and the stimulation or suppression of T cell activation. The second signal, acting as a co-stimulatory or co-inhibitory signal, is often referred to as an "immune checkpoint" for CD8(+) T cell function. Immune checkpoints help maintain the balance of T-cell activation, immune tolerance, and immune-mediated tissue damage[50]. Both co-stimulatory and co-inhibitory ligands and their receptors are present on T cells and antigen-presenting cells. Inhibitory checkpoint molecules displayed by CD8(+) T cells can respond to and aid the tumor in evading the immune system[51].

There are four main ICIs named after the corresponding Food and Drug Administration (FDA)-approved monoclonal antibody therapies: Cytotoxic T lymphocyte antigen-4 (CTLA-4), PD-1, PD-L1/L2, and lymphocyte activation gene-3 (LAG-3)[52]. CTLA-4 and PD-1 are members of the CD28 receptor family expressed on T-cells, which bind to their corresponding targets of the B7 family[53]. CTLA-4 is an intracellular protein often found on regulatory T cells, inhibiting CD8(+) T cell activity. Ipilimumab, approved by the FDA in 2011, targets CTLA-4[54]. PD-1 is a transmembrane protein upregulated by repeated stimulation of T cells. PD-1 has two ligands, PD-L1 and PD-L2, which are cell surface proteins expressed on tumor cells and some immune cells within the TME. When PD-1 binds to these ligands, T cell function is inhibited. Overexpression of PD-L1 is associated with tumor progression, as cancer cells exploit the PD-1/PD-L1 and PD-1/PD-L2 pathways to create an immunosuppressive environment[55]. Nivolumab and Pembrolizumab are ICIs that target the PD-1 molecule, both FDA-approved in 2014. In 2018 and 2021, Cemiplimab and Dostarlimab were also approved, respectively[56,57]. Atezolizumab, Avelumab, and Durvalumab are FDA-approved PD-L1 inhibitors[58-60]. LAG-3 is a transmembrane receptor expressed on CD8(+) T cells, further upregulated by T cell activation. Relatlimab is the only FDA-approved LAG-3 inhibitor[61].

In recent years, several domestic anti-PD-1 monoclonal antibodies have been approved as drugs for various tumors by the China National Medical Product Administration. Notably, Camrelizumab, Sintilimab, Toripalimab, and Tislelizumab are representative drugs that are currently undergoing in-depth research. Camrelizumab, a humanized anti-PD-1 monoclonal antibody developed in China, has shown promising activity and manageable toxicity when combined with Apatinib, an anti-angiogenic drug. This combination may serve as a potential second-line treatment option for patients with advanced ESCC[62] or patients with recurrent or metastatic ESCC[63].

Neoadjuvant immunotherapy of ESCC

As previously mentioned, ICI immunotherapy has demonstrated improved outcomes in terms of OS and disease-free survival (DFS) for both second-line and first-line treatments of ESCC. In the context of resectable locally advanced ESCC, there has been a growing interest in perioperative immunotherapy combined with chemotherapy or radiotherapy, representing a key research direction for this disease. Preoperative neoadjuvant immunotherapy aims to activate the patient's immune system, leading to the formation of immune memory cells, thereby enabling the immune system to assume an immune surveillance role[64,65]. This review will summarize the current status of neoadjuvant immunotherapy as a treatment for ESCC.

Completed and reported clinical studies of neoadjuvant immunotherapy

Numerous clinical studies have investigated the efficacy and safety of immunotherapy for resectable ESCC in the neoadjuvant setting, as detailed in Table 1. Most neoadjuvant immunotherapy trials are conducted in conjunction with chemotherapy or CRT. Given the high incidence of this disease in China, numerous clinical trials on this subject are carried out in the country. Specifically, six ICIs targeting PD-1/PD-L1, namely, Pembrolizumab (4 studies), Camrelizumab (10 studies), Sintilimab (4 studies), Toripalimab (5 studies), and Tislelizumab (1 study), have been studied as neoadjuvant therapy. Additionally, there is an ongoing drug-based neoadjuvant therapy RCT involving Nivolumab, the first ICI used in adjuvant immunotherapy in the CheckMate-577 study[66]. The results of this trial, known as the FRONTiER study (NCT03914443), are eagerly anticipated[67]. In Table 1, four reports were retrospective in nature, while the other 21 reports were prospective, with 20 of them being single-arm trials. Only three studies employed neoadjuvant immunotherapy in combination with concurrent CRT as an intervention. In studies involving neoadjuvant immunotherapy combined with chemotherapy, the chemotherapy drugs used included 5-fluorouracil (5-FU), cisplatin (DDP), carboplatin (CBP), nedaplatin (NDP), paclitaxel (PTX), docetaxel (DTX), albumin-bound paclitaxel (nab-PTX), and PTX liposomes. Over the past few years, the use and dosages of these chemotherapy drugs have demonstrated efficacy for ESCC treatment in clinical settings. Most surgeons have chosen an interval time of 4-6 wk from the end of neoadjuvant therapy to surgery. The primary outcomes of utmost concern to doctors are safety, feasibility, and pCR, while MPR and R0 resection rate are commonly selected as primary or secondary outcomes.

Ensuring the safety of participants is of utmost importance in clinical trials, and the occurrence of trAEs is a key indicator in assessing the safety of neoadjuvant immunotherapy[68]. When ICIs are combined with other anti-cancer therapies, such as chemotherapy, immunotherapy, targeted therapy, or radiotherapy, the incidence of trAEs is significantly higher compared to the use of ICIs alone[69]. These trAEs can affect various organs, with the most common being endocrine (hypothyroidism and hyperthyroidism), gastrointestinal (diarrhea and colitis), pulmonary (pneumonitis), dermatological (rash and pruritus), and hepatic (elevated liver enzymes) complications[70,71]. The majority of trAEs (grades 1-2) are self-limiting or can be managed with immunosuppressive therapy, such as corticosteroids. However, persistent trAEs that do not respond to corticosteroids require close monitoring and appropriate treatment. Fatal trAEs are extremely rare for anti-PD-1 antibodies, with an incidence of less than 0.5% in a meta-analysis of ICI monotherapy studies across various cancer types, most commonly associated with pneumonitis[71]. The incidence of serious trAEs (grade ≥ 3) in neoadjuvant ICI plus chemotherapy ranged from 0% to 36.7% in the studies presented in Table 1. Notably, the combination of chemotherapy with Camrelizumab and Apatinib resulted in the highest incidence of patients experiencing serious trAEs (36.7%). In another meta-analysis comparing the efficacy and safety of various ICIs for patients with advanced or metastatic ESCC, Camrelizumab and Nivolumab were found to have a lower incidence of serious trAEs in the first-line and refractory settings, respectively[72]. Close monitoring and early recognition of relevant symptoms and signs are essential to ensure appropriate management.

Feasibility can be assessed by comparing the completion rate of the trial. In a pooled analysis, the rates of completion of neoadjuvant therapy and surgery ranged from 49.4% (Camrelizumab + nab-PTX + NDP) to 100% (Sintilimab + PTX liposome, DDP, and S-1). Failures in the study were mainly attributed to trAEs[73,74], patient decisions[75-77], or disease progression[78]. As most trials achieved a treatment completion rate of over 60%, interpreting the data in the conference abstract (ChiCTR2000039170) is challenging.

The definition of pCR is the absence of any signs of cancer on a histological resection specimen. The pCR rate is a crucial efficacy-related parameter reported in all studies, with some studies choosing it as a secondary outcome. In a meta-analysis of seven clinical trials involving 815 patients, the pooled pCR rate was 32.4% (95% confidence interval [CI]: 28.2%-36.8%)[79]. Data from Table 1 shows that the pCR rate ranges from 6.7% to 46.1%. The definition of MPR is the presence of less than 10% of the remaining viable tumor cells in the resected primary tumor. In the aforementioned meta-analysis, the pooled MPR rate was 49.4% (95%CI: 42.1%-56.7%)[79]. MPR rate was chosen as the primary outcome in four studies and seemed to be a second primary outcome in the main studies verified in Table 1, with reported rates ranging from 42% to 72.3%[73,76,77,80-83]. The R0 resection rate is defined as a complete resection of the tumor with a negative microscopic edge, indicating no residual tumor. It is another crucial indicator to evaluate the effectiveness of neoadjuvant therapy. The R0 resection rate in Table 1 ranges from 80.4% to 100%, which indicates positive outcomes.

Table 1 Reported clinical results of neoadjuvant immunotherapy for resectable esophageal squamous cell carcinoma

Drug & Ref.	Trial No.	Phase	Number of enrollments	Clinical stage	Design	Chemotherapy drugs	Chemotherapy cycles	Radiotherapy	Interval time to surgery	Primary outcome	Safety (rate of grade ≥ 3 trAEs)	Feasibility (therapy completion rate)	pCR	MPR	Surgical outcome (R0 rate)
Pembrolizumab [111]	Park *et al*[111] (NR)	NA	38	IA-IVA	Retrospective	5-FU + DDP/PTX + CBP	NA	41.4 Gy/23 f	6-8 wk	Operative risk	18.75% (3/16)	100% (16/16)	NA	NA	100%
Pembrolizumab [112]	Huang *et al*[112] (NR)	NA	54	II–IVA	Retrospective	DTX + NDP	2, Q3W		4-6 wk	pCR	13.04% (4/23)	NA	30.4% (7/23)	NA	100%
Pembrolizumab [113]	NCT02844075	II	28	IB-III	Single- arm	PTX + CBP	5, Q1W	41.4 Gy/23 f	5 wk	pCR	NA	92.9% (26/28)	46.1% (12/26)	NA	NA
Pembrolizumab [80]	Keystone-001/NCT04389177	II	50	IIIA-IIIB	Single-arm	PTX + DDP	3, Q3W		4-6 wk	pCR, MPR, safety	0	69.0% (29/42)	41.4% (12/29)	72.4% (21/29)	100%
Camrelizumab [114]	Qiao *et al*[114] (NR)	NA	254	IA-IVA	Retrospective	PTX, nab-PTX/DTX	2, Q3W		NA	pCR	6.25% (3/48)	NA	41.7% (20/48)	60.4 (29/48)	NA
Camrelizumab [74]	ChiCTR1900026240	II	60	IIIA-IVA	Single-arm	nab-PTX + CBP	2, Q3W		4-6 wk	pCR	56.7% (34/60)	85.0% (51/60)	39.2% (20/51)	NA	98.0%
Camrelizumab [115]	NCT04506138	I-II	46	II-IVA	Single-arm	nab-PTX + CBP			4-6 wk	pCR	15.2% (7/46)	82.6% (38/46)	21.6% (8/37)	48.6% (18/37)	80.4%
Camrelizumab [82]	GASTO1056/ChiCTR2000028900	II	23	II-III	Single-arm	nab-PTX + CBP	2, Q3W		3-6 wk	Safety	47.8%	87.0% (20/23)	25% (5/20)	50% (10/20)	100%
Camrelizumab [116]	Yang *et al*[116] (NR)	II	12	II-III	Single-arm	nab-PTX + S1	3, Q3W		3-6 wk	pCR	0	75.0% (9/12)	33.3% (4/12)	41.7% (5/12)	100%
Camrelizumab [75]	NIC-ESCC2019/NCT04225364	II	56	II-IVA	Single-arm	nab-PTX + DDP	2, Q3W		6 wk	pCR	10.7% (6/51)	91.1% (51/56)	35.3% (18/51)	23.5% (12/21)	100%
Camrelizumab [117]	ChiCTR1900023880	Ib	30	IC-IIIB	Single-arm	nab-PTX + NDP + Apatinib	2-4, Q3W		4-8 wk	Safety, feasibility	36.7% (11/30)	96.7% (29/30)	24.1% (7/29)	51.7% (15/29)	NA
Camrelizumab [118]	ESPRIT/ChiCTR2000033761	II	48	IIA-IIIB	Single-arm	PTX + NDP	2-4, Q3W		NA	pCR	4.2%	62.5% (30/48)	35.0% (7/20)	NA	NA
Camrelizumab [119]	NCT 03917966	II	40	IC-IVA	Single-arm	DTX + NDP	2, Q3W		4-6 wk	MPR	3%	70.6% (12/17)	25.0% (3/12)	41.6% (5/12)	100%
Camrelizumab [120]	ChiCTR2000039170	II	166	Locally advanced	Single-arm	nab-PTX + NDP	NA		NA	Safety	7.8% (13/166)	49.4% (82/166)	18.5% (15/81)	63.0% (51/81)	97.5% (79/82)
Sintilimab[121]	ChiCTR1900026593	II	47	II-IVA	Single-arm	PTX liposome +	2, Q3W		3-6 wk	pCR	29.8%	95.7%	22.2%	44.4%	97.8%

						CBP					(14/47)	(45/47)	(10/45)	(20/45)	(44/45)
Sintilimab[81]	SIN-ICE study/ChiCTR2100048917	II	23	IC-IVA	Single-arm	Platinum	3, Q3W		4-6 wk	pCR, safety	30.4% (7/23)	73.9% (17/23)	35.3%, (6/17)	52.9% (9/17)	94.1% (16/17)
Sintilimab[73]	ESONICT-1/ChiCTR2100045659	II	30	IIB-IVA	Single-arm	DDP + nab-PTX	2, Q3W		4-6 wk	pCR, safety	3.3% (1/30)	76.6% (23/30)	21.7% (5/23)	52.2% (12/23)	100%
Sintilimab[88]	KEEP-G03/NCT03946969	II	30	IB-IVA	Single-arm	PTX liposom + DDP + S1	2, Q3W		Within 6 wk	Safety, feasibility	36.7%	100.0% (30/30)	20% (6/30)	50% (15/30)	100%
Toripalimab [122,123]	NCT03985670	II	30	II-IVA	Two-arm	PTX + DDP	2, Q3-4W		4-6 wk	pCR	8.33% (2/24)	80.0% (24/30)	20.8% (5/24)	NA	100%
Toripalimab [124]	ChiCTR1900025318	II	23	IIB-IVA	Single-arm	PTX + DDP	2, Q3W		4-6 wk	pCR, R0 rate	8.70% (2/23)	78.3% (18/23)	33.3% (6/18)	NA	100%
Toripalimab [77]	NCT04177797	II	20	IIIA-IVA	Single-arm	PTX + CBP	2, Q3W		4-6 wk	Safety, feasibility, MPR, pCR	20.0% (4/20)	80.0% (16/20)	18.8% (3/16)	43.8% (7/16)	87.5% (14/16)
Toripalimab [125]	ESONICT-2/ChiCTR2100052784	II	20	IIB-IVA	Single-arm	DTX + DDP	2, Q3W		4-6 wk	pCR, safety	15.0% (3/20)	60.0% (12/20)	16.7% (2/12)	41.7% (5/12)	100%
Toripalimab [126]	SCALE-1/ChiCTR2100045104	Ib	20	IIB-IVA	Single-arm	PTX + CBP	2, Q3W	30 Gy/12 f	4-7 wk	Safety	NA	87.0% (20/23)	55% (11/20)	80% (16/20)	
Tislelizumab [76]	TD-NICE/ChiCTR2000037488	II	45	IIIA-IVA	Single-arm	CBP + nab-PTX	2, Q3W		3-6 wk	MPR	33.3% (15/45)	80.0% (36/45)	50% (18/36)	72% (26/36)	97.2% (35/36)
Multiple[127]	CHICTR2100045659		27	IC-IVA	Retrospectively, two-arm	Platinum+ PTX or platinum + 5-Fu	2, Q3w		4–8 wk	30-d major complications	11.1% (3/27)	NA	NA	NA	100%

NR: Not registered; NA: Not available; 5-FU: 5-fluorouracil; DDP: Cisplatin; PTX: Paclitaxel; DTX: Docetaxel; CBP: Carboplatin; NDP: Nedaplatin; nab-PTX: Albumin bound paclitaxel; S1: Tegafur (Gimeracil and Oteracil Potassium Capsules); pCR: Pathological complete response; MPR: Major pathological response; trAEs: Treatment-related adverse events.

Ongoing clinical trials in neoadjuvant immunotherapy

This period marks a surge in clinical trials focused on neoadjuvant immunotherapy, particularly for perioperative treatment of ESCC, with a significant number of ongoing RCTs, especially led by Chinese investigators (Table 2). Eight ICIs are currently under investigation, with dozens of trials in progress. PD-1 is the primary target in seven of these trials, while Adebrelimab targets PD-L1. Camrelizumab is the most extensively studied ICI, involved in ten clinical trials, followed by Toripalimab with seven trials. Among these trials, there are 23 single-arm studies, 11 two-arm studies, two three-arm studies, and one four-arm study.

An array of combinations of new adjuvant therapies for ESCC are constantly emerging. Most ICIs are being utilized as neoadjuvant adjuncts, combined with chemotherapy in 13 trials or CRT in 18 trials. Adebrelimab, a PD-L1-targeting ICI, is used alone in one trial (NCT04215471), as is Nivolumab in another (NCT03987815). Camrelizumab, on the other hand, is being combined with radiotherapy (NCT05176002 and NCT03200691), or paired with multitargeted small molecule inhibitors and CRT or chemotherapy (NCT04666090), or further combined with both CRT and an anti-EGFR antibody

Table 2 Ongoing clinical trials of neoadjuvant immunotherapy for resectable esophageal squamous cell carcinoma

Drug & target	Trial name/No./Ref.	Phase	Sample size	Clinical stage	Design	Chemotherapy drugs	Chemotherapy cycles	Radiotherapy	Interval to surgery	Primary endpoint	Start date
Nivolumab	FRONTiER/NCT03914443[67]	I	36	IC-IVA	Two-arm	5-FU + DDP	2, Q3W		12 wk	Incidence of dose-limiting toxicities	07-May-19
	NCT03987815	II	20	NA	Single-arm	NA				MPR	01-Aug-19
	NCT05213312	II-III	90	II-III	Two-arm	PTX/5-FU + DDP	2, Q3W		4-6 wk	pCR	01-Jun-22
Pembrolizumab	PALACE-1/NCT03792347[85]	I	20	IC-IVA	Single-arm	CBP + PTX	5, Q1W	41.4 Gy/23 f	4-6 wk	Safety	21-Jan-19
	PALACE-2/NCT04435197[84]	II	143	IC-IVA	Single-arm	CBP + PTX	5, Q1 W	41.4 Gy/23 f	4-6 wk	pCR	11-Aug-20
	NCT05302011	II	30	IIB/IIIB/IVA	Single-arm	CBP/DDP + DTX	4, Q3W			Tumor response, pCR	01-Jun-20
	NCT05281003	II	128	IC-IVA	Single-arm	PTX + DDP	4, Q4W			pCR	20-Feb-23
Camrelizumab	NCT04520035	II	60	IIB-IVA	Single-arm	PTX + DDP	2, Q3W			pCR	01-Aug-20
	NCT04767295	II	28	IA-IVA	Single-arm	nab-PTX + CBP	2, Q3W		5-8 wk	pCR	01-Mar-21
	NICE-2 Study/NCT 05043688 [128]	II	204	Locally advanced	Three-arm	nab-PTX, CBP, PTX	2, Q3W	41.4 Gy/23 f	4-12 wk	pCR	14-Sep-21
	NCT05476380	II	39	IIIB-IVA	Single-arm	PTX + DDP	3, Q3W			pCR	19-Feb-21
	NCT05182944	II	130	IIB-IVA	Four-arm	nab-PTX + DDP	2, Q3W			pCR, 3-yr DFS	15-Jan-22
	NCT04937673	II	40	IIB-IVA	Two-arm	PTX/nab-PTX + DDP	3, Q3W		NA	Biomarkers related to pCR	01-Jul-21
	NCT05176002	I-II	26	II-IVA	Single-arm	NA	NA	Radiotherapy, NA	NA	Efficacy Safety	23-Sep-21
	NCT04666090	II	42	IIA-IVA	Single-arm	nab-PTX + NDP + Apatinib	2-3, Q2W		4-6wk	pCR	23-Nov-20
	NCT05355168	I-II	57	IC-IVA	Single-arm	Nimotuzumab + CRT	NA			pCR, MPR	01-Nov-21
	NCT03200691	II	21	IIA-III	Single-			40 Gy/20 f	2-4 wk	pCR	10-Aug-

					arm					17
Sintilimab	NCT03940001	I	20	IIB-IVA	Single-arm	PTX + CBP	2, Q3W	41.4 Gy/23 f	NA	Unacceptable toxicity; pCR; MPR	01-May-19
	(NICCE)NCT05028231	NA	46	IIB-IVA	Single-arm	nab-PTX + DDP	2, Q3W			pCR	05-Jun-21
	NCT05357846	III	422	IIB-IVA	Two-arm	PTX + DDP	4, Q1W	40 or 45 Gy / 20 f	6-8 wk	OS	01-Nov-22
	NCT05244798	III	420	IC-IVA	Three-arm	nab-PTX + CBP	2, Q3	41.4 Gy/23 f	6-8 wk	pCR	01-Nov-22
Toripalimab	NCT04280822	III	400	IC-IVA	Two-arm	DDP + PTX	2, Q3W		2-3 wk	3 yr EFS; 5 yr EFS	21-Apr-20
	NCT04804696	II	53	NA	Single-arm	PTX + DDP	NA		NA	pCR	10-Feb-21
	NCT04177875	II	44	IC-IIIB	Single-arm	DTX/PTX + DDP	2, Q3W	40 Gy/20 f	NA	MPR; ORR	01-May-19
	NCT04888403	II	45	IIB-IVA	Single-arm	nab-PTX + NDP	5, Q1W	41.4 Gy/23 f	Within 7 wk	pCR	31-Dec-21
	NCT04644250	II	32	IIB-IVA	Single-arm	CBP + PTX liposome	5, Q1W	41.4 Gy/23 f	2-4 wk	pCR	01-Sep-20
	NCT04848753	III	632	IC-IVA	Two-arm	DDP + PTX	NA		NA	EFS	18-Jun-21
	NCT04006041	II	44	IIB-IVA	Single-arm	PTX + DDP	4, Q1W	44 Gy/20 f	6-8 wk	pCR	25-Jun-19
Tislelizumab	iCROSS/NCT04973306	II-III	176	II-III	Two-arm	CBP + PTX	5, Q1W	41.4 Gy/23 f	NA	pCR; OS	02-Mar-22
	NCT05323890	II	15	IIB-IVA	Single-arm	nab-PTX + DDP	5, Q1W	41.4 Gy/23 f	NA	MPR, pCR	20-Apr-22
	NCT04974047	II	70	IIB-IVA	Two-arm	PTX/5-FU + DDP	2, NA	40 or 45 Gy/20 fractions	NA	pCR	17-Aug-21
	NCT05189730	II	80	II-III	Single-arm	PTX + CBP	2, Q3W	40 Gy/20 f	4-6 wk	pCR, incidence of adverse events	01-Jul-21
Adebrelimab (PD-L1)	NATION1907II/NCT04215471	II	30	Resectable	Single-arm					ORR	01-Feb-20
Durvalumab	NCT04568200	II	60	IIB-IVA	Two-arm	CBP + PTX	4, Q3W	41.4 Gy/23 f		pCR	19-Jun-20
Pembrolizumab (+ Adjuvant)	KEYSTONE-002/NCT04807673 [86]	III	342	IC-IIIB	Two-arm	PTX + DDP	3, Q3W	41.4 Gy/23 f	4-6 wk	EFS	01-Dec-21

PD-1 Inhibitor	REVO/NCT05007145	II	92	IB-IVA	Two-arm	nab-PTX + DDP	2-4, Q3W	40 Gy/20 f		pCR	15-Aug-21
Toripalimab (+ Adjuvant)	NCT 04437212	II	20	IIB-IVA	Single-arm	PTX/DDP	5, Q3W	41.4 Gy/23 f	6-8 wk	MPR	01-Jul-20

EFS: Events-free survival; DFS: Disease-free survival; OS: Overall survival; ORR: Objective response rate; NA: Not available; 5-FU: 5-fluorouracil; DDP: Cisplatin; PTX: Paclitaxel; DTX: Docetaxel; CBP: Carboplatin; NDP: Nedaplatin; nab-PTX: Paclitaxel for injection (albumin bound); pCR: Pathological complete response; MPR: Major pathological response.

(NCT05355168).

Several large medical centers are now conducting phases II and III clinical studies based on promising results from phases I and II studies. Examples include PALACE-2 (NCT04435197)[84], an advancement of PALACE-1 (NCT03792347)[85], and KEYSTONE-002 (NCT04807673)[86], another advancement based on Keystone-001 (NCT04389177)[80]. Although Pembrolizumab is the ICI being studied in both series of trials, the PALACE trial was designed as neoadjuvant immunotherapy combined with chemotherapy, while the Keystone trial was designed as neoadjuvant combined with chemotherapy and adjuvant immunotherapy. Most chemotherapy regimens include taxols and platinum, with 5-FU being chosen in only two trials. The mainstream radiotherapy method utilizes 41.4 GY divided into 23 fractions, and the interval between neoadjuvant therapy and surgery ranges from 2 to 12 wk, with 4-6 wk being the most common choice. The primary outcome sought by most ongoing trials is pCR.

Ongoing clinical trials of adjuvant immunotherapy

Despite the benefits of neoadjuvant chemoradiation in improving survival compared to surgery alone, achieving a pCR remains challenging, with persistent disease in LNs leading to decreased survival[66]. An RCT involving 346 patients with ESCC compared preoperative and perioperative chemotherapy. Both groups received two cycles of paclitaxel, cisplatin, and 5-fluorouracil before surgery, but only half received two cycles after surgery. The group receiving adjuvant chemotherapy showed an estimated 16% improvement in 5-year survival[87].

In contrast to neoadjuvant methods, adjuvant immunotherapy has received relatively little attention. The global CheckMate-577 trial, a randomized, double-blind, placebo-controlled phase III trial, demonstrated the DFS benefit of Nivolumab for ESCC (29.7 *vs* 11.0 mo)[66]. Despite the promising results of CheckMate-577 for adjuvant immunotherapy after surgery, there are currently only three ongoing trials in this area. One trial is investigating the effectiveness of Toripalimab (NCT04437212) in both neoadjuvant and adjuvant settings. The other two RCTs are assessing postoperative adjuvant therapy with Tislelizumab, with one in phase II as a single-arm study and the other in phase III with two-arm trials. The phase II trial involves adjuvant immunotherapy combined with CRT, while the phase III trial is adjuvant immunotherapy combined with chemotherapy (Table 3). Further details and results from these ongoing trials are eagerly awaited.

ISSUES SHOULD BE CONCERNED IN FUTURE

The majority of neoadjuvant immunotherapy trials in ESCC are currently single-arm, phase II clinical trials. These trials explore various combinations of different drugs and different methods of other therapies, leading to a continuous emergence of new clinical trials in this field. However, it is important to acknowledge that progress in some cases has

Table 3 Clinical trials of adjuvant immunotherapy for resectable esophageal squamous cell carcinoma

Drug	Trial name/No.	Phase	Sample size	Clinical stage	Design	Chemotherapy drugs	Chemotherapy cycles	Radiotherapy	Interval time to surgery	Primary endpoint	Start date	Outcome
Nivolumab	CheckMate-577/NCT02743494	III	784 (ESCC29%)	NA	Two-arm	NA				DFS	Completed	22.1:11.0 mo
Toripalimab (+ Neoadjuvant)	NCT 04437212	II	20	IIB-IVA	Single-arm	PTX + DDP	5, Q3W	41.4 Gy/23 f	6-8 wk	MPR	Jul 1, 2020	
Tislelizumab	AIRE/ChiCTR2100045651	III	110	High-risk resected locally advanced	Two-arm	Platinum-based doublets	2, Q3W			DFS	May 1, 2021	
Tislelizumab	CRISEC/NCT04776590	II	30	NA	Single-arm	PTX + CBP	5, Q1W	41.4 Gy/23 f		pCR	Jan 28, 2021	

DFS: Disease-free survival; NA: Not available; DDP: Cisplatin; PTX: Paclitaxel; CBP: Carboplatin; pCR: Pathological complete response; MPR: Major pathological response.

been slow or stagnant.

Ethical conduct should be a primary concern in the development of new therapies. As the development of immunotherapy is often driven by related industries, methodological, legal, and ethical frameworks can sometimes be overlooked. Currently, a significant portion of scientific research in immunotherapy is industry-driven, with various pharmaceutical companies involved in registering RCTs. Despite the existence of international research registries aimed at improving the transparency of medical research, there are still uncertainties and "not applicable" rules and regulations. Consequently, there may be a lack of control over data mining and publication bias. Even if there are significant differences between the research protocol and the reported results, most trial outcomes are still published. To ensure the reliability, quality, and expected clinical benefits of ongoing and future trials in this field, the medical community and relevant stakeholders should focus on curbing the significant increase in "feasibility" trials with unclear expected benefits. Emphasizing a few multi-center phase III trials, conducted by leading centers in ESCC research, could be a crucial approach to prevent unclear or contradictory results and uphold the integrity of the research.

The second issue of concern in clinical trials is safety, which should be carefully considered throughout the perioperative treatment of ESCC. One of the major safety risks is the occurrence of trAEs, especially immune-related adverse events. Perioperative immunotherapy trials for ESCC typically consist of three parts: Preoperative neoadjuvant therapy, surgery, and postoperative adjuvant therapy. Different immunotherapy drugs are administered at varying intervals: Pembrolizumab, Tislelizumab, Atilizumab, Toripalimab, and Sintilimab are usually given at 3-wk intervals, while Nivolumab, Camrelizumab, and Durvalumab are given at 2-wk intervals. The treatment cycles generally involve 2-4 cycles, and multiple factors such as treatment efficacy, surgical timing, economic considerations, and patient compliance are taken into account. Since most RCTs in this field are single-arm or two-arm studies within phase I or II, the safety data obtained may be limited and not fully comprehensive. This might result in an underestimation of the occurrence and severity of trAEs, especially those of grade 3 or above. Additionally, the introduction of new emerging drugs into clinical trials adds uncertain factors that could impact the results. Therefore, researchers should be attentive to the incidence and severity of trAEs, even when they are below grade 2. In cases where the trAEs are grade 3 or higher in severity, special attention should be given to the subjects to avoid fatal consequences. Furthermore, if three or more anti-cancer therapies, including immunotherapy, are administered to a subject simultaneously, researchers should exercise caution due to the

higher risk of trAEs for the patient. Vigilance and thorough monitoring are essential to ensure the safety of subjects throughout the course of treatment.

Neoadjuvant immunotherapy presents a dual challenge, aiming to achieve better treatment outcomes while minimizing harm to normal organs caused by immunotherapy. The impact of trAEs during preoperative therapy on surgery must be carefully considered. In the trial "KEEP-G 03"[88], 36.7% (11/30) of patients experienced grades 3-4 TRAEs, but fortunately, these did not result in any surgical delays. However, in another multicenter, single-arm, phase II trial using Camrelizumab and chemotherapy as neoadjuvant treatment for locally advanced ESCC[74], 34 patients (56.7%) experienced adverse events of grade 3 or worse, with one patient (1.7%) experiencing a fatal grade 5 adverse event due to pneumonia and acute respiratory failure. The risk of increased surgical complications after immunotherapy is a concern, emphasizing the importance of forming a multidisciplinary team to address trAEs and conduct comprehensive evaluations during immunotherapy. Early detection and management of trAEs can minimize the impact on subsequent treatment and related complications. Additionally, exploring biomarkers related to trAEs is crucial in the research field.

Surgery itself poses another safety concern. ESCC radical resection is a complex procedure with a high incidence of complications, and surgical team experience significantly influences the rate of complications. Patients undergoing neoadjuvant treatment may face unexpected surgical challenges. High-volume medical units with stable and mature treatment processes, including neoadjuvant therapy and operations, generally have lower complication and mortality rates[89]. Therefore, RCTs involving neoadjuvant treatment should preferably be conducted in high-volume centers to reduce surgical risks and avoid any adverse impacts. Even in multi-center clinical trials, it is advisable to select larger surgical units or include surgeons with significant experience in performing over 100 operations on ESCC, both open and minimally invasive surgeries. Such measures ensure optimal surgical outcomes and minimize potential complications.

The third issue pertains to how we can accurately assess the efficacy of chosen drugs or treatments. Imaging is a crucial tool for preoperative efficacy assessment. Circulating tumor DNA (ct-DNA) has shown promise as an effective predictive method[90]. Positron emission tomography (PET) also has reference value as an assessment method[91,92]. Typically, pCR and MPR rates are used to predict efficacy, based on the examination of residual tumor cells in postoperative pathology. However, this method has certain limitations[93,94]. First, accurately assessing the pathological conditions of ESCC before immunotherapy, especially in cases of LN metastasis, is challenging. Detection can only be done in resected specimens after neoadjuvant immunotherapy, leading to an inability to make accurate comparisons with pathological specimens before surgery. Second, there is currently no universal standard for evaluating pathological response in ESCC after neoadjuvant immunotherapy. Pathologists are relied upon for positioning, measuring, sampling, slicing, and labeling, introducing variability. The different patterns of resection after neoadjuvant treatment, involving thoracic surgeons and pathologists, may also impact ESCC prognosis[95]. Thus, there is a need for a highly sensitive, specific, and preferably repeatable, simple, and feasible biomarker to predict efficacy in clinical practice.

PET is an integral part of the standard staging for ESCC. Its utility and acceptance in initial staging and recurrence detection have led to the hypothesis that PET could be used to differentiate responders from non-responders during neoadjuvant treatment. However, the precise PET parameters with the best predictive values are still a subject of debate. Several traditional PET parameters, such as the maximum and mean standardized uptake value (SUVmax and SUVmean), metabolic tumor volume (MTV), and total lesion glycolysis (TLG)[96], have been studied to correlate with pathological response. In a study of 31 patients with resectable ESCC or EAC, PET was used prospectively during treatment with trimodality therapy, and it was found that baseline TLG and post-chemoradiotherapy TLG were associated with OS[97]. More recently, efforts have been made to develop radiomic signatures and more robust predictive models. Simoni *et al*[98] investigated multiple traditional PET parameters and identified several radiomic features, as well as tumor regression grade, which correlated with pathological response in a retrospective analysis[98]. However, further research is necessary to develop more reliable predictive models and to validate them in prospective randomized trials. The credibility of PET evaluations in the era of immunotherapy remains largely unknown. Although PET has shown promise in predicting efficacy, especially with regard to OS, its applicability to immunotherapy response assessment is not fully understood. If sufficient high-quality CT or PET data, correlating with pathological response in ESCC, can be obtained, machine learning and artificial intelligence (AI) may emerge as new methods for evaluating neoadjuvant immunotherapy in ESCC. Such advancements could potentially enhance our ability to predict treatment outcomes and optimize patient care.

As of the current writing, specific biomarkers that can precisely determine the efficacy or predict perioperative surgery outcomes of ESCC have not been identified. However, several biomarkers have been explored mainly based on immunological and genetic criteria, including PD-L1 expression, intertumoral lymphoid infiltrates, dMMR/microsatellite instable (MSI), tumor mutation burden (TMB)/tumor neoantigen burden (TNB), and human leukocyte antigen (HLA)[99]. Among these biomarkers, PD-L1 expression is one of the best characterized for anti-PD-1/PD-L1 therapy. It is assessed using immunohistochemistry (IHC) staining and evaluated by the combined positive score (CPS) or tumor proportional score (TPS). CPS is determined by dividing the number of PD-L1-positive cells (tumor cells and other lymphocytes) by the total number of tumor cells[100], while TPS is calculated by dividing the number of PD-L1-positive tumor cells by the total number of tumor cells. In general, high PD-L1 expression usually correlates with an improved objective response to anti-PD-1/PD-L1 therapy[101]. However, some clinical studies have failed to consistently demonstrate this correlation, showing that patients with tumors showing high PD-L1 expression do not always respond to PD-1/PD-L1 blockade [102]. The relationship between PD-L1 expression and clinical outcome in ESCC remains a topic of controversy[103]. While some studies have shown that PD-L1 overexpression is associated with poor clinical outcomes[104], others have indicated a favorable prognosis[105].

Studies have also shown that circulating tumor cells (CTCs) and ct-DNA have a predictive role in evaluating the treatment efficacy of PD-1/PD-L1 inhibition[106,107]. CTCs have been found to be associated with a poor response to PD-L1 inhibitors in non-small cell lung cancer (NSCLC)[106]. Similarly, ct-DNA minimal residual disease (ct-DNA MRD) is

an important indicator for monitoring the efficacy of treating NSCLC[108]. Therefore, it is worth exploring whether CTCs and ct-DNA can be introduced into the long-term follow-up of ESCC to help assess treatment response and predict patient outcomes. However, further research is needed to validate the predictive value of these biomarkers in ESCC and determine their potential role in guiding treatment decisions for patients undergoing perioperative immunotherapy.

The fourth issue pertains to the long-term benefits of perioperative immunotherapy. Many clinical trials on perioperative immunotherapy have focused on short-term or mid-term outcomes, such as safety, feasibility, and pCR. However, the true primary outcomes that need to be concerned with are long-term OS and PFS, regardless of the type of immunological drugs selected or the combination with other anti-cancer therapies. For neoadjuvant anti-PD-1 therapy in resectable NSCLC, a trial with a median follow-up of 63 mo (NCT02259621) reported promising long-term outcomes. The 5-year recurrence-free survival (RFS) and OS rates were 60% and 80%, respectively[109]. Similarly, a study evaluating neoadjuvant anti-PD-1 treatment for localized dMMR colorectal cancer (CRC) also reported positive long-term follow-up data. Among patients who underwent surgery or achieved complete response, the 2-year tumor-specific disease-free and OS rates were both 100%[110].

In the context of resectable locally advanced ESCC, neoadjuvant chemotherapy and nCRT remain the standard treatments before surgery. While immune checkpoint-based therapy shows promise, it currently benefits only a small proportion of ESCC patients. Therefore, perioperative immunotherapy should be strictly monitored with ethical confirmation and preferably conducted within clinical trials. Patients must be fully informed about the potential benefits and risks and give informed consent before participating. Accurate screening of target populations and appropriate choice of combination therapy will be crucial for future research in this field. The importance of monitoring and managing trAEs, especially when combining immunotherapies with other anti-cancer therapies, cannot be ignored. Robust predictive and prognostic biomarkers or comprehensive biomarkers need to be identified to optimize treatment strategies and ensure the most effective therapy for patients. The development of clinical consensus or guidelines based on research findings will also be necessary to ensure that patients receive the most applicable and effective immunotherapy treatments.

CONCLUSION

The utilization of immunotherapy is progressively transitioning from a second-line approach for advanced or metastatic cases to a perioperative strategy for resectable locally advanced ESCC. Despite the current results lacking comprehensiveness and robustness, substantial advancements in perioperative immunotherapy for ESCC are evident. With the assurance derived from existing outcomes, numerous EC centers are now engaged in conducting multicenter, multi-arm RCTs. These RCTs hold the promise of providing further insights into the value of perioperative immunotherapy. It is plausible that in the near future, perioperative immunotherapy will emerge as a pivotal component of comprehensive treatment for resectable locally advanced ESCC. However, the determination of the optimal drug or the most effective combination of therapies, as well as the potential role of AI as an assistant, will require further observation and investigation.

FOOTNOTES

Author contributions: Liu Y designed the paper, collected and analyzed the data in the references, and wrote the manuscript.

Conflict-of-interest statement: The author declares no conflicts of interest related to this article.

Country/Territory of origin: China

ORCID number: Yong Liu 0000-0002-4048-5837.

S-Editor: Yan JP
L-Editor: Wang TQ
P-Editor: Cai YX

REFERENCES

1 **Sung H**, Ferlay J, Siegel RL, Laversanne M, Soerjomataram I, Jemal A, Bray F. Global Cancer Statistics 2020: GLOBOCAN Estimates of Incidence and Mortality Worldwide for 36 Cancers in 185 Countries. *CA Cancer J Clin* 2021; **71**: 209-249 [PMID: 33538338 DOI: 10.3322/caac.21660]

2 **Rustgi AK**, El-Serag HB. Esophageal carcinoma. *N Engl J Med* 2014; **371**: 2499-2509 [PMID: 25539106 DOI: 10.1056/NEJMra1314530]

3 **Yan Y**, Feng X, Li C, Lerut T, Li H. Treatments for resectable esophageal cancer: from traditional systemic therapy to immunotherapy. *Chin Med J (Engl)* 2022; **135**: 2143-2156 [PMID: 36525602 DOI: 10.1097/CM9.0000000000002371]

4 **Plum PS**, Hölscher AH, Pacheco Godoy K, Schmidt H, Berlth F, Chon SH, Alakus H, Bollschweiler E. Prognosis of patients with superficial T1 esophageal cancer who underwent endoscopic resection before esophagectomy-A propensity score-matched comparison. *Surg Endosc* 2018; **32**: 3972-3980 [PMID: 29536160 DOI: 10.1007/s00464-018-6139-7]

5 **Omloo JM**, Lagarde SM, Hulscher JB, Reitsma JB, Fockens P, van Dekken H, Ten Kate FJ, Obertop H, Tilanus HW, van Lanschot JJ. Extended transthoracic resection compared with limited transhiatal resection for adenocarcinoma of the mid/distal esophagus: five-year survival of a randomized clinical trial. *Ann Surg* 2007; **246**: 992-1000; discussion 1000 [PMID: 18043101 DOI: 10.1097/SLA.0b013e31815c4037]

6 **Oppedijk V**, van der Gaast A, van Lanschot JJ, van Hagen P, van Os R, van Rij CM, van der Sangen MJ, Beukema JC, Rütten H, Spruit PH, Reinders JG, Richel DJ, van Berge Henegouwen MI, Hulshof MC. Patterns of recurrence after surgery alone versus preoperative chemoradiotherapy and surgery in the CROSS trials. *J Clin Oncol* 2014; **32**: 385-391 [PMID: 24419108 DOI: 10.1200/JCO.2013.51.2186]

7 **Chen G**, Wang Z, Liu XY, Liu FY. Recurrence pattern of squamous cell carcinoma in the middle thoracic esophagus after modified Ivor-Lewis esophagectomy. *World J Surg* 2007; **31**: 1107-1114 [PMID: 17426905 DOI: 10.1007/s00268-006-0551-1]

8 **Leng XF**, Daiko H, Han YT, Mao YS. Optimal preoperative neoadjuvant therapy for resectable locally advanced esophageal squamous cell carcinoma. *Ann N Y Acad Sci* 2020; **1482**: 213-224 [PMID: 33067818 DOI: 10.1111/nyas.14508]

9 **Yang H**, Liu H, Chen Y, Zhu C, Fang W, Yu Z, Mao W, Xiang J, Han Y, Chen Z, Yang H, Wang J, Pang Q, Zheng X, Li T, Lordick F, D'Journo XB, Cerfolio RJ, Korst RJ, Novoa NM, Swanson SJ, Brunelli A, Ismail M, Fernando HC, Zhang X, Li Q, Wang G, Chen B, Mao T, Kong M, Guo X, Lin T, Liu M, Fu J; AME Thoracic Surgery Collaborative Group. Neoadjuvant Chemoradiotherapy Followed by Surgery Versus Surgery Alone for Locally Advanced Squamous Cell Carcinoma of the Esophagus (NEOCRTEC5010): A Phase III Multicenter, Randomized, Open-Label Clinical Trial. *J Clin Oncol* 2018; **36**: 2796-2803 [PMID: 30089078 DOI: 10.1200/JCO.2018.79.1483]

10 **Lewis S**, Lukovic J. Neoadjuvant Therapy in Esophageal Cancer. *Thorac Surg Clin* 2022; **32**: 447-456 [PMID: 36266032 DOI: 10.1016/j.thorsurg.2022.06.003]

11 **Shah MA**, Kennedy EB, Catenacci DV, Deighton DC, Goodman KA, Malhotra NK, Willett C, Stiles B, Sharma P, Tang L, Wijnhoven BPL, Hofstetter WL. Treatment of Locally Advanced Esophageal Carcinoma: ASCO Guideline. *J Clin Oncol* 2020; **38**: 2677-2694 [PMID: 32568633 DOI: 10.1200/JCO.20.00866]

12 **Puetz K**, Bollschweiler E, Semrau R, Mönig SP, Hölscher AH, Drebber U. Neoadjuvant chemoradiation for patients with advanced oesophageal cancer - which response grading system best impacts prognostic discrimination? *Histopathology* 2019; **74**: 731-743 [PMID: 30636069 DOI: 10.1111/his.13811]

13 **Shapiro J**, van Lanschot JJB, Hulshof MCCM, van Hagen P, van Berge Henegouwen MI, Wijnhoven BPL, van Laarhoven HWM, Nieuwenhuijzen GAP, Hospers GAP, Bonenkamp JJ, Cuesta MA, Blaisse RJB, Busch ORC, Ten Kate FJW, Creemers GM, Punt CJA, Plukker JTM, Verheul HMW, Bilgen EJS, van Dekken H, van der Sangen MJC, Rozema T, Biermann K, Beukema JC, Piet AHM, van Rij CM, Reinders JG, Tilanus HW, Steyerberg EW, van der Gaast A; CROSS study group. Neoadjuvant chemoradiotherapy plus surgery versus surgery alone for oesophageal or junctional cancer (CROSS): long-term results of a randomised controlled trial. *Lancet Oncol* 2015; **16**: 1090-1098 [PMID: 26254683 DOI: 10.1016/S1470-2045(15)00040-6]

14 **Sun HB**, Xing WQ, Liu XB, Zheng Y, Yang SJ, Wang ZF, Liu SL, Ba YF, Zhang RX, Liu BX, Fan CC, Chen PN, Liang GH, Yu YK, Liu Q, Wang HR, Li HM, Li ZX; written on Henan Cancer Hospital Thoracic Oncology Group (HCHTOG). Neoadjuvant chemotherapy versus neoadjuvant chemoradiotherapy for locally advanced oesophageal squamous cell carcinoma: a single-Centre, open-label, randomized, controlled, clinical trial (HCHTOG1903). *BMC Cancer* 2020; **20**: 303 [PMID: 32293362 DOI: 10.1186/s12885-020-06824-2]

15 **Tepper J**, Krasna MJ, Niedzwiecki D, Hollis D, Reed CE, Goldberg R, Kiel K, Willett C, Sugarbaker D, Mayer R. Phase III trial of trimodality therapy with cisplatin, fluorouracil, radiotherapy, and surgery compared with surgery alone for esophageal cancer: CALGB 9781. *J Clin Oncol* 2008; **26**: 1086-1092 [PMID: 18309943 DOI: 10.1200/JCO.2007.12.9593]

16 **van Hagen P**, Hulshof MC, van Lanschot JJ, Steyerberg EW, van Berge Henegouwen MI, Wijnhoven BP, Richel DJ, Nieuwenhuijzen GA, Hospers GA, Bonenkamp JJ, Cuesta MA, Blaisse RJ, Busch OR, ten Kate FJ, Creemers GJ, Punt CJ, Plukker JT, Verheul HM, Spillenaar Bilgen EJ, van Dekken H, van der Sangen MJ, Rozema T, Biermann K, Beukema JC, Piet AH, van Rij CM, Reinders JG, Tilanus HW, van der Gaast A; CROSS Group. Preoperative chemoradiotherapy for esophageal or junctional cancer. *N Engl J Med* 2012; **366**: 2074-2084 [PMID: 22646630 DOI: 10.1056/NEJMoa1112088]

17 **Zhou HY**, Zheng SP, Li AL, Gao QL, Ou QY, Chen YJ, Wu ST, Lin DG, Liu SB, Huang LY, Li FS, Zhu HY, Qiao GB, Lanuti M, Yao HR, Yu YF. Clinical evidence for association of neoadjuvant chemotherapy or chemoradiotherapy with efficacy and safety in patients with resectable esophageal carcinoma (NewEC study). *EClinicalMedicine* 2020; **24**: 100422 [PMID: 32637899 DOI: 10.1016/j.eclinm.2020.100422]

18 **Chan KKW**, Saluja R, Delos Santos K, Lien K, Shah K, Cramarossa G, Zhu X, Wong RKS. Neoadjuvant treatments for locally advanced, resectable esophageal cancer: A network meta-analysis. *Int J Cancer* 2018; **143**: 430-437 [PMID: 29441562 DOI: 10.1002/ijc.31312]

19 **Pasquali S**, Yim G, Vohra RS, Mocellin S, Nyanhongo D, Marriott P, Geh JI, Griffiths EA. Survival After Neoadjuvant and Adjuvant Treatments Compared to Surgery Alone for Resectable Esophageal Carcinoma: A Network Meta-analysis. *Ann Surg* 2017; **265**: 481-491 [PMID: 27429017 DOI: 10.1097/SLA.0000000000001905]

20 **Mariette C**, Dahan L, Mornex F, Maillard E, Thomas PA, Meunier B, Boige V, Pezet D, Robb WB, Le Brun-Ly V, Bosset JF, Mabrut JY, Triboulet JP, Bedenne L, Seitz JF. Surgery alone versus chemoradiotherapy followed by surgery for stage I and II esophageal cancer: final analysis of randomized controlled phase III trial FFCD 9901. *J Clin Oncol* 2014; **32**: 2416-2422 [PMID: 24982463 DOI: 10.1200/JCO.2013.53.6532]

21 **Murakami Y**, Hamai Y, Emi M, Hihara J, Imano N, Takeuchi Y, Takahashi I, Nishibuchi I, Kimura T, Okada M, Nagata Y. Long-term results of neoadjuvant chemoradiotherapy using cisplatin and 5-fluorouracil followed by esophagectomy for resectable, locally advanced esophageal squamous cell carcinoma. *J Radiat Res* 2018; **59**: 616-624 [PMID: 29939306 DOI: 10.1093/jrr/rry047]

22 **Ajani JA**, D'Amico TA, Bentrem DJ, Chao J, Corvera C, Das P, Denlinger CS, Enzinger PC, Fanta P, Farjah F, Gerdes H, Gibson M, Glasgow RE, Hayman JA, Hochwald S, Hofstetter WL, Ilson DH, Jaroszewski D, Johung KL, Keswani RN, Kleinberg LR, Leong S, Ly QP, Matkowskyj KA, McNamara M, Mulcahy MF, Paluri RK, Park H, Perry KA, Pimiento J, Poultsides GA, Roses R, Strong VE, Wiesner G, Willett CG, Wright CD, McMillian NR, Pluchino LA. Esophageal and Esophagogastric Junction Cancers, Version 2.2019, NCCN Clinical Practice Guidelines in Oncology. *J Natl Compr Canc Netw* 2019; **17**: 855-883 [PMID: 31319389 DOI: 10.6004/jnccn.2019.0033]

23 **Ajani JA**, D'Amico TA, Bentrem DJ, Cooke D, Corvera C, Das P, Enzinger PC, Enzler T, Farjah F, Gerdes H, Gibson M, Grierson P,

Hofstetter WL, Ilson DH, Jalal S, Keswani RN, Kim S, Kleinberg LR, Klempner S, Lacy J, Licciardi F, Ly QP, Matkowskyj KA, McNamara M, Miller A, Mukherjee S, Mulcahy MF, Outlaw D, Perry KA, Pimiento J, Poultsides GA, Reznik S, Roses RE, Strong VE, Su S, Wang HL, Wiesner G, Willett CG, Yakoub D, Yoon H, McMillian NR, Pluchino LA. Esophageal and Esophagogastric Junction Cancers, Version 2.2023, NCCN Clinical Practice Guidelines in Oncology. *J Natl Compr Canc Netw* 2023; **21**: 393-422 [PMID: 37015332 DOI: 10.6004/jnccn.2023.0019]

24 **Muro K**, Lordick F, Tsushima T, Pentheroudakis G, Baba E, Lu Z, Cho BC, Nor IM, Ng M, Chen LT, Kato K, Li J, Ryu MH, Zamaniah WIW, Yong WP, Yeh KH, Nakajima TE, Shitara K, Kawakami H, Narita Y, Yoshino T, Van Cutsem E, Martinelli E, Smyth EC, Arnold D, Minami H, Tabernero J, Douillard JY. Pan-Asian adapted ESMO Clinical Practice Guidelines for the management of patients with metastatic oesophageal cancer: a JSMO-ESMO initiative endorsed by CSCO, KSMO, MOS, SSO and TOS. *Ann Oncol* 2019; **30**: 34-43 [PMID: 30475943 DOI: 10.1093/annonc/mdy498]

25 **Zhang W**, Wang P, Pang Q. Immune checkpoint inhibitors for esophageal squamous cell carcinoma: a narrative review. *Ann Transl Med* 2020; **8**: 1193 [PMID: 33241042 DOI: 10.21037/atm-20-4625]

26 **Eyck BM**, van Lanschot JJB, Hulshof MCCM, van der Wilk BJ, Shapiro J, van Hagen P, van Berge Henegouwen MI, Wijnhoven BPL, van Laarhoven HWM, Nieuwenhuijzen GAP, Hospers GAP, Bonenkamp JJ, Cuesta MA, Blaisse RJB, Busch OR, Creemers GM, Punt CJA, Plukker JTM, Verheul HMW, Spillenaar Bilgen EJ, van der Sangen MJC, Rozema T, Ten Kate FJW, Beukema JC, Piet AHM, van Rij CM, Reinders JG, Tilanus HW, Steyerberg EW, van der Gaast A; CROSS Study Group. Ten-Year Outcome of Neoadjuvant Chemoradiotherapy Plus Surgery for Esophageal Cancer: The Randomized Controlled CROSS Trial. *J Clin Oncol* 2021; **39**: 1995-2004 [PMID: 33891478 DOI: 10.1200/JCO.20.03614]

27 **Groom JR**. Regulators of T-cell fate: Integration of cell migration, differentiation and function. *Immunol Rev* 2019; **289**: 101-114 [PMID: 30977199 DOI: 10.1111/imr.12742]

28 **Masopust D**, Schenkel JM. The integration of T cell migration, differentiation and function. *Nat Rev Immunol* 2013; **13**: 309-320 [PMID: 23598650 DOI: 10.1038/nri3442]

29 **Baba Y**, Nomoto D, Okadome K, Ishimoto T, Iwatsuki M, Miyamoto Y, Yoshida N, Baba H. Tumor immune microenvironment and immune checkpoint inhibitors in esophageal squamous cell carcinoma. *Cancer Sci* 2020; **111**: 3132-3141 [PMID: 32579769 DOI: 10.1111/cas.14541]

30 **Janjigian YY**, Bendell J, Calvo E, Kim JW, Ascierto PA, Sharma P, Ott PA, Peltola K, Jaeger D, Evans J, de Braud F, Chau I, Harbison CT, Dorange C, Tschaika M, Le DT. CheckMate-032 Study: Efficacy and Safety of Nivolumab and Nivolumab Plus Ipilimumab in Patients With Metastatic Esophagogastric Cancer. *J Clin Oncol* 2018; **36**: 2836-2844 [PMID: 30110194 DOI: 10.1200/JCO.2017.76.6212]

31 **Kudo T**, Hamamoto Y, Kato K, Ura T, Kojima T, Tsushima T, Hironaka S, Hara H, Satoh T, Iwasa S, Muro K, Yasui H, Minashi K, Yamaguchi K, Ohtsu A, Doki Y, Kitagawa Y. Nivolumab treatment for oesophageal squamous-cell carcinoma: an open-label, multicentre, phase 2 trial. *Lancet Oncol* 2017; **18**: 631-639 [PMID: 28314688 DOI: 10.1016/S1470-2045(17)30181-X]

32 **Kojima T**, Shah MA, Muro K, Francois E, Adenis A, Hsu CH, Doi T, Moriwaki T, Kim SB, Lee SH, Bennouna J, Kato K, Shen L, Enzinger P, Qin SK, Ferreira P, Chen J, Girotto G, de la Fouchardiere C, Senellart H, Al-Rajabi R, Lordick F, Wang R, Suryawanshi S, Bhagia P, Kang SP, Metges JP; KEYNOTE-181 Investigators. Randomized Phase III KEYNOTE-181 Study of Pembrolizumab Versus Chemotherapy in Advanced Esophageal Cancer. *J Clin Oncol* 2020; **38**: 4138-4148 [PMID: 33026938 DOI: 10.1200/JCO.20.01888]

33 **Shen L**, Kato K, Kim SB, Ajani JA, Zhao K, He Z, Yu X, Shu Y, Luo Q, Wang J, Chen Z, Niu Z, Zhang L, Yi T, Sun JM, Chen J, Yu G, Lin CY, Hara H, Bi Q, Satoh T, Pazo-Cid R, Arkenau HT, Borg C, Lordick F, Li L, Ding N, Tao A, Shi J, Van Cutsem E; RATIONALE-302 Investigators. Tislelizumab Versus Chemotherapy as Second-Line Treatment for Advanced or Metastatic Esophageal Squamous Cell Carcinoma (RATIONALE-302): A Randomized Phase III Study. *J Clin Oncol* 2022; **40**: 3065-3076 [PMID: 35442766 DOI: 10.1200/JCO.21.01926]

34 **Kato K**, Cho BC, Takahashi M, Okada M, Lin CY, Chin K, Kadowaki S, Ahn MJ, Hamamoto Y, Doki Y, Yen CC, Kubota Y, Kim SB, Hsu CH, Holtved E, Xynos I, Kodani M, Kitagawa Y. Nivolumab versus chemotherapy in patients with advanced oesophageal squamous cell carcinoma refractory or intolerant to previous chemotherapy (ATTRACTION-3): a multicentre, randomised, open-label, phase 3 trial. *Lancet Oncol* 2019; **20**: 1506-1517 [PMID: 31582355 DOI: 10.1016/S1470-2045(19)30626-6]

35 **Huang J**, Xu J, Chen Y, Zhuang W, Zhang Y, Chen Z, Chen J, Zhang H, Niu Z, Fan Q, Lin L, Gu K, Liu Y, Ba Y, Miao Z, Jiang X, Zeng M, Fu Z, Gan L, Wang J, Zhan X, Liu T, Li Z, Shen L, Shu Y, Zhang T, Yang Q, Zou J; ESCORT Study Group. Camrelizumab versus investigator's choice of chemotherapy as second-line therapy for advanced or metastatic oesophageal squamous cell carcinoma (ESCORT): a multicentre, randomised, open-label, phase 3 study. *Lancet Oncol* 2020; **21**: 832-842 [PMID: 32416073 DOI: 10.1016/S1470-2045(20)30110-8]

36 **Wang ZX**, Cui C, Yao J, Zhang Y, Li M, Feng J, Yang S, Fan Y, Shi J, Zhang X, Shen L, Shu Y, Wang C, Dai T, Mao T, Chen L, Guo Z, Liu B, Pan H, Cang S, Jiang Y, Wang J, Ye M, Chen Z, Jiang D, Lin Q, Ren W, Wu L, Xu Y, Miao Z, Sun M, Xie C, Liu Y, Wang Q, Zhao L, Li Q, Huang C, Jiang K, Yang K, Li D, Zhu Z, Chen R, Jia L, Li W, Liao W, Liu HX, Ma D, Ma J, Qin Y, Shi Z, Wei Q, Xiao K, Chen X, Dai G, He J, Li J, Li G, Liu Z, Yuan X, Zhang J, Fu Z, He Y, Ju F, Tang P, Wang T, Wang W, Luo X, Tang X, May R, Feng H, Yao S, Keegan P, Xu RH, Wang F. Toripalimab plus chemotherapy in treatment-naïve, advanced esophageal squamous cell carcinoma (JUPITER-06): A multi-center phase 3 trial. *Cancer Cell* 2022; **40**: 277-288.e3 [PMID: 35245446 DOI: 10.1016/j.ccell.2022.02.007]

37 **Doki Y**, Ajani JA, Kato K, Xu J, Wyrwicz L, Motoyama S, Ogata T, Kawakami H, Hsu CH, Adenis A, El Hajbi F, Di Bartolomeo M, Braghiroli MI, Holtved E, Ostoich SA, Kim HR, Ueno M, Mansoor W, Yang WC, Liu T, Bridgewater J, Makino T, Xynos I, Liu X, Lei M, Kondo K, Patel A, Gricar J, Chau I, Kitagawa Y; CheckMate 648 Trial Investigators. Nivolumab Combination Therapy in Advanced Esophageal Squamous-Cell Carcinoma. *N Engl J Med* 2022; **386**: 449-462 [PMID: 35108470 DOI: 10.1056/NEJMoa2111380]

38 **Lu Z**, Wang J, Shu Y, Liu L, Kong L, Yang L, Wang B, Sun G, Ji Y, Cao G, Liu H, Cui T, Li N, Qiu W, Li G, Hou X, Luo H, Xue L, Zhang Y, Yue W, Liu Z, Wang X, Gao S, Pan Y, Galais MP, Zaanan A, Ma Z, Li H, Wang Y, Shen L; ORIENT-15 study group. Sintilimab versus placebo in combination with chemotherapy as first line treatment for locally advanced or metastatic oesophageal squamous cell carcinoma (ORIENT-15): multicentre, randomised, double blind, phase 3 trial. *BMJ* 2022; **377**: e068714 [PMID: 35440464 DOI: 10.1136/bmj-2021-068714]

39 **Luo H**, Lu J, Bai Y, Mao T, Wang J, Fan Q, Zhang Y, Zhao K, Chen Z, Gao S, Li J, Fu Z, Gu K, Liu Z, Wu L, Zhang X, Feng J, Niu Z, Ba Y, Zhang H, Liu Y, Zhang L, Min X, Huang J, Cheng Y, Wang D, Shen Y, Yang Q, Zou J, Xu RH; ESCORT-1st Investigators. Effect of Camrelizumab vs Placebo Added to Chemotherapy on Survival and Progression-Free Survival in Patients With Advanced or Metastatic Esophageal Squamous Cell Carcinoma: The ESCORT-1st Randomized Clinical Trial. *JAMA* 2021; **326**: 916-925 [PMID: 34519801 DOI: 10.1001/jama.2021.12836]

40 **Sun JM**, Shen L, Shah MA, Enzinger P, Adenis A, Doi T, Kojima T, Metges JP, Li Z, Kim SB, Cho BC, Mansoor W, Li SH, Sunpaweravong

P, Maqueda MA, Goekkurt E, Hara H, Antunes L, Fountzilas C, Tsuji A, Oliden VC, Liu Q, Shah S, Bhagia P, Kato K; KEYNOTE-590 Investigators. Pembrolizumab plus chemotherapy versus chemotherapy alone for first-line treatment of advanced oesophageal cancer (KEYNOTE-590): a randomised, placebo-controlled, phase 3 study. *Lancet* 2021; **398**: 759-771 [PMID: 34454674 DOI: 10.1016/S0140-6736(21)01234-4]

41 **Forde PM**, Chaft JE, Smith KN, Anagnostou V, Cottrell TR, Hellmann MD, Zahurak M, Yang SC, Jones DR, Broderick S, Battafarano RJ, Velez MJ, Rekhtman N, Olah Z, Naidoo J, Marrone KA, Verde F, Guo H, Zhang J, Caushi JX, Chan HY, Sidhom JW, Scharpf RB, White J, Gabrielson E, Wang H, Rosner GL, Rusch V, Wolchok JD, Merghoub T, Taube JM, Velculescu VE, Topalian SL, Brahmer JR, Pardoll DM. Neoadjuvant PD-1 Blockade in Resectable Lung Cancer. *N Engl J Med* 2018; **378**: 1976-1986 [PMID: 29658848 DOI: 10.1056/NEJMoa1716078]

42 **Provencio M**, Nadal E, Insa A, García-Campelo MR, Casal-Rubio J, Dómine M, Majem M, Rodríguez-Abreu D, Martínez-Martí A, De Castro Carpeño J, Cobo M, López Vivanco G, Del Barco E, Bernabé Caro R, Viñolas N, Barneto Aranda I, Viteri S, Pereira E, Royuela A, Casarrubios M, Salas Antón C, Parra ER, Wistuba I, Calvo V, Laza-Briviesca R, Romero A, Massuti B, Cruz-Bermúdez A. Neoadjuvant chemotherapy and nivolumab in resectable non-small-cell lung cancer (NADIM): an open-label, multicentre, single-arm, phase 2 trial. *Lancet Oncol* 2020; **21**: 1413-1422 [PMID: 32979984 DOI: 10.1016/S1470-2045(20)30453-8]

43 **Huang AC**, Orlowski RJ, Xu X, Mick R, George SM, Yan PK, Manne S, Kraya AA, Wubbenhorst B, Dorfman L, D'Andrea K, Wenz BM, Liu S, Chilukuri L, Kozlov A, Carberry M, Giles L, Kier MW, Quagliarello F, McGettigan S, Kreider K, Annamalai L, Zhao Q, Mogg R, Xu W, Blumenschein WM, Yearley JH, Linette GP, Amaravadi RK, Schuchter LM, Herati RS, Bengsch B, Nathanson KL, Farwell MD, Karakousis GC, Wherry EJ, Mitchell TC. A single dose of neoadjuvant PD-1 blockade predicts clinical outcomes in resectable melanoma. *Nat Med* 2019; **25**: 454-461 [PMID: 30804515 DOI: 10.1038/s41591-019-0357-y]

44 **Powles T**, Kockx M, Rodriguez-Vida A, Duran I, Crabb SJ, Van Der Heijden MS, Szabados B, Pous AF, Gravis G, Herranz UA, Protheroe A, Ravaud A, Maillet D, Mendez MJ, Suarez C, Linch M, Prendergast A, van Dam PJ, Stanoeva D, Daelemans S, Mariathasan S, Tea JS, Mousa K, Banchereau R, Castellano D. Clinical efficacy and biomarker analysis of neoadjuvant atezolizumab in operable urothelial carcinoma in the ABACUS trial. *Nat Med* 2019; **25**: 1706-1714 [PMID: 31686036 DOI: 10.1038/s41591-019-0628-7]

45 **Chalabi M**, Fanchi LF, Dijkstra KK, Van den Berg JG, Aalbers AG, Sikorska K, Lopez-Yurda M, Grootscholten C, Beets GL, Snaebjornsson P, Maas M, Mertz M, Veninga V, Bounova G, Broeks A, Beets-Tan RG, de Wijkerslooth TR, van Lent AU, Marsman HA, Nuijten E, Kok NF, Kuiper M, Verbeek WH, Kok M, Van Leerdam ME, Schumacher TN, Voest EE, Haanen JB. Neoadjuvant immunotherapy leads to pathological responses in MMR-proficient and MMR-deficient early-stage colon cancers. *Nat Med* 2020; **26**: 566-576 [PMID: 32251400 DOI: 10.1038/s41591-020-0805-8]

46 **Schalper KA**, Rodriguez-Ruiz ME, Diez-Valle R, López-Janeiro A, Porciuncula A, Idoate MA, Inogés S, de Andrea C, López-Diaz de Cerio A, Tejada S, Berraondo P, Villarroel-Espindola F, Choi J, Gúrpide A, Giraldez M, Goicoechea I, Gallego Perez-Larraya J, Sanmamed MF, Perez-Gracia JL, Melero I. Neoadjuvant nivolumab modifies the tumor immune microenvironment in resectable glioblastoma. *Nat Med* 2019; **25**: 470-476 [PMID: 30742120 DOI: 10.1038/s41591-018-0339-5]

47 **Whiteside TL**. The tumor microenvironment and its role in promoting tumor growth. *Oncogene* 2008; **27**: 5904-5912 [PMID: 18836471 DOI: 10.1038/onc.2008.271]

48 **Blessin NC**, Li W, Mandelkow T, Jansen HL, Yang C, Raedler JB, Simon R, Büscheck F, Dum D, Luebke AM, Hinsch A, Möller K, Menz A, Bernreuther C, Lebok P, Clauditz T, Sauter G, Marx A, Uhlig R, Wilczak W, Minner S, Krech T, Fraune C, Höflmayer D, Burandt E, Steurer S. Prognostic role of proliferating CD8(+) cytotoxic Tcells in human cancers. *Cell Oncol (Dordr)* 2021; **44**: 793-803 [PMID: 33864611 DOI: 10.1007/s13402-021-00601-4]

49 **Zhang N**, Bevan MJ. CD8(+) T cells: foot soldiers of the immune system. *Immunity* 2011; **35**: 161-168 [PMID: 21867926 DOI: 10.1016/j.immuni.2011.07.010]

50 **Nurieva RI**, Liu X, Dong C. Yin-Yang of costimulation: crucial controls of immune tolerance and function. *Immunol Rev* 2009; **229**: 88-100 [PMID: 19426216 DOI: 10.1111/j.1600-065X.2009.00769.x]

51 **Vinay DS**, Ryan EP, Pawelec G, Talib WH, Stagg J, Elkord E, Lichtor T, Decker WK, Whelan RL, Kumara HMCS, Signori E, Honoki K, Georgakilas AG, Amin A, Helferich WG, Boosani CS, Guha G, Ciriolo MR, Chen S, Mohammed SI, Azmi AS, Keith WN, Bilsland A, Bhakta D, Halicka D, Fujii H, Aquilano K, Ashraf SS, Nowsheen S, Yang X, Choi BK, Kwon BS. Immune evasion in cancer: Mechanistic basis and therapeutic strategies. *Semin Cancer Biol* 2015; **35** Suppl: S185-S198 [PMID: 25818339 DOI: 10.1016/j.semcancer.2015.03.004]

52 **Baldwin XL**, Spanheimer PM, Downs-Canner S. A Review of Immune Checkpoint Blockade for the General Surgeon. *J Surg Res* 2023; **281**: 289-298 [PMID: 36228339 DOI: 10.1016/j.jss.2022.08.040]

53 **Buchbinder EI**, Desai A. CTLA-4 and PD-1 Pathways: Similarities, Differences, and Implications of Their Inhibition. *Am J Clin Oncol* 2016; **39**: 98-106 [PMID: 26558876 DOI: 10.1097/COC.0000000000000239]

54 **Ribas A**, Wolchok JD. Cancer immunotherapy using checkpoint blockade. *Science* 2018; **359**: 1350-1355 [PMID: 29567705 DOI: 10.1126/science.aar4060]

55 **Sharpe AH**, Pauken KE. The diverse functions of the PD1 inhibitory pathway. *Nat Rev Immunol* 2018; **18**: 153-167 [PMID: 28990585 DOI: 10.1038/nri.2017.108]

56 **Geng Q**, Rohondia SO, Khan HJ, Jiao P, Dou QP. Small molecules as antagonists of co-inhibitory pathways for cancer immunotherapy: a patent review (2018-2019). *Expert Opin Ther Pat* 2020; **30**: 677-694 [PMID: 32715813 DOI: 10.1080/13543776.2020.1801640]

57 **Baumeister SH**, Freeman GJ, Dranoff G, Sharpe AH. Coinhibitory Pathways in Immunotherapy for Cancer. *Annu Rev Immunol* 2016; **34**: 539-573 [PMID: 26927206 DOI: 10.1146/annurev-immunol-032414-112049]

58 **Yi M**, Zheng X, Niu M, Zhu S, Ge H, Wu K. Combination strategies with PD-1/PD-L1 blockade: current advances and future directions. *Mol Cancer* 2022; **21**: 28 [PMID: 35062949 DOI: 10.1186/s12943-021-01489-2]

59 **Awadasseid A**, Wu Y, Zhang W. Advance investigation on synthetic small-molecule inhibitors targeting PD-1/PD-L1 signaling pathway. *Life Sci* 2021; **282**: 119813 [PMID: 34256042 DOI: 10.1016/j.lfs.2021.119813]

60 **Wu Q**, Jiang L, Li SC, He QJ, Yang B, Cao J. Small molecule inhibitors targeting the PD-1/PD-L1 signaling pathway. *Acta Pharmacol Sin* 2021; **42**: 1-9 [PMID: 32152439 DOI: 10.1038/s41401-020-0366-x]

61 **Maruhashi T**, Sugiura D, Okazaki IM, Okazaki T. LAG-3: from molecular functions to clinical applications. *J Immunother Cancer* 2020; **8** [PMID: 32929051 DOI: 10.1136/jitc-2020-001014]

62 **Meng X**, Wu T, Hong Y, Fan Q, Ren Z, Guo Y, Yang X, Shi P, Yang J, Yin X, Luo Z, Xia J, Zhou Y, Xu M, Liu E, Jiang G, Li S, Zhao F, Ma C, Hou Z, Li J, Wang J, Wang F. Camrelizumab plus apatinib as second-line treatment for advanced oesophageal squamous cell carcinoma (CAP 02): a single-arm, open-label, phase 2 trial. *Lancet Gastroenterol Hepatol* 2022; **7**: 245-253 [PMID: 34998471 DOI:

10.1016/S2468-1253(21)00378-2]

63 **Huang J**, Xu B, Mo H, Zhang W, Chen X, Wu D, Qu D, Wang X, Lan B, Yang B, Wang P, Zhang H, Yang Q, Jiao Y. Safety, Activity, and Biomarkers of SHR-1210, an Anti-PD-1 Antibody, for Patients with Advanced Esophageal Carcinoma. *Clin Cancer Res* 2018; **24**: 1296-1304 [PMID: 29358502 DOI: 10.1158/1078-0432.CCR-17-2439]

64 **O'Donnell JS**, Hoefsmit EP, Smyth MJ, Blank CU, Teng MWL. The Promise of Neoadjuvant Immunotherapy and Surgery for Cancer Treatment. *Clin Cancer Res* 2019; **25**: 5743-5751 [PMID: 31040150 DOI: 10.1158/1078-0432.CCR-18-2641]

65 **Topalian SL**, Taube JM, Pardoll DM. Neoadjuvant checkpoint blockade for cancer immunotherapy. *Science* 2020; **367** [PMID: 32001626 DOI: 10.1126/science.aax0182]

66 **Kelly RJ**, Ajani JA, Kuzdzal J, Zander T, Van Cutsem E, Piessen G, Mendez G, Feliciano J, Motoyama S, Lièvre A, Uronis H, Elimova E, Grootscholten C, Geboes K, Zafar S, Snow S, Ko AH, Feeney K, Schenker M, Kocon P, Zhang J, Zhu L, Lei M, Singh P, Kondo K, Cleary JM, Moehler M; CheckMate 577 Investigators. Adjuvant Nivolumab in Resected Esophageal or Gastroesophageal Junction Cancer. *N Engl J Med* 2021; **384**: 1191-1203 [PMID: 33789008 DOI: 10.1056/NEJMoa2032125]

67 **Yamamoto S**, Kato K, Daiko H, Kojima T, Hara H, Abe T, Tsubosa Y, Nagashima K, Aoki K, Mizoguchi Y, Kitano S, Yachida S, Shiba S, Kitagawa Y. Feasibility study of nivolumab as neoadjuvant chemotherapy for locally esophageal carcinoma: FRONTiER (JCOG1804E). *Future Oncol* 2020; **16**: 1351-1357 [PMID: 32396014 DOI: 10.2217/fon-2020-0189]

68 **Jia XH**, Xu H, Geng LY, Jiao M, Wang WJ, Jiang LL, Guo H. Efficacy and safety of neoadjuvant immunotherapy in resectable nonsmall cell lung cancer: A meta-analysis. *Lung Cancer* 2020; **147**: 143-153 [PMID: 32717571 DOI: 10.1016/j.lungcan.2020.07.001]

69 **Zhou X**, Yao Z, Bai H, Duan J, Wang Z, Wang X, Zhang X, Xu J, Fei K, Zhang Z, Tan F, Xue Q, Gao S, Gao Y, Wang J, He J. Treatment-related adverse events of PD-1 and PD-L1 inhibitor-based combination therapies in clinical trials: a systematic review and meta-analysis. *Lancet Oncol* 2021; **22**: 1265-1274 [PMID: 34391508 DOI: 10.1016/S1470-2045(21)00333-8]

70 **Wang Y**, Zhou S, Yang F, Qi X, Wang X, Guan X, Shen C, Duma N, Vera Aguilera J, Chintakuntlawar A, Price KA, Molina JR, Pagliaro LC, Halfdanarson TR, Grothey A, Markovic SN, Nowakowski GS, Ansell SM, Wang ML. Treatment-Related Adverse Events of PD-1 and PD-L1 Inhibitors in Clinical Trials: A Systematic Review and Meta-analysis. *JAMA Oncol* 2019; **5**: 1008-1019 [PMID: 31021376 DOI: 10.1001/jamaoncol.2019.0393]

71 **Khoja L**, Day D, Wei-Wu Chen T, Siu LL, Hansen AR. Tumour- and class-specific patterns of immune-related adverse events of immune checkpoint inhibitors: a systematic review. *Ann Oncol* 2017; **28**: 2377-2385 [PMID: 28945858 DOI: 10.1093/annonc/mdx286]

72 **Gao TT**, Shan JH, Yang YX, Zhang ZW, Liu SL, Xi M, Liu MZ, Zhao L. Comparative efficacy and safety of immunotherapy for patients with advanced or metastatic esophageal squamous cell carcinoma: a systematic review and network Meta-analysis. *BMC Cancer* 2022; **22**: 992 [PMID: 36115960 DOI: 10.1186/s12885-022-10086-5]

73 **Zhang Z**, Hong ZN, Xie S, Lin W, Lin Y, Zhu J, Yang X, Lin Z, Lin J, Kang M. Neoadjuvant sintilimab plus chemotherapy for locally advanced esophageal squamous cell carcinoma: a single-arm, single-center, phase 2 trial (ESONICT-1). *Ann Transl Med* 2021; **9**: 1623 [PMID: 34926667 DOI: 10.21037/atm-21-5381]

74 **Liu J**, Yang Y, Liu Z, Fu X, Cai X, Li H, Zhu L, Shen Y, Zhang H, Sun Y, Chen H, Yu B, Zhang R, Shao J, Zhang M, Li Z. Multicenter, single-arm, phase II trial of camrelizumab and chemotherapy as neoadjuvant treatment for locally advanced esophageal squamous cell carcinoma. *J Immunother Cancer* 2022; **10** [PMID: 35338088 DOI: 10.1136/jitc-2021-004291]

75 **Liu J**, Li J, Lin W, Shao D, Depypere L, Zhang Z, Li Z, Cui F, Du Z, Zeng Y, Jiang S, He P, Gu X, Chen H, Zhang H, Lin X, Huang H, Lv W, Cai W, Liang W, Liang H, Jiang W, Wang W, Xu K, Wu K, Lerut T, Fu J, He J. Neoadjuvant camrelizumab plus chemotherapy for resectable, locally advanced esophageal squamous cell carcinoma (NIC-ESCC2019): A multicenter, phase 2 study. *Int J Cancer* 2022; **151**: 128-137 [PMID: 35188268 DOI: 10.1002/ijc.33976]

76 **Yan X**, Duan H, Ni Y, Zhou Y, Wang X, Qi H, Gong L, Liu H, Tian F, Lu Q, Sun J, Yang E, Zhong D, Wang T, Huang L, Wang J, Chaoyang Wang, Wang Y, Wan Z, Lei J, Zhao J, Jiang T. Tislelizumab combined with chemotherapy as neoadjuvant therapy for surgically resectable esophageal cancer: A prospective, single-arm, phase II study (TD-NICE). *Int J Surg* 2022; **103**: 106680 [PMID: 35595021 DOI: 10.1016/j.ijsu.2022.106680]

77 **He W**, Leng X, Mao T, Luo X, Zhou L, Yan J, Peng L, Fang Q, Liu G, Wei X, Wang K, Wang C, Zhang S, Zhang X, Shen X, Huang D, Yi H, Bei T, She X, Xiao W, Han Y. Toripalimab Plus Paclitaxel and Carboplatin as Neoadjuvant Therapy in Locally Advanced Resectable Esophageal Squamous Cell Carcinoma. *Oncologist* 2022; **27**: e18-e28 [PMID: 35305102 DOI: 10.1093/oncolo/oyab011]

78 **van den Ende T**, de Clercq NC, van Berge Henegouwen MI, Gisbertz SS, Geijsen ED, Verhoeven RHA, Meijer SL, Schokker S, Dings MPG, Bergman JJGHM, Haj Mohammad N, Ruurda JP, van Hillegersberg R, Mook S, Nieuwdorp M, de Gruijl TD, Soeratram TTD, Ylstra B, van Grieken NCT, Bijlsma MF, Hulshof MCCM, van Laarhoven HWM. Neoadjuvant Chemoradiotherapy Combined with Atezolizumab for Resectable Esophageal Adenocarcinoma: A Single-arm Phase II Feasibility Trial (PERFECT). *Clin Cancer Res* 2021; **27**: 3351-3359 [PMID: 33504550 DOI: 10.1158/1078-0432.CCR-20-4443]

79 **Ge F**, Huo Z, Cai X, Hu Q, Chen W, Lin G, Zhong R, You Z, Wang R, Lu Y, Huang Q, Zhang H, Song A, Li C, Wen Y, Jiang Y, Liang H, He J, Liang W, Liu J. Evaluation of Clinical and Safety Outcomes of Neoadjuvant Immunotherapy Combined With Chemotherapy for Patients With Resectable Esophageal Cancer: A Systematic Review and Meta-analysis. *JAMA Netw Open* 2022; **5**: e2239778 [PMID: 36322089 DOI: 10.1001/jamanetworkopen.2022.39778]

80 **Shang X**, Zhao G, Liang F, Zhang C, Zhang W, Liu L, Li R, Duan X, Ma Z, Yue J, Chen C, Meng B, Ren X, Jiang H. Safety and effectiveness of pembrolizumab combined with paclitaxel and cisplatin as neoadjuvant therapy followed by surgery for locally advanced resectable (stage III) esophageal squamous cell carcinoma: a study protocol for a prospective, single-arm, single-center, open-label, phase-II trial (Keystone-001). *Ann Transl Med* 2022; **10**: 229 [PMID: 35280363 DOI: 10.21037/atm-22-513]

81 **Duan H**, Wang T, Luo Z, Wang X, Liu H, Tong L, Dong X, Zhang Y, Valmasoni M, Kidane B, Almhanna K, Wiesel O, Pang S, Ma J, Yan X. A multicenter single-arm trial of sintilimab in combination with chemotherapy for neoadjuvant treatment of resectable esophageal cancer (SIN-ICE study). *Ann Transl Med* 2021; **9**: 1700 [PMID: 34988209 DOI: 10.21037/atm-21-6102]

82 **Yang W**, Xing X, Yeung SJ, Wang S, Chen W, Bao Y, Wang F, Feng S, Peng F, Wang X, Chen S, He M, Zhang N, Wang H, Zeng B, Liu Z, Kidane B, Seder CW, Koyanagi K, Shargall Y, Luo H, Peng S, Cheng C. Neoadjuvant programmed cell death 1 blockade combined with chemotherapy for resectable esophageal squamous cell carcinoma. *J Immunother Cancer* 2022; **10** [PMID: 35022193 DOI: 10.1136/jitc-2021-003497]

83 **Duan H**, Shao C, Pan M, Liu H, Dong X, Zhang Y, Tong L, Feng Y, Wang Y, Wang L, Newman NB, Sarkaria IS, Reynolds JV, De Cobelli F, Ma Z, Jiang T, Yan X. Neoadjuvant Pembrolizumab and Chemotherapy in Resectable Esophageal Cancer: An Open-Label, Single-Arm Study (PEN-ICE). *Front Immunol* 2022; **13**: 849984 [PMID: 35720388 DOI: 10.3389/fimmu.2022.849984]

84 **Zheng Y**, Li C, Yu B, Zhao S, Li J, Chen X, Li H. Preoperative pembrolizumab combined with chemoradiotherapy for esophageal squamous cell carcinoma: Trial design. *JTCVS Open* 2022; **9**: 293-299 [PMID: 36003437 DOI: 10.1016/j.xjon.2021.11.003]

85 **Li C**, Zhao S, Zheng Y, Han Y, Chen X, Cheng Z, Wu Y, Feng X, Qi W, Chen K, Xiang J, Li J, Lerut T, Li H. Preoperative pembrolizumab combined with chemoradiotherapy for oesophageal squamous cell carcinoma (PALACE-1). *Eur J Cancer* 2021; **144**: 232-241 [PMID: 33373868 DOI: 10.1016/j.ejca.2020.11.039]

86 **Shang X**, Zhang W, Zhao G, Liang F, Zhang C, Yue J, Duan X, Ma Z, Chen C, Pang Q, Liu L, Ren X, Meng B, Zhang P, Ma Y, Zhang L, Li H, Kang X, Li Y, Jiang H. Pembrolizumab Combined With Neoadjuvant Chemotherapy Versus Neoadjuvant Chemoradiotherapy Followed by Surgery for Locally Advanced Oesophageal Squamous Cell Carcinoma: Protocol for a Multicentre, Prospective, Randomized-Controlled, Phase III Clinical Study (Keystone-002). *Front Oncol* 2022; **12**: 831345 [PMID: 35433421 DOI: 10.3389/fonc.2022.831345]

87 **Zhao Y**, Dai Z, Min W, Sui X, Kang H, Zhang Y, Ren H, Wang XJ. Perioperative versus Preoperative Chemotherapy with Surgery in Patients with Resectable Squamous Cell Carcinoma of Esophagus: A Phase III Randomized Trial. *J Thorac Oncol* 2015; **10**: 1349-1356 [PMID: 26287319 DOI: 10.1097/JTO.0000000000000612]

88 **Chen X**, Xu X, Wang D, Liu J, Sun J, Lu M, Wang R, Hui B, Li X, Zhou C, Wang M, Qiu T, Cui S, Sun N, Li Y, Wang F, Liu C, Shao Y, Luo J, Gu Y. Neoadjuvant sintilimab and chemotherapy in patients with potentially resectable esophageal squamous cell carcinoma (KEEP-G 03): an open-label, single-arm, phase 2 trial. *J Immunother Cancer* 2023; **11** [PMID: 36759013 DOI: 10.1136/jitc-2022-005830]

89 **Feo CV**, Villaflor VM, Patti MG. Should esophageal resections for cancer be performed in high-volume centers only? *Updates Surg* 2011; **63**: 147-150 [PMID: 21695513 DOI: 10.1007/s13304-011-0090-7]

90 **Forschner A**, Battke F, Hadaschik D, Schulze M, Weißgraeber S, Han CT, Kopp M, Frick M, Klumpp B, Tietze N, Amaral T, Martus P, Sinnberg T, Eigentler T, Keim U, Garbe C, Döcker D, Biskup S. Tumor mutation burden and circulating tumor DNA in combined CTLA-4 and PD-1 antibody therapy in metastatic melanoma - results of a prospective biomarker study. *J Immunother Cancer* 2019; **7**: 180 [PMID: 31300034 DOI: 10.1186/s40425-019-0659-0]

91 **Jreige M**, Letovanec I, Chaba K, Renaud S, Rusakiewicz S, Cristina V, Peters S, Krueger T, de Leval L, Kandalaft LE, Nicod-Lalonde M, Romero P, Prior JO, Coukos G, Schaefer N. (18)F-FDG PET metabolic-to-morphological volume ratio predicts PD-L1 tumour expression and response to PD-1 blockade in non-small-cell lung cancer. *Eur J Nucl Med Mol Imaging* 2019; **46**: 1859-1868 [PMID: 31214790 DOI: 10.1007/s00259-019-04348-x]

92 **Lv G**, Sun X, Qiu L, Sun Y, Li K, Liu Q, Zhao Q, Qin S, Lin J. PET Imaging of Tumor PD-L1 Expression with a Highly Specific Nonblocking Single-Domain Antibody. *J Nucl Med* 2020; **61**: 117-122 [PMID: 31253743 DOI: 10.2967/jnumed.119.226712]

93 **Sholl LM**. Understanding patterns of pathologic response following neoadjuvant immunotherapy for solid tumors. *Ann Oncol* 2018; **29**: 1630-1632 [PMID: 30052725 DOI: 10.1093/annonc/mdy227]

94 **Cottrell TR**, Thompson ED, Forde PM, Stein JE, Duffield AS, Anagnostou V, Rekhtman N, Anders RA, Cuda JD, Illei PB, Gabrielson E, Askin FB, Niknafs N, Smith KN, Velez MJ, Sauter JL, Isbell JM, Jones DR, Battafarano RJ, Yang SC, Danilova L, Wolchok JD, Topalian SL, Velculescu VE, Pardoll DM, Brahmer JR, Hellmann MD, Chaft JE, Cimino-Mathews A, Taube JM. Pathologic features of response to neoadjuvant anti-PD-1 in resected non-small-cell lung carcinoma: a proposal for quantitative immune-related pathologic response criteria (irPRC). *Ann Oncol* 2018; **29**: 1853-1860 [PMID: 29982279 DOI: 10.1093/annonc/mdy218]

95 **Tang H**, Jiang D, Zhang S, Zeng Z, Tan L, Hou Y, Wang Q; Zhongshan NCRT-EC working group, Wang H, Zhu J, Shen Y, Yin J, Ge D. Residual tumor characteristics of esophageal squamous cell carcinoma after neoadjuvant chemoradiotherapy. *J Thorac Cardiovasc Surg* 2021; **162**: 1632-1641 [PMID: 33268125 DOI: 10.1016/j.jtcvs.2020.09.042]

96 **van Rossum PSN**, Fried DV, Zhang L, Hofstetter WL, Ho L, Meijer GJ, Carter BW, Court LE, Lin SH. The value of (18)F-FDG PET before and after induction chemotherapy for the early prediction of a poor pathologic response to subsequent preoperative chemoradiotherapy in oesophageal adenocarcinoma. *Eur J Nucl Med Mol Imaging* 2017; **44**: 71-80 [PMID: 27511188 DOI: 10.1007/s00259-016-3478-2]

97 **Elimova E**, Wang X, Etchebehere E, Shiozaki H, Shimodaira Y, Wadhwa R, Planjery V, Charalampakis N, Blum MA, Hofstetter W, Lee JH, Weston BR, Bhutani MS, Rogers JE, Maru D, Skinner HD, Macapinlac HA, Ajani JA. 18-fluorodeoxy-glucose positron emission computed tomography as predictive of response after chemoradiation in oesophageal cancer patients. *Eur J Cancer* 2015; **51**: 2545-2552 [PMID: 26321501 DOI: 10.1016/j.ejca.2015.07.044]

98 **Simoni N**, Rossi G, Benetti G, Zuffante M, Micera R, Pavarana M, Guariglia S, Zivelonghi E, Mengardo V, Weindelmayer J, Giacopuzzi S, de Manzoni G, Cavedon C, Mazzarotto R. (18)F-FDG PET/CT Metrics Are Correlated to the Pathological Response in Esophageal Cancer Patients Treated With Induction Chemotherapy Followed by Neoadjuvant Chemo-Radiotherapy. *Front Oncol* 2020; **10**: 599907 [PMID: 33330097 DOI: 10.3389/fonc.2020.599907]

99 **Fan J**, Shen X, Wang Y, Zhou HL, Liu G, Li YL, Xu ZX. Biomarkers for immune checkpoint therapy targeting programmed death 1 and programmed death ligand 1. *Biomed Pharmacother* 2020; **130**: 110621 [PMID: 34321165 DOI: 10.1016/j.biopha.2020.110621]

100 **Shah MA**, Kojima T, Hochhauser D, Enzinger P, Raimbourg J, Hollebecque A, Lordick F, Kim SB, Tajika M, Kim HT, Lockhart AC, Arkenau HT, El-Hajbi F, Gupta M, Pfeiffer P, Liu Q, Lunceford J, Kang SP, Bhagia P, Kato K. Efficacy and Safety of Pembrolizumab for Heavily Pretreated Patients With Advanced, Metastatic Adenocarcinoma or Squamous Cell Carcinoma of the Esophagus: The Phase 2 KEYNOTE-180 Study. *JAMA Oncol* 2019; **5**: 546-550 [PMID: 30570649 DOI: 10.1001/jamaoncol.2018.5441]

101 **Aguiar PN Jr**, De Mello RA, Hall P, Tadokoro H, Lima Lopes G. PD-L1 expression as a predictive biomarker in advanced non-small-cell lung cancer: updated survival data. *Immunotherapy* 2017; **9**: 499-506 [PMID: 28472902 DOI: 10.2217/imt-2016-0150]

102 **Paz-Ares L**, Spira A, Raben D, Planchard D, Cho BC, Özgüroğlu M, Daniel D, Villegas A, Vicente D, Hui R, Murakami S, Spigel D, Senan S, Langer CJ, Perez BA, Boothman AM, Broadhurst H, Wadsworth C, Dennis PA, Antonia SJ, Faivre-Finn C. Outcomes with durvalumab by tumour PD-L1 expression in unresectable, stage III non-small-cell lung cancer in the PACIFIC trial. *Ann Oncol* 2020; **31**: 798-806 [PMID: 32209338 DOI: 10.1016/j.annonc.2020.03.287]

103 **Doroshow DB**, Bhalla S, Beasley MB, Sholl LM, Kerr KM, Gnjatic S, Wistuba II, Rimm DL, Tsao MS, Hirsch FR. PD-L1 as a biomarker of response to immune-checkpoint inhibitors. *Nat Rev Clin Oncol* 2021; **18**: 345-362 [PMID: 33580222 DOI: 10.1038/s41571-021-00473-5]

104 **Yagi T**, Baba Y, Ishimoto T, Iwatsuki M, Miyamoto Y, Yoshida N, Watanabe M, Baba H. PD-L1 Expression, Tumor-infiltrating Lymphocytes, and Clinical Outcome in Patients With Surgically Resected Esophageal Cancer. *Ann Surg* 2019; **269**: 471-478 [PMID: 29206673 DOI: 10.1097/SLA.0000000000002616]

105 **Wakita A**, Motoyama S, Nanjo H, Sato Y, Yoshino K, Sasaki T, Kawakita Y, Liu J, Imai K, Saito H, Minamiya Y. PD-L1 Expression Is a Prognostic Factor in Patients with Thoracic Esophageal Cancer Treated Without Adjuvant Chemotherapy. *Anticancer Res* 2017; **37**: 1433-1441 [PMID: 28314315 DOI: 10.21873/anticanres.11467]

106 **Tamminga M**, de Wit S, Hiltermann TJN, Timens W, Schuuring E, Terstappen LWMM, Groen HJM. Circulating tumor cells in advanced non-small cell lung cancer patients are associated with worse tumor response to checkpoint inhibitors. *J Immunother Cancer* 2019; **7**: 173 [PMID: 31291995 DOI: 10.1186/s40425-019-0649-2]

107 **Lipson EJ**, Velculescu VE, Pritchard TS, Sausen M, Pardoll DM, Topalian SL, Diaz LA Jr. Circulating tumor DNA analysis as a real-time method for monitoring tumor burden in melanoma patients undergoing treatment with immune checkpoint blockade. *J Immunother Cancer* 2014; **2**: 42 [PMID: 25516806 DOI: 10.1186/s40425-014-0042-0]

108 **Pellini B**, Chaudhuri AA. Circulating Tumor DNA Minimal Residual Disease Detection of Non-Small-Cell Lung Cancer Treated With Curative Intent. *J Clin Oncol* 2022; **40**: 567-575 [PMID: 34985936 DOI: 10.1200/JCO.21.01929]

109 **Rosner S**, Reuss JE, Zahurak M, Zhang J, Zeng Z, Taube J, Anagnostou V, Smith KN, Riemer J, Illei PB, Broderick SR, Jones DR, Topalian SL, Pardoll DM, Brahmer JR, Chaft JE, Forde PM. Five-Year Clinical Outcomes after Neoadjuvant Nivolumab in Resectable Non-Small Cell Lung Cancer. *Clin Cancer Res* 2023; **29**: 705-710 [PMID: 36794455 DOI: 10.1158/1078-0432.CCR-22-2994]

110 **Xiao BY**, Zhang X, Cao TY, Li DD, Jiang W, Kong LH, Tang JH, Han K, Zhang CZ, Mei WJ, Xiao J, Pan ZZ, Li YF, Zhang XS, Ding PR. Neoadjuvant Immunotherapy Leads to Major Response and Low Recurrence in Localized Mismatch Repair-Deficient Colorectal Cancer. *J Natl Compr Canc Netw* 2023; **21**: 60-66.e5 [PMID: 36630898 DOI: 10.6004/jnccn.2022.7060]

111 **Park SY**, Hong MH, Kim HR, Lee CG, Cho JH, Cho BC, Kim DJ. The feasibility and safety of radical esophagectomy in patients receiving neoadjuvant chemoradiotherapy with pembrolizumab for esophageal squamous cell carcinoma. *J Thorac Dis* 2020; **12**: 6426-6434 [PMID: 33282345 DOI: 10.21037/jtd-20-1088]

112 **Huang B**, Shi H, Gong X, Yu J, Xiao C, Zhou B, Liang Z, Li X. Comparison of efficacy and safety between pembrolizumab combined with chemotherapy and simple chemotherapy in neoadjuvant therapy for esophageal squamous cell carcinoma. *J Gastrointest Oncol* 2021; **12**: 2013-2021 [PMID: 34790369 DOI: 10.21037/jgo-21-610]

113 **Lee S**, Ahn BC, Park SY, Kim DJ, Lee CG, Cho J, Kim JH, Kim HR, Kim YH, Park SR, Chun YJ, Hong MH, Cho B. A phase II trial of preoperative chemoradiotherapy and pembrolizumab for locally advanced esophageal squamous cell carcinoma (ESCC). *Ann Oncol* 2019; **30**: 754 [DOI: 10.1093/annonc/mdz266.018]

114 **Qiao Y**, Zhao C, Li X, Zhao J, Huang Q, Ding Z, Zhang Y, Jiao J, Zhang G, Zhao S. Efficacy and safety of camrelizumab in combination with neoadjuvant chemotherapy for ESCC and its impact on esophagectomy. *Front Immunol* 2022; **13**: 953229 [PMID: 35911723 DOI: 10.3389/fimmu.2022.953229]

115 **Xu WL**, Jiang YH, Wang CC, Wu J, Li JQ, Hu YQ, Lu WS, Shen DJ, Wang YJ, Chen QX. The efficacy and safety of neoadjuvant camrelizumab and chemotherapy for locally advanced thoracic esophageal squamous cell carcinoma. *J Clin Oncol* 2022; **40**: 278 [DOI: 10.1200/JCO.2022.40.4_suppl.278]

116 **Yang G**, Su X, Yang H, Luo G, Gao C, Zheng Y, Xie W, Huang M, Bei T, Bai Y, Wang Z, Cai P, He H, Xiang J, Cai M, Zhang Y, Qu C, Fu J, Liu Q, Hu Y, Zhong J, Huang Y, Guo Q, Zhang X. Neoadjuvant programmed death-1 blockade plus chemotherapy in locally advanced esophageal squamous cell carcinoma. *Ann Transl Med* 2021; **9**: 1254 [PMID: 34532391 DOI: 10.21037/atm-21-3352]

117 **Wang Z**. Neoadjuvant camrelizumab combined with chemotherapy and apatinib for locally advanced thoracic esophageal squamous cell carcinoma (ESCC): A single-arm, open-label, phase Ib study. *J Clin Oncol* 2021; **39**: 4047 [DOI: 10.1200/JCO.2021.39.15_suppl.4047]

118 **Ma JQ**, Zhang JF, Yang YN, Zheng DY, Wang XY, Liang H, Zhang LQ, Xin YZ, Ling XD, Fang CY, Jiang H, Zheng W. Camrelizumab combined with paclitaxel and nedaplatin as neoadjuvant therapy for locally advanced esophageal squamous cell carcinoma (ESPRIT): A phase II, single-arm, exploratory research. *J Clin Oncol* 2021; **39**: e16033 [DOI: 10.1200/JCO.2021.39.15_suppl.e16033]

119 **Wang F**, Yu Q, Meng XG, Fan QX. Camrelizumab in combination with preoperative chemotherapy for locally advanced esophageal squamous cell carcinoma: A single-arm, open-label, phase II study. *J Clin Oncol* 2021; **39**: 222 [DOI: 10.1200/JCO.2021.39.3_suppl.222]

120 **Zhang Y**, Shen GY, Xu RY, Huang GZ, Yang SS, Zheng QF, Huang ZJ, Duan HB, Ma LY, Yang LB, Yi YF, Liu RX, Li KZ, Chen SG. Real-world effectiveness and safety of camrelizumab-based neoadjuvant therapy in resectable esophageal cancer: Initial results of a prospective multicenter observational study. *J Clin Oncol* 2022; **40**: 250 [DOI: 10.1200/JCO.2022.40.4_suppl.250]

121 **Zhang Z**, Ye J, Li H, Gu D, Du M, Ai D, Chen W, Fang Y, Xu X, Bai C, Zhao K, Zhou G. Neoadjuvant sintilimab and chemotherapy in patients with resectable esophageal squamous cell carcinoma: A prospective, single-arm, phase 2 trial. *Front Immunol* 2022; **13**: 1031171 [PMID: 36311804 DOI: 10.3389/fimmu.2022.1031171]

122 **Xing W**, Zhao L, Zheng Y, Liu B, Liu X, Li T, Zhang Y, Ma B, Yang Y, Shang Y, Fu X, Liang G, Yuan D, Qu J, Chai X, Zhang H, Wang Z, Lin H, Liu L, Ren X, Zhang J, Gao Q. The Sequence of Chemotherapy and Toripalimab Might Influence the Efficacy of Neoadjuvant Chemoimmunotherapy in Locally Advanced Esophageal Squamous Cell Cancer-A Phase II Study. *Front Immunol* 2021; **12**: 772450 [PMID: 34938292 DOI: 10.3389/fimmu.2021.772450]

123 **Xing W**, Zhao L, Fu X, Liang G, Zhang Y, Yuan D, Li Z, Gao Q, Zheng Y; written on Henan Cancer Hospital Thoracic Oncology Group (HCHTOG). A phase II, single-centre trial of neoadjuvant toripalimab plus chemotherapy in locally advanced esophageal squamous cell carcinoma. *J Thorac Dis* 2020; **12**: 6861-6867 [PMID: 33282388 DOI: 10.21037/jtd-20-2198]

124 **Liu DL**, Zhang Q, Zhu JH, Qian T, Yin R, Fan ZH, Jiang F, Li HH, Lu JW, Cao GC. Phase-II study of toripalimab combined with neoadjuvant chemotherapy for the treatment of resectable esophageal squamous cell carcinoma. *J Clin Oncol* 2021; **39**: e16029 [DOI: 10.1200/JCO.2021.39.15_suppl.e16029]

125 **Gao L**, Lu J, Zhang P, Hong ZN, Kang M. Toripalimab combined with docetaxel and cisplatin neoadjuvant therapy for locally advanced esophageal squamous cell carcinoma: a single-center, single-arm clinical trial (ESONICT-2). *J Gastrointest Oncol* 2022; **13**: 478-487 [PMID: 35557591 DOI: 10.21037/jgo-22-131]

126 **Jiang N**, Jiang M, Zhu XZ, Ren BH, Zhang JY, Guo Z, Wu YA, Song X, Zhao LJ, Kong C, Cao GC, Qian PD, Zhao Y, Li S, Luo SF. SCALE-1: Safety and efficacy of short course neoadjuvant chemo-radiotherapy plus toripalimab for locally advanced resectable squamous cell carcinoma of esophagus. *J Clin Oncol* 2022; **40**: 4063 [DOI: 10.1200/JCO.2022.40.16_suppl.4063]

127 **Hong ZN**, Zhang Z, Chen Z, Weng K, Peng K, Lin J, Kang M. Safety and feasibility of esophagectomy following combined neoadjuvant immunotherapy and chemotherapy for locally advanced esophageal cancer: a propensity score matching. *Esophagus* 2022; **19**: 224-232 [PMID: 34988773 DOI: 10.1007/s10388-021-00899-x]

128 **Yang Y**, Zhu L, Cheng Y, Liu Z, Cai X, Shao J, Zhang M, Liu J, Sun Y, Li Y, Yi J, Yu B, Jiang H, Chen H, Yang H, Tan L, Li Z. Three-arm phase II trial comparing camrelizumab plus chemotherapy versus camrelizumab plus chemoradiation versus chemoradiation as preoperative treatment for locally advanced esophageal squamous cell carcinoma (NICE-2 Study). *BMC Cancer* 2022; **22**: 506 [PMID: 35524205 DOI: 10.1186/s12885-022-09573-6]

World Journal of Gastroenterology

Submit a Manuscript: https://www.f6publishing.com

World J Gastroenterol 2023 September 14; 29(34): 5038-5053

DOI: 10.3748/wjg.v29.i34.5038

ISSN 1007-9327 (print) ISSN 2219-2840 (online)

ORIGINAL ARTICLE

Basic Study

Suberoylanilide hydroxamic acid upregulates reticulophagy receptor expression and promotes cell death in hepatocellular carcinoma cells

Jia-Yao Li, Tian Tian, Bing Han, Ting Yang, Yi-Xin Guo, Jia-Yu Wu, Yu-Si Chen, Qin Yang, Ru-Jia Xie

Specialty type: Gastroenterology and hepatology

Provenance and peer review: Unsolicited article; Externally peer reviewed.

Peer-review model: Single blind

Peer-review report's scientific quality classification

Grade A (Excellent): A
Grade B (Very good): B
Grade C (Good): C
Grade D (Fair): 0
Grade E (Poor): 0

P-Reviewer: Franci G, Italy; Rizzo A, Italy

Received: March 23, 2023
Peer-review started: March 23, 2023
First decision: June 17, 2023
Revised: July 15, 2023
Accepted: August 15, 2023
Article in press: August 15, 2023
Published online: September 14, 2023

Jia-Yao Li, Bing Han, Ting Yang, Yi-Xin Guo, Jia-Yu Wu, Yu-Si Chen, Qin Yang, Ru-Jia Xie, Guizhou Provincial Key Laboratory of Pathogenesis and Drug Research on Common Chronic Diseases, College of Basic Medical Sciences, Guizhou Medical University, Guiyang 550025, Guizhou Province, China

Jia-Yao Li, Bing Han, Ting Yang, Yi-Xin Guo, Jia-Yu Wu, Yu-Si Chen, Qin Yang, Ru-Jia Xie, Department of Pathophysiology, College of Basic Medical Sciences, Guizhou Medical University, Guiyang 550025, Guizhou Province, China

Tian Tian, Department of Eugenic Genetics, Guiyang Maternal and Child Health Care Hospital, Guiyang 550003, Guizhou Province, China

Corresponding author: Ru-Jia Xie, MD, Academic Research, Department of Pathophysiology, College of Basic Medical Sciences, Guizhou Medical University, Dongqing Road, Guiyang 550025, Guizhou Province, China. 592153968@qq.com

Abstract

BACKGROUND

Hepatocellular carcinoma (HCC) is a common clinical condition with a poor prognosis and few effective treatment options. Potent anticancer agents for treating HCC must be identified. Epigenetics plays an essential role in HCC tumorigenesis. Suberoylanilide hydroxamic acid (SAHA), the most common histone deacetylase inhibitor agent, triggers many forms of cell death in HCC. However, the underlying mechanism of action remains unclear. Family with sequence similarity 134 member B (FAM134B)-induced reticulophagy, a selective autophagic pathway, participates in the decision of cell fate and exhibits anti-cancer activity. This study focused on the relationship between FAM134B-induced reticulophagy and SAHA-mediated cell death.

AIM

To elucidate potential roles and underlying molecular mechanisms of reticulophagy in SAHA-induced HCC cell death.

METHODS

The viability, apoptosis, cell cycle, migration, and invasion of SAHA-treated Huh7 and MHCC97L cells were measured. Proteins related to the reticulophagy

pathway, mitochondria-endoplasmic reticulum (ER) contact sites, intrinsic mitochondrial apoptosis, and histone acetylation were quantified using western blotting. ER and lysosome colocalization, and mitochondrial Ca^{2+} levels were characterized *via* confocal microscopy. The level of cell death was evaluated through Hoechst 33342 staining and propidium iodide colocalization. Chromatin immunoprecipitation was used to verify histone H4 lysine-16 acetylation in the *FAM134B* promoter region.

RESULTS

After SAHA treatment, the proliferation of Huh7 and MHCC97L cells was significantly inhibited, and the migration and invasion abilities were greatly blocked *in vitro*. This promoted apoptosis and caused G1 phase cells to increase in a concentration-dependent manner. Following treatment with SAHA, ER-phagy was activated, thereby triggering autophagy-mediated cell death of HCC cells *in vitro*. Western blotting and chromatin immunoprecipitation assays confirmed that SAHA regulated FAM134B expression by enhancing the histone H4 lysine-16 acetylation in the *FAM134B* promoter region. Further, SAHA disturbed the Ca^{2+} homeostasis and upregulated the level of autocrine motility factor receptor and proteins related to mitochondria-endoplasmic reticulum contact sites in HCC cells. Additionally, SAHA decreased the mitochondrial membrane potential levels, thereby accelerating the activation of the reticulophagy-mediated mitochondrial apoptosis pathway and promoting HCC cell death *in vitro*.

CONCLUSION

SAHA stimulates FAM134B-mediated ER-phagy to synergistically enhance the mitochondrial apoptotic pathway, thereby enhancing HCC cell death.

Key Words: Suberoylanilide hydroxamic acid; Histone H4 lysine-16; Reticulophagy; Apoptosis; Autophagic cell death; Hepatocellular carcinoma

Core Tip: Family with sequence similarity 134 member B (FAM134B) is considered to be a tumor suppressor protein that can play a pivotal role in inhibiting hepatocellular carcinoma (HCC) cells. In addition, FAM134B acts as a putative reticulophagy receptor in the regulation of the reticulophagy process. Furthermore, suberoylanilide hydroxamic acid (SAHA) upregulates FAM134B expression in HCC cells and promotes apoptosis and autophagy-mediated cell death. Thus, FAM134B-mediated reticulophagy synergizes with SAHA to induce HCC cell death. Our findings offer novel insights into the mechanism underlying SAHA-induced HCC cell death.

Citation: Li JY, Tian T, Han B, Yang T, Guo YX, Wu JY, Chen YS, Yang Q, Xie RJ. Suberoylanilide hydroxamic acid upregulates reticulophagy receptor expression and promotes cell death in hepatocellular carcinoma cells. *World J Gastroenterol* 2023; 29(34): 5038-5053

URL: https://www.wjgnet.com/1007-9327/full/v29/i34/5038.htm

DOI: https://dx.doi.org/10.3748/wjg.v29.i34.5038

INTRODUCTION

Hepatocellular carcinoma (HCC) represents the most well-known and prevalent primary liver cancer in China. The mortality rates with HCC have consistently increased annually[1]. Immune checkpoint therapies have recently emerged as noteworthy treatments for HCC[2-4]. A considerable proportion of patients, approximately 70% with advanced HCC, fail to derive benefits from immunotherapy[5]. Thus, pursuing more potent anticancer medications to combat HCC must persist. Owing to its high degree of malignancy, poor prognosis, and relatively limited range of treatment strategies, it is necessary to seek more powerful anticancer agents for treating HCC. In the past decade, accumulating evidence has validated the role that epigenetics plays in HCC tumorigenesis[6,7]. Epigenetic regulation changes the transcriptional activity of key genes without altering DNA sequences[8,9].

Epigenetic regulation occurs primarily through DNA methylation, post-translational histone modification, chromatin remodeling, and non-coding RNA-mediated gene silencing[10]. Current therapies targeting epigenetic modifications to cancer mainly include DNA methyltransferases and histone deacetylases (HDACs) as well as microRNAs (miRNAs). Due to the widespread existence of DNA methylation variation in HCC, a variety of corresponding regulators of DNA methyltransferase have been developed[11]. At the same time, miRNAs such as miRNA-148a are used in anti-HCC therapy by combining with oncolytic viruses.

Histone acetylation modification, induced by HDACs and histone acetyltransferases, is a prominent mode of epigenetic regulation[12]. The histone acetylation/deacetylation balance is dynamically regulated to maintain global chromatin structure[13]. Therefore, any dysregulation may contribute to altered gene expression, leading to pathological conditions, such as HCC. Suberoylanilide hydroxamic acid (SAHA) represents the most typical HDAC inhibitor (HDACi)

and was the first of its kind to be approved for human treatment. So far, SAHA has been found to induce the differentiation of malignant tumor cells and accelerate apoptosis *in vitro* and *in vivo*[14]. According to our previous results, SAHA may act as a potential initiator of endoplasmic reticulum (ER) stress-associated apoptosis in HepG2 hepatoma cells by activating ER stress-related apoptotic pathways[15]. However, it is still unknown whether SAHA utilizes a new mechanism to induce HCC cell death through some different therapeutic targets.

Acetylation of histone H4 lysine 16 (H4K16ac) is important for gene initiation[16]. Recently, researchers have found that H4K16ac is closely associated with autophagy induction and significantly correlated with autophagy regulation. Moreover, deacetylase inhibitors can promote the upregulation of H4K16ac and lead to autophagic death of cancer cells [17]. However, the regulatory mechanism underlying the induction of H4K16ac-mediated reticulophagy is unclear.

Family with sequence similarity 134 member B (*FAM134B*) has been proposed as a cancer suppressor gene[18,19]. Numerous researchers have demonstrated that in colorectal carcinoma, the presence of FAM134B limits the overgrowth and suppresses the proliferation of cancer cells[20,21]. In addition, FAM134B acts as a putative reticulophagy receptor in regulating ER turnover and maintaining calcium homeostasis by remodeling ER[22,23]. Recent findings have also identified that FAM134B-mediated ER-phagy may regulate ER-mitochondrion interaction[24]. As the largest cellular organelle, the ER can interact with mitochondria through multiple contact sites, termed mitochondria-ER contact sites (MERCS).

Many ER-related and mitochondria-related proteins have been discovered at MERCS, including the inositol 1, 4, 5-trisphosphate receptor type 1 (IP3R1)/glucose-regulated protein 75 (GRP75)/voltage-dependent anion channel 1 (VDAC1) complex, which is a central component of MERCS that contributes to calcium exchange regulation[25,26]. Recent research has suggested that Ca^{2+} deregulation between ER and mitochondria by MERCS led to mitochondrial calcium overload, thereby activating the mitochondria-associated apoptotic pathway[27]. In the present study, we verified that SAHA treatment augmented FAM134B expression and facilitated Huh7 and MHCC97L HCC cell apoptosis; however, the regulatory mechanisms underlying this effect remain unknown. In our study, we elucidated potential roles and underlying molecular mechanisms of reticulophagy in SAHA-induced HCC cell death. Our findings may offer new perspectives for clinical trials of HCC.

MATERIALS AND METHODS

Cell culture and treatments

The human Huh7 and MHCC97L cell lines were derived from the cell bank of the Chinese Academy of Sciences (Shanghai, China). Both cell lines were cultivated at 37 °C in a 5% CO_2-supplemented atmosphere and maintained in high-glucose Dulbecco's modified Eagle's medium (ESscience, Shanghai, China) supplemented with 10% fetal bovine serum (Gibco, Grand Island, NY, United States) and 1% penicillin-streptomycin (BioInd, Beit-Haemek, Israel). SAHA (Abcam, Cambridge, United Kingdom) was dissolved in dimethyl sulfoxide as a 5 mmol/L stock solution and then diluted with the complete medium to achieve ultimate concentrations of 0-24 μmol/L. Both cell lines were exposed to SAHA or vehicle treated with 0.1% dimethyl sulfoxide.

Cell counting kit-8 assay

Cell counting kit-8 (CCK-8) assay was applied to evaluate the anti-proliferative effects of SAHA. Briefly, MHCC97L and Huh7 cells (5×10^3) were plated onto 96-well plates and given 24 h to adhere before being treated with SAHA. The cells were then exposed to various doses of SAHA (0, 0.5, 1, 3, 6, 9, 12, 18, and 24 μmol/L) for 48 h. Subsequently, 10 μL CCK-8 reagent (Solarbio, Beijing, China) was added to each well and incubated for 4 h. Absorbance at 450 nm was recorded using a spectrophotometer (BioRad, Hercules, United States). The IC_{50} of SAHA was calculated using GraphPad Prism software (v9.0.0, GraphPad Software, La Jolla, CA, United States).

Flow cytometry

The data regarding the apoptosis and cell cycle of HCC cells treated with 0, 1, 3, 6, and 12 μmol/L SAHA were obtained *via* standard flow cytometry (NovoCyte, Agilent, Santa Clara, CA, United States). The apoptosis assay was carried out using a cellular apoptosis detection kit (KeyGEN BioTECH, Nanjing, China) following the manufacturer's protocol. Briefly, Huh7 and MHCC97L cells were plated onto 6-well plates at 1×10^5 cells per well before adding SAHA solution. Then, each group of cells was harvested, rinsed with chilled phosphate buffered saline (PBS), and loaded with binding buffer. The cells were labelled with Annexin V-FITC/propidium iodide (PI) solution, and the stained cells were calculated using the flow cytometer. Similarly, cell cycle analysis was conducted using the flow cytometer following the manufacturer's instructions. Each group of cells was collected and washed thrice with chilled PBS. The cells were fixed with 70% ethanol and stained with PI/RNase I solution (KeyGEN BioTECH), and the percentages of cells in the G1, S, and G2 stages were measured using the flow cytometer. The inbuilt software NovoExpress® 1.4.1 was used for statistical analysis.

Wound healing assay

The wound healing assay was monitored to evaluate the effect of SAHA on HCC cell migration. Briefly, Huh7 and MHCC97L cells (3×10^4) were planted onto 6-well plates, grown until they formed an optically confluent monolayer, and then wounded with a sterile 200 μL micropipette tip. Upon treatment with 0 μmol/L or 3 μmol/L SAHA for 48 h, HCC cells were photographed using a microscope (× 40).

Transwell assay

The cell invasion and migration assay *in vitro* was carried out using 24 transwell plates divided into upper and lower chambers using sterile polycarbonate with 8 μm pore size (Corning Life Science, Corning, NY, United States). The sterile polycarbonate covered 200 μL Matrigel (BD Biosciences, San Jose, CA, United States) in the cell invasion assay but not in the cell migration assay. Upon treatment with 0 μmol/L or 3 μmol/L SAHA for 48 h, cells that passed through the pore were stained with crystal violet, photographed, and quantified.

Western blot analysis

Huh7 and MHCC97L cells were exposed to 0, 1, 3, 6, and 12 μmol/L SAHA for 48 h. Then, the cells were rinsed with pre-chilled PBS, lysed in 100 μL RIPA lysis buffer with protease inhibitor (Solarbio), and collected with cell scrapers. Protein samples were boiled for 5 min, and total protein extracts were subjected to standard sodium-dodecyl sulfate gel electrophoresis and subsequently removed to polyvinylidene difluoride membranes (Merck Millipore, Burlington, MA, United States). The membranes were blocked with rapid blocking solution and stained overnight with the corresponding primary antibodies, including FAM134B (Proteintech; Wuhan, China 1:1500), CCPG1 (Proteintech; 1:1500), LC3 (Abcam; 1:2000), ATG12 (Cell Signaling Technology; Danvers, MA, United States 1:1500), H4 (Proteintech; 1:2000), total acH4 (Proteintech; 1:2000), H3K27ac (Cell Signaling Technology; 1:6000), H4K5ac (Cell Signaling Technology; 1:6000), H4K12ac (Cell Signaling Technology; 1:6000), H4K16ac (Abcam; 1:10000), GRP75 (Abcam; 1:2000), VDAC1 (Abcam; 1:2000), IP3R (Abcam; 1:1000), autocrine motility factor receptor (AMFR) (Proteintech; 1:500), cyt c (Cell Signaling Technology; 1:1500), cleaved caspase-3 (Cell Signaling Technology; 1:1500), Bax (Cell Signaling Technology; 1:1500), Bcl-2 (Cell Signaling Technology; 1;1500), and β-actin (Abcam; 1:1000), followed by incubation with the corresponding secondary antibodies (1:8000). Polyvinylidene fluoride membranes carrying proteins were treated with enhanced chemiluminescence reagent (Solarbio), and ImageLab software was used to observe the protein bands.

Live imaging of the ER and lysosomes

ER-trackers and Lyso-trackers (Beyotime; Nanjing, China), the specific organelle dyes, were applied to stain and locate ER and lysosomes, respectively. Huh7 and MHCC97L cells were exposed to 0, 1, 3, 6, and 12 μmol/L SAHA for 48 h. Then, the cells were coincubated with the two tracking dyes at 37 °C for 45 min and rinsed thrice with PBS. The stained cells were viewed at × 200 magnification under a confocal microscope (Olympus, Tokyo, Japan) and immediately imaged.

Hoechst 33342/PI double chromatin staining assay

Huh7 and MHCC97L cells (3×10^4) were seeded in confocal laser Petri dishes. The cells were pretreated with 0.5 nmol/L bafilomycin A1 (MedChemexpress, NJ, United States) for 12 h and then exposed with 12 μmol/L SAHA for 48 h. Subsequently, Hoechst 33342/PI double fluorescent chromatin staining assay was conducted using a Viastain™ Hoechst 33342/PI viability kit (Beyotime). Cells were stained with Hoechst 33342 and PI for 30 min at 25 °C in the dark. The labelled cells were observed with a confocal microscope under × 400 magnification.

Mitochondrial calcium labeling

Rhod-2 AM Red (Abcam), a specific Ca^{2+} indicator, was applied to detect the level of mitochondrial Ca^{2+}. Huh7 and MHCC97L cells were exposed to 0, 1, 3, 6, and 12 μmol/L SAHA for 48 h and rinsed thrice with Hank's balanced salt solution. The treated cells were labelled with a mixture of Mito-Tracker Green (Beyotime) and Rhod-2 AM Red (Beyotime) and incubated for 50 min. The labelled cells were observed with a confocal microscope under × 400 magnification.

Chromatin immunoprecipitation

Chromatin immunoprecipitation (ChIP) assay of Huh7 cells was conducted as described previously[28]. Huh7 cells treated with 0 μmol/L or 6 μmol/L SAHA were subjected to ChIP assay using a ChIP Kit (Thermo Fisher Scientific, Waltham, MA, United States). In brief, the Huh7 cells were cross-linked with 1% formaldehyde and lysed with sodium-dodecyl sulfate lysis buffer. The lysate was sonicated and centrifuged (9000 × g/min) to harvest chromatin fragments (200-1000 bp). Immunoprecipitation was conducted with the following antibodies: anti-H4K16ac (1:50); rabbit IgG (1:50); and anti-RNA polymerase II (1:50). A no-antibody sample was used as input control. Input DNA and ChIP DNA were detected *via* quantitative polymerase chain reaction.

JC-1 fluorescence mitochondrial imaging

The JC-1 fluorescence mitochondrial imaging technique was applied to examine the mitochondrial membrane potential of HCC cells treated with 0, 1, 3, 6, and 12 μmol/L SAHA. Briefly, Huh7 and MHCC97L cells (1×10^5) were plated onto 6-well plates before adding SAHA solution and incubated with JC-1 fluorescence solution in an incubator for 20 min. Analysis was performed using a flow cytometer.

Statistical analysis

Data were processed and analyzed, and experimental graphs were prepared using GraphPad Prism software. All experiments were conducted in biological triplicate. All data are shown as means ± standard deviation. One-way analysis of variance was conducted for multigroup comparisons. *P* values less than 0.05 were considered to indicate significance.

RESULTS

SAHA suppressed the overgrowth of HCC cells by inducing G1 phase arrest and apoptosis in vitro

In our previous study, we confirmed that SAHA suppressed the overgrowth of HepG2 cells and mediated apoptosis by promoting the ER stress-associated apoptotic pathway[15]. However, this was not demonstrated in Huh7 and MHCC97L cells. As presented in Figure 1A, HCC cell growth was notably suppressed in SAHA-treated cells; the semi-lethal dose was 12 μmol/L. Apoptosis in Huh7 and MHCC97L cells was determined using flow cytometry with different SAHA concentrations. Consistent with previous studies, SAHA induced apoptosis in Huh7 and MHCC97L cells (Figures 1B and C). The percentage of specific cell populations that were early apoptotic and late apoptotic throughout the apoptotic stage is shown in Figure 1C. In addition, cell cycle assay results showed that an increasing number of cells were blocked in the G1 phase (Figures 1D-F).

SAHA suppressed the migration and invasion of HCC cells

Both Huh7 and MHCC97L cells were tested under various treatment conditions (0 μmol/L or 3 μmol/L SAHA) to assess their ability to cross a membrane from low to high nutrient solution *in vitro*. Serum was used as an inducer, mimicking the process of tumor cell invasion into adjacent tissues *in vivo*. Cells invading through the semiporous membrane into the underlying medium containing a high serum concentration were photographed under an optical microscope (Figures 2A and B) and quantitatively analyzed (Figures 2C and D). The model cells were compared with the control sample, which was assumed to represent 100% invasion without any treatment. Huh7 and MHCC97L cells showed 78% and 68% lower migration and 44% and 30% lower invasion following treatment with 3 μmol/L SAHA, respectively. Further wound-healing tests were used to verify how cancer cells interact and move. The results showed a gradual decrease in cell migration distance after SAHA treatment (Figure 2E). Overall, SAHA resulted in reduced cell invasion and migration in HCC cells.

SAHA enhanced the level of ER-phagy and augmented autophagy-mediated cell death in HCC cells

The effect of SAHA on FAM134B-mediated ER-phagy was assessed using western blotting. In HCC cells, SAHA increases the expression of proteins linked to the reticulophagy-related signaling pathway. We found increases in the expression of FAM134B, CCPG1, and autophagy-related protein Atg12 and the LC3-II/LC3-I ratio (Figures 3A-C). In the process of reticulophagy, ER fragments were delivered to lysosomes for final degradation. To detect the final state of ER autophagic lysosome formation, we used organelle markers that could trace the ER and lysosomes to detect the colocalization of both. We found that colocalization coverage of the ER and lysosomes increased in Huh7 and MHCC97L cells under SAHA treatment (Figure 3D). The above results suggested that SAHA could enhance the level of ER-phagy in HCC cells.

Previous research has reported that appropriate autophagy is a protective response under cellular stress conditions, but uncontrolled autophagy leads to autophagy-mediated cell death[29]. To further verify whether autophagic death mode exists in HCC cells under SAHA treatment, Huh7 and MHCC97L cells were pretreated with BafA1, a specific inhibitor of the late phase of autophagy that restrains autophagosomal fusion with lysosomes, 12 h before SAHA treatment. Nuclear double staining with Hoechst 33342 and PI was conducted to observe the level of cell death in the treated cells. The results showed that HCC cells treated with 12 μmol/L SAHA for 48 h after pretreatment with BafA1 exhibited significantly lower cell death rates compared with cells treated with 12 μmol/L SAHA alone, indicating that autophagy-mediated cell death was involved in SAHA-induced HCC cell death (Figure 3E).

SAHA upregulated the level of histone acetylation modification and enhanced H4K16ac in the promoter region of FAM134B in HCC cells

After SAHA treatment, the levels of H3K27ac, total H4ac, H4K5ac, H4K12ac, and H4K16ac in Huh7 and MHCC97L cells were determined using western blotting. We found that various doses of SAHA could upregulate the levels of these proteins (Figures 4A-C). Histone hyperacetylation results in gene transcription activation, and recent findings have shown that H4K16ac is linked to the regulation of autophagy-related genes; therefore, we further focused on the regulatory role of H4K16ac in gene expression. We conducted ChIP assays to confirm whether the regulation of *FAM134B* transcription by SAHA was mediated by H4K16ac upregulation. Our results showed that H4K16ac in the *FAM134B* promoter region was significantly increased in Huh7 cells (Figure 4D).

SAHA disturbed Ca^{2+} homeostasis and upregulated the expression of AMFR and MERCS-related proteins in HCC cells

After SAHA treatment, the level of cytosolic Ca^{2+} in Huh7 and MHCC97L cells was determined using Rhod-2 AM Red staining, and mitochondrial Ca^{2+} was colocalized with Mito-Tracker Green and Rhod-2 AM Red. The results showed that SAHA markedly elevated cytosolic and mitochondrial Ca^{2+} levels (Figures 5A and B). Classical papers reported that increased cytosolic Ca^{2+} could increase the expression of AMFR, which targets the outer mitochondrial membrane (OMM) for ubiquitination and degradation[30-32]. We evaluated the protein level of AMFR in Huh7 and MHCC97L cells and found that SAHA could considerably increase AMFR protein levels. The IP3R-GRP75-VDAC1 complex is one of the most significant components of MERCS, which regulates ER-mitochondrial calcium flux. To determine the altered expression of MERCS in response to SAHA, the levels of IP3R, GRP75, and VDAC1 were examined using protein blots. Similar to our hypothesis, SAHA administration raised the protein levels of the above three proteins relative to the control group (Figures 5C-E). These findings showed that SAHA contributed to calcium buildup in the mitochondria by enhancing the interaction between the ER and mitochondria.

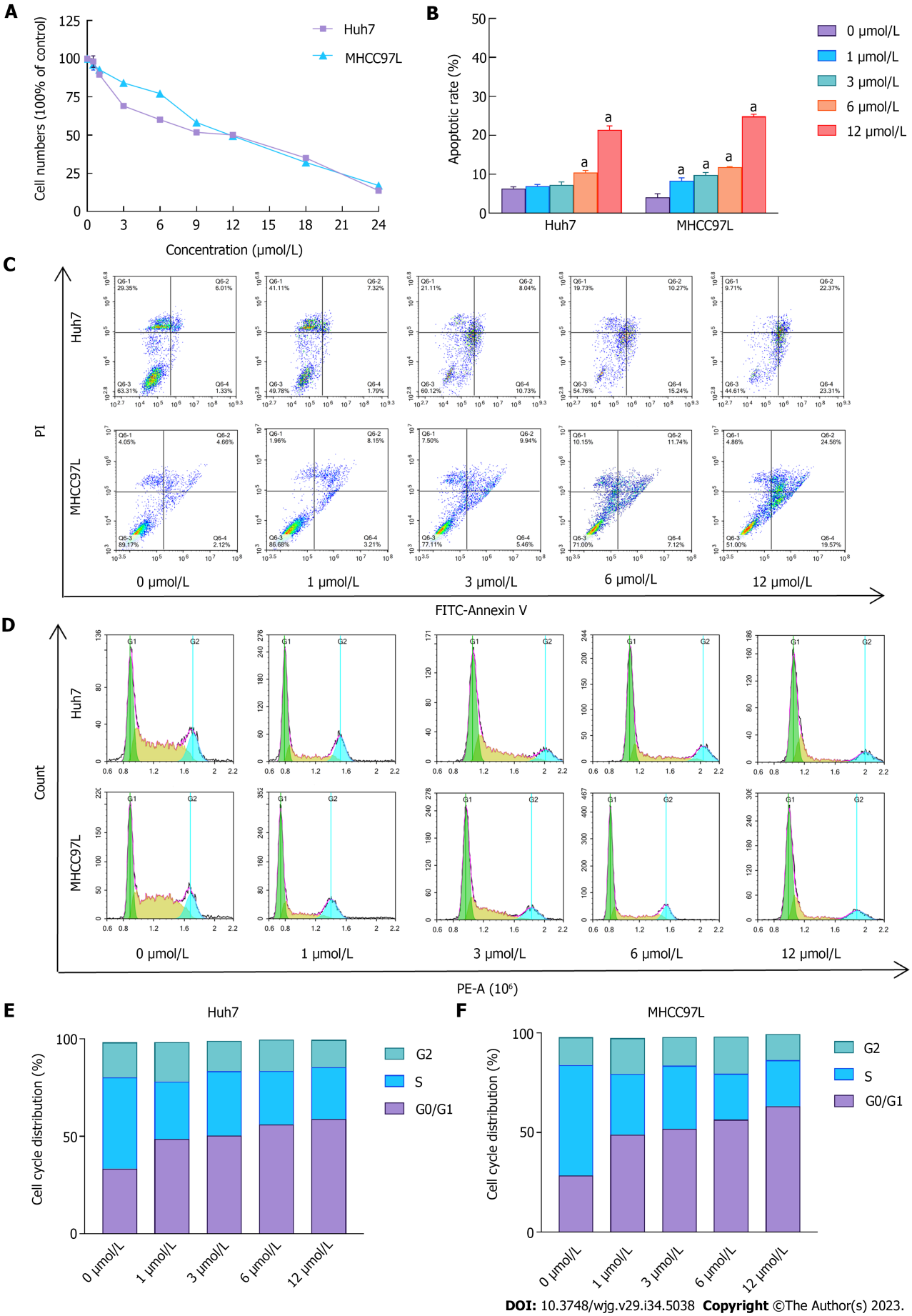

DOI: 10.3748/wjg.v29.i34.5038

Figure 1 Impact of suberoylanilide hydroxamic acid treatment on cell viability, cell cycle dispersion, and cellular apoptosis in Huh7 and

MHCC97L cells. A: Huh7 and MHCC97L cells were treated with 0, 0.5, 1, 3, 6, 9, 12, 18, and 24 μmol/L suberoylanilide hydroxamic acid (SAHA) for 48 h. The proliferation of Huh7 and MHCC97L cells upon SAHA treatment was monitored using a cell counting kit-8 assay; B-F: Huh7 and MHCC97L cells were exposed to 0, 1, 3, 6, and 12 μmol/L SAHA for 48 h. The proportions of apoptotic cells and the cell cycle dispersion were detected using flow cytometer. Experiments were repeated thrice. Representative results from three independent replicate assays are shown. Data are exhibited as mean ± standard deviation. $^{a}P < 0.05$ *vs* 0 μmol/L group (n = 3). PI: Propidium iodide.

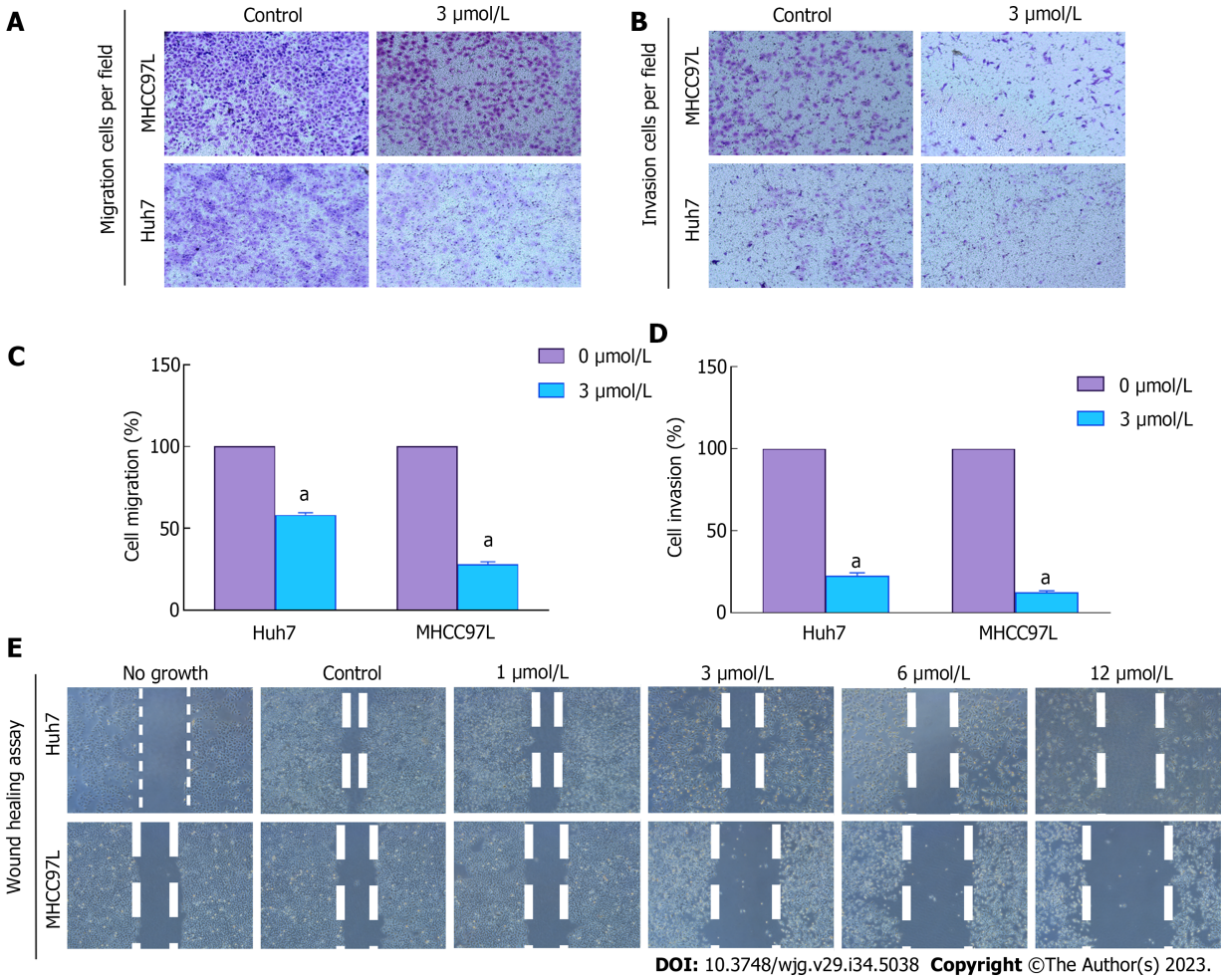

DOI: 10.3748/wjg.v29.i34.5038

Figure 2 Impact of suberoylanilide hydroxamic acid treatment on the migration and invasion of Huh7 and MHCC97L cells. A and B: During experimental verification, the mobile ability of hepatocellular carcinoma cells could not be observed in the 6 μmol/L and 12 μmol/L suberoylanilide hydroxamic acid (SAHA) groups and even the cell growth was directly inhibited. Therefore, we selected 3 μmol/L SAHA to treat Huh7 and MHCC97L cells in a transwell assay. Both cell lines were vehicle-treated with 0.1% dimethyl sulfoxide or exposed to 3 μmol/L SAHA for 48 h. The migration and invasion behavior of cells was evaluated by calculating the cells stained using crystal violet. Representative pictures of invaded hepatocellular carcinoma cells from three independent replicate assays are exhibited; C and D: Statistical graphs; E: In the cell scratch experiment, the space in the middle was artificially divided into regions to observe the motility of Huh7 and MHCC97L cells upon treatment with various doses of SAHA (0, 1, 3, 6, and 12 μmol/L) for 48 h. All cells were observed under an inverted microscope with a 40-fold objective lens. Data are exhibited as mean ± standard deviation. $^{a}P < 0.05$ *vs* control group (n = 3).

SAHA treatment activated the mitochondrial apoptotic pathway by decreasing mitochondrial membrane potential

After SAHA treatment, mitochondrial membrane potential was monitored *via* JC-1 staining. We found that SAHA treatment reduced mitochondrial membrane potential (Figures 6A and B). To investigate the particular SAHA-induced apoptotic processes, the levels of cyt c, caspase-3, and proteins related to the Bcl-2 family were detected using western blotting. The experimental results revealed that SAHA upregulated the expression of cyt c, cleaved caspase-3, and Bax and downregulated the expression of Bcl-2 (Figures 6C-E). These results clearly indicated that the mitochondrial membrane potential was at a lower level, and the mitochondrial apoptotic pathway was activated under the action of SAHA.

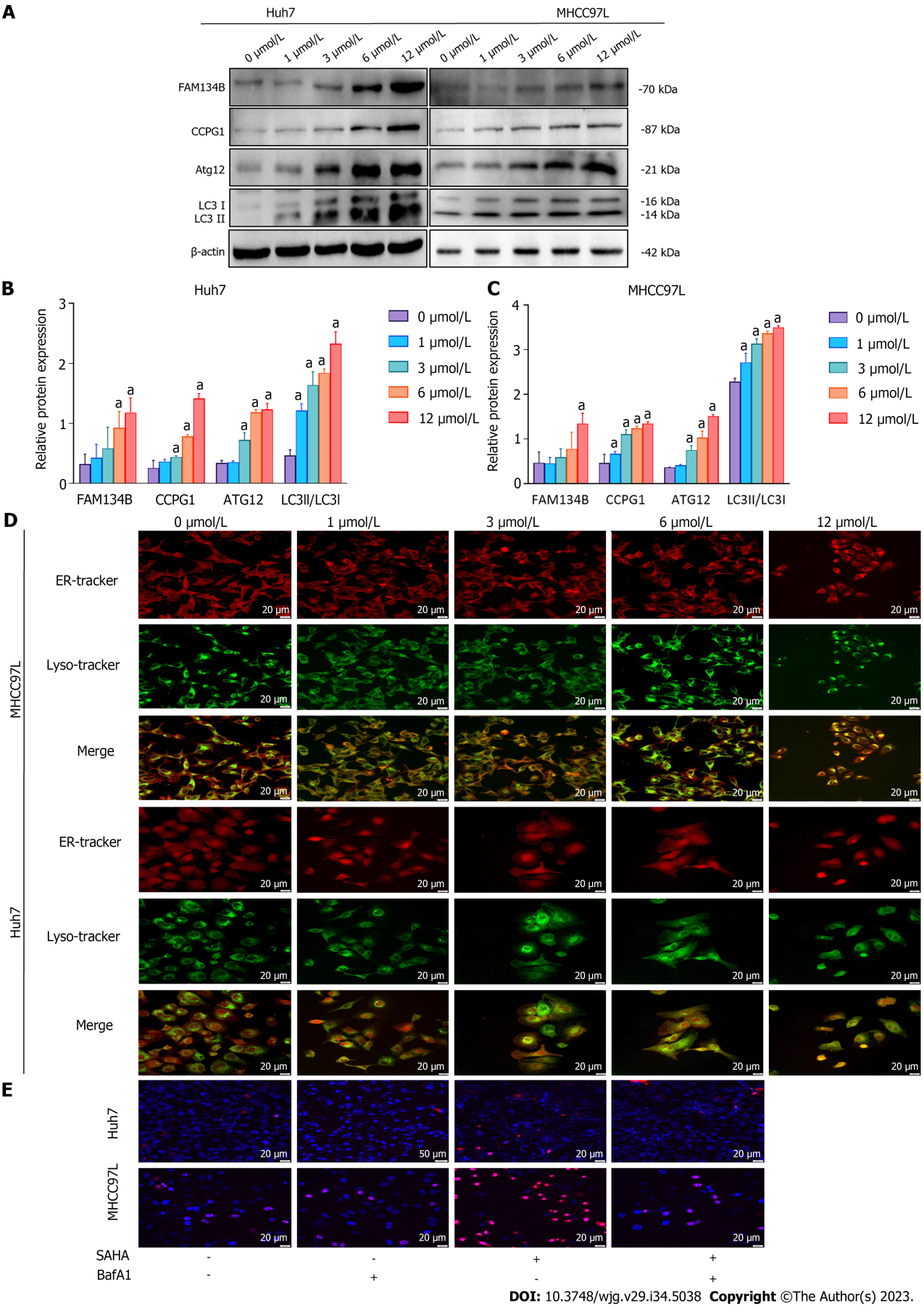

DOI: 10.3748/wjg.v29.i34.5038

Figure 3 Impact of suberoylanilide hydroxamic acid treatment on the level of endoplasmic reticulum-phagy and autophagy-mediated cell death in Huh7 and MHCC97L cells. A-C: Huh7 and MHCC97L cells were exposed to 0, 1, 3, 6, and 12 μmol/L suberoylanilide hydroxamic acid for 48 h.

Proteins related to the reticulophagy pathway were detected using western blotting. Relative protein expression levels were normalized to β-actin; D: The colocalization coverage of the endoplasmic reticulum and lysosomes were observed using a confocal microscope (× 400). Representative pictures from three independent replicate assays are exhibited; E: Huh7 and MHCC97L cells were pretreated with 0.5 nmol/L BafA1 for 12 h, followed by 12 μmol/L suberoylanilide hydroxamic acid treatment for 48 h. Hoechst 33342/propidium iodide (PI) double staining localization assay was utilized to observe nuclear coagulation. After Hoechst 33342/PI double staining, the death rate of hepatocellular carcinoma cells was quantified based on the ratio of pink cells/blue cells. Experiments were repeated thrice. Representative pictures from three independent replicate assays are shown. Data are exhibited as mean ± standard deviation. $^{a}P < 0.05$ *vs* 0 μmol/L group. SAHA: Suberoylanilide hydroxamic acid; ER: Endoplasmic reticulum; FAM134B: Family with sequence similarity 134 member B.

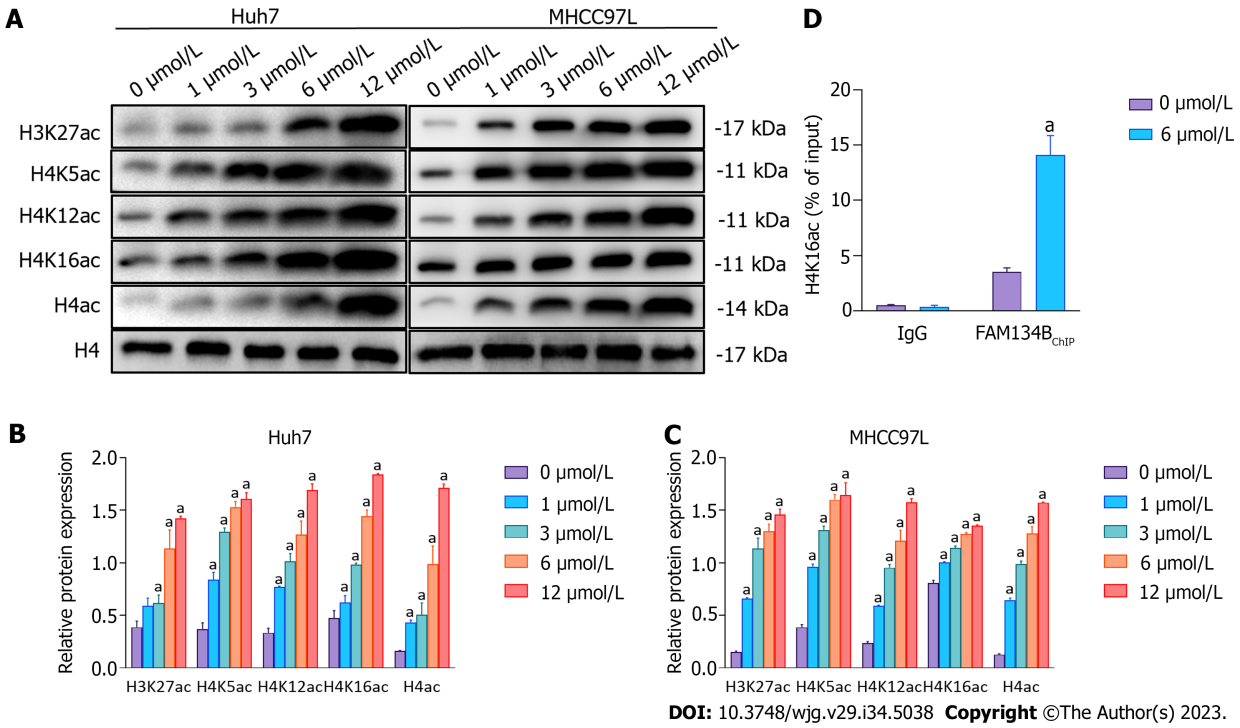

DOI: 10.3748/wjg.v29.i34.5038

Figure 4 Impact of suberoylanilide hydroxamic acid treatment on the levels of histone H4 lysine 16 acetylation in the promoter region of family with sequence similarity 134 member B in Huh7 and MHCC97L cells. A-C: Huh7 and MHCC97L cells were exposed to 0, 1, 3, 6, and 12 μmol/L suberoylanilide hydroxamic acid for 48 h. Relative protein levels of histone H3 lysine 27 acetylation (H3K27ac), total H4ac, H4K5ac, H4K12ac, and H4K16ac were normalized to total histone H4. Representative western blot images from three independent replicate assays are exhibited; D: Huh7 cells were exposed to 0 μmol/L or 6 μmol/L suberoylanilide hydroxamic acid for 48 h. Quantification of the acetylated histone H4K16-related promoter region of family with sequence similarity 134 member B in Huh7 cells was measured using chromatin immunoprecipitation assay and quantitative polymerase chain reaction. Data are exhibited as mean ± standard deviation. $^{a}P < 0.05$ *vs* 0 μmol/L group ($n = 3$). FAM134B: Family with sequence similarity 134 member B; ChIP: Chromatin immunoprecipitation.

DISCUSSION

SAHA, also known as vorinostat, is an HDACi that has shown tumor-suppressive properties in clinical trials[33]. Findings have revealed that SAHA could suppress cell proliferation and accelerate apoptosis in multiple malignant tumor cells. Scholars have demonstrated that SAHA increased the expression of death receptor 5 in liver cancer cells, which led to the initiation of the death receptor-mediated apoptosis pathway[34]. Furthermore, SAHA contributed to the initiation of the mitochondria-related apoptosis pathway by enhancing the protein level of Bim and Bax[35]. Our previous study found that SAHA could initiate the ER stress-related apoptotic pathway to foster apoptosis in liver cancer cells by upregulating the protein level of CHOP, a transcription factor that accelerates proapoptotic gene transcription[15]. In the present study, we found that SAHA suppressed the proliferation and induced cell cycle arrest in Huh7 and MHCC97L cells. Moreover, SAHA initiated Huh7 and MHCC97L cell apoptosis.

We also indicated that SAHA could augment the expression of *FAM134B*, a putative cancer suppressor gene. Studies have uncovered the pivotal role of FAM134B in multiple malignancies. Lee *et al*[20] reported that FAM134B may exert anticancer effects by influencing mitochondrial function and inducing cell cycle arrest in colon cancer. FAM134B also acts as a cancer suppressor in breast carcinoma. Upregulating FAM134B expression was significantly correlated with a higher survival in patients with breast carcinoma[36]. Zhong[37] confirmed that FAM134B was decreased in liver cancer, and its decreased expression was correlated with malignant liver cancer. In contrast, upregulation of FAM134B inhibited HepG2 cell proliferation and enhanced cell apoptosis. FAM134B was proposed as the first discovered mammalian receptor of reticulophagy[38,39], a type of selective phagocytosis. As an ER-anchored protein, FAM134B mediates the sequestration of ER fragments into phagophore membranes through its LC3-interacting region, which binds the autophagy modifier protein LC3[40-42]. In the present study, we detected the proteins related to ER-phagy in Huh7 and MHCC97L cells

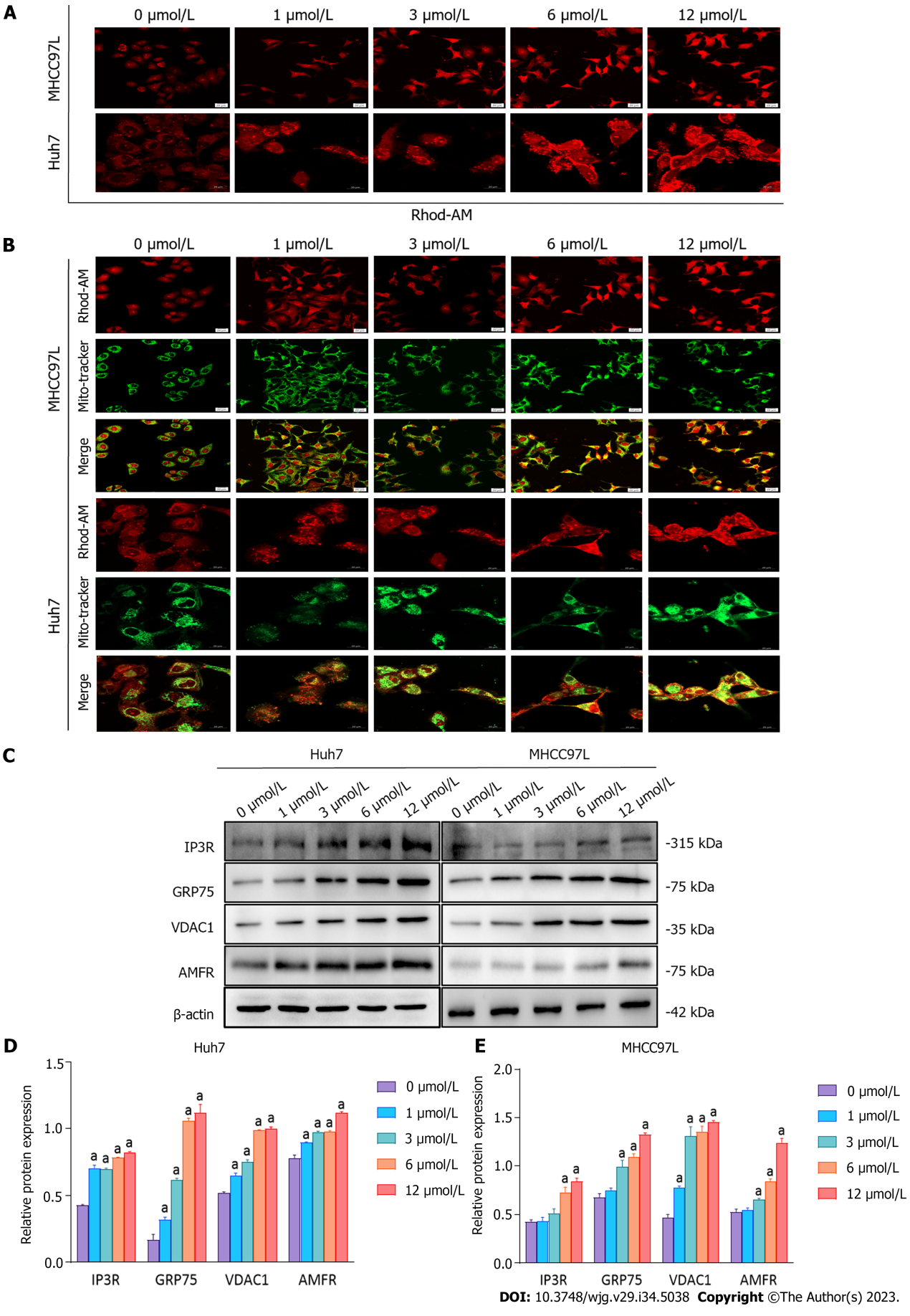

DOI: 10.3748/wjg.v29.i34.5038

Figure 5 Impact of suberoylanilide hydroxamic acid treatment on Ca^{2+} homeostasis and the expression of autocrine motility factor

receptor and proteins related to mitochondria-endoplasmic reticulum contact sites in Huh7 and MHCC97L cells. A: Huh7 and MHCC97L cells were exposed to 0, 1, 3, 6, and 12 μmol/L suberoylanilide hydroxamic acid (SAHA) for 48 h and stained with Rhod-2 AM. The cells were observed under a confocal microscope (× 400 magnification); B: Huh7 and MHCC97L cells were exposed to 0, 1, 3, 6, and 12 μmol/L SAHA for 48 h and simultaneously stained with Mito-Tracker Green and Rhod-2 AM Red. The cells were observed under a confocal microscope (× 400 magnification). The scale is 100 μm; C-E: Representative western blot images showed the expression of inositol 1, 4, 5-trisphosphate receptor type 1, glucose-regulated protein 75, voltage-dependent anion channel 1, and autocrine motility factor receptor in Huh7 and MHCC97L cells treated with SAHA for 48 h. Relative protein expression levels were normalized to β-actin. Data are exhibited as mean ± standard deviation. $^{a}P < 0.05$ *vs* 0 μmol/L group ($n = 3$). AMFR: Autocrine motility factor receptor; IP3R1: Inositol 1, 4, 5-trisphosphate receptor type 1; GRP75: Glucose-regulated protein 75; VDAC1: Voltage-dependent anion channel 1.

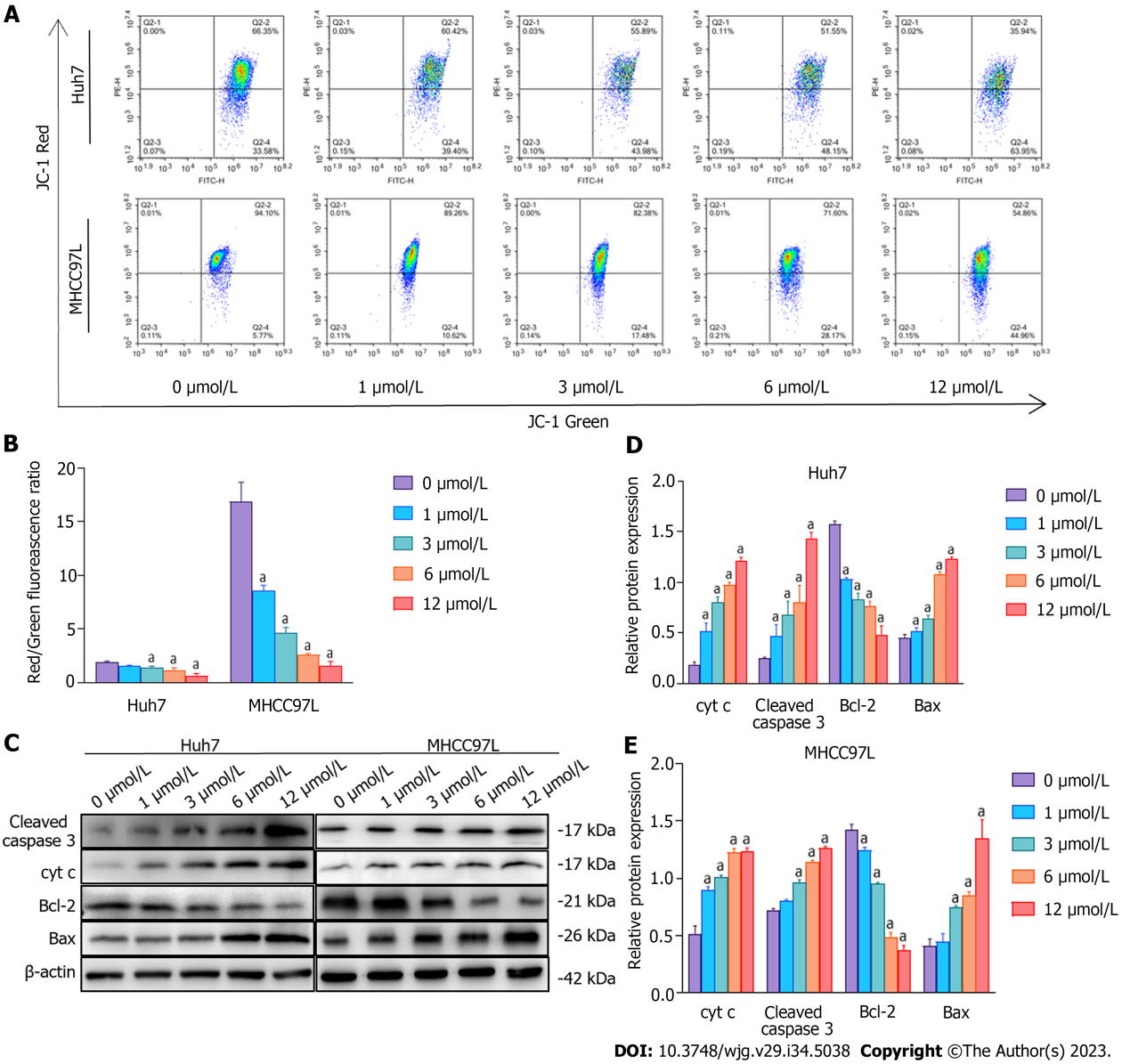

DOI: 10.3748/wjg.v29.i34.5038

Figure 6 The impact of suberoylanilide hydroxamic acid treatment on mitochondrial membrane potential and the expression of proteins related to the mitochondrial apoptotic pathway in Huh7 and MHCC97L cells. A and B: After being treated with 0, 1, 3, 6, and 12 μmol/L suberoylanilide hydroxamic acid for 48 h, the mitochondrial membrane potential in Huh7 and MHCC97L cells was analyzed using flow cytometry with bivariable JC-1 dye (mitochondrial membrane potential probe). Representative pictures from three independent replicate assays are exhibited; C-E: Representative western blot images showed the related protein expression in Huh7 and MHCC97L cells treated with 0, 1, 3, 6, and 12 μmol/L suberoylanilide hydroxamic acid for 48 h. Relative protein expression levels were normalized to β-actin. Data are exhibited as mean ± standard deviation. $^{a}P < 0.05$ *vs* 0 μmol/L group ($n = 3$).

treated with various doses of SAHA. We found that the expression levels of FAM134B, Atg12, and LC3II/LC3I were considerably upregulated. Moreover, SAHA augmented the colocalization of ER and lysosomes in Huh7 and MHCC97L cells. The above results indicated that SAHA treatment enhanced the level of ER-phagy.

ER-phagy is a protective response under cellular stress conditions, but uncontrolled autophagy leads to the depletion of organelles and key proteins, which in turn lead to caspase-independent cell death, also known as autophagy-mediated

cell death[43]. Recent findings have revealed that SAHA could induce autophagy-mediated cell death in malignant tumor cells[44,45]. In fact, a decrease in cell viability detected using CCK-8 was not the same as apoptosis induction, as revealed in this study. We found that 12 μmol/L SAHA resulted in markedly reduced Huh7 and MHCC97L cell proliferation levels (Figure 1), with proliferation being inhibited by approximately 50%; however, the rate of early apoptosis was only about 25%. This phenomenon reveals that SAHA may also elicit other types of cell death to suppress the proliferation of Huh7 and MHCC97L cells, such as autophagy-mediated cell death.

To confirm this hypothesis, we investigated cells with or without pretreatment with BafA1, a specific inhibitor of the late phase of autophagy that restrains autophagosomal fusion with lysosomes. Notably, BafA1-mediated autophagy inhibition reduced SAHA-induced cell death. These results confirmed that SAHA could enhance autophagy-mediated cell death, potentially by promoting FAM134B-mediated ER-phagy. However, the specific mechanism by which SAHA regulated FAM134B expression in Huh7 and MHCC97L cells remains elusive. As an HDACi, the essential role of SAHA is the enhancement of histone acetylation. In previous research, we revealed that SAHA markedly augmented the acetylated histones H4K5 and H4K12 in HepG2 cells[15]. In the present study, SAHA was shown to augment H4K16ac. In addition, Füllgrabe *et al*[17] reported that H4K16ac was linked to altered gene expression, including the modulation of autophagy-related genes; however, it was unclear whether H4K16ac regulated *FAM134B* transcription and its associated ER-phagy. We used ChIP to detect H4K16ac in the *FAM134B* promoter region. Our findings revealed that FAM134B promoter H4K16ac was considerably elevated in Huh7 cells exposed to SAHA, which enhanced the *FAM134B* transcription.

As a key organelle in eukaryotic cells, the ER contributes to protein synthesis and maintenance of calcium homeostasis [46,47]; hence, ER dysfunction results in the agglomeration of protein aggregates and disturbance of calcium homeostasis in the ER. Moreover, the ER contributes to organelle communication[27,48]. For example, the ER can interact with mitochondria through MERCS, as the short distance (15-20 nm) between the ER and OMM enables ER-anchored proteins to interact with OMM proteins[49]. The IP3R1-GRP75-VDAC1 complex is a central component of MERCS, which is involved in regulating calcium flow[50]. Emerging evidence has indicated that the imbalance of Ca^{2+} between the ER and mitochondria by MERCS leads to calcium overload in the mitochondria, which activates the mitochondria-associated apoptotic pathway[51].

Furthermore, under ER stress conditions, increased cytosolic Ca^{2+} would elevate the level of ER E3 ligase AMFR, which targets the OMM for ubiquitination and degradation[32]. High AMFR levels accelerate OMM degradation, which brings the inner mitochondrial membrane closer to the ER, thus promoting interplay between the ER and mitochondria[30]. In the present study, we revealed that SAHA upregulated the expression of MERCS-related proteins, including IP3R1, GRP75, and VDAC1, thereby enhancing the exchange of Ca^{2+} from the ER to the mitochondria, along with mitochondrial Ca^{2+} overload. Additionally, SAHA augmented cytosolic Ca^{2+} and increased AMFR expression, thus decreasing mitochondrial membrane potential and elevating mitochondrial membrane permeability, resulting in the release of proapoptotic proteins. As expected, we found that SAHA upregulated the expression level of mitochondria-dependent apoptotic proteins, including cytochrome c, cleaved caspase-3, and Bax but downregulated the expression of Bcl-2. The above results revealed that SAHA treatment enhanced the interplay between the ER and mitochondria and promoted Ca^{2+} transmission from the ER to the mitochondria, thereby activating the mitochondria-related apoptotic pathway.

This study had a few limitations. Despite the presence of numerous reticulophagy receptors, we focused on only FAM134B in this manuscript. For comprehensive knowledge, our team will verify multiple receptors in subsequent laboratory studies. Knocking down the gene encoding FAM134B could verify if it is a key gene in the pathway leading to HCC death. In this experiment, H4K16ac, a highly relevant acetylation site, was selected for the study. However, SAHA acts as a broad-spectrum deacetylase inhibitor influencing numerous acetylation sites, which need to be further verified in subsequent experiments. Results of this study indicated that SAHA can inhibit the proliferation of liver cancer cells *in vitro*; however, *in vivo* analyses could confirm the consistency of its effectiveness. Basic medical research serves the clinic, and the clinical verification of various aspects is more persuasive. Our study provided basic information that aids ongoing and prospective *in vivo* experiment.

CONCLUSION

The HDACi SAHA initiated apoptosis and autophagy-mediated cell death in Huh7 and MHCC97L cells to exert antitumor activity in HCC. Our results underscore a crucial link between the induction of ER-phagy and H4K16ac-linked *FAM134B* gene expression, which facilitates FAM134B-mediated ER-phagy. Moreover, we presented evidence that suggested that SAHA induced the mitochondria-associated apoptotic pathway in Huh7 and MHCC97L cells by enhancing the interplay between the ER and mitochondria and promoting Ca^{2+} exchange. In summary, SAHA promoted FAM134B-mediated ER-phagy, which acted synergistically with the mitochondrial apoptotic pathway to promote HCC cell death.

ARTICLE HIGHLIGHTS

Research background

Suberoylanilide hydroxamic acid (SAHA) has been demonstrated to trigger multiple forms of cell death in hepatocellular carcinoma (HCC). Family with sequence similarity 134 member B (FAM134B), a reticulophagy receptor, has been

recognized as a cancer suppressor protein in multiple tumors, including HCC. However, few researchers have focused on the relationship between reticulophagy and SAHA-induced HCC cell death.

Research motivation

Reticulophagy is involved in a variety of human cancer pathologies. However, its specific function in the modulation of SAHA-initiated HCC cell death remains unproven.

Research objectives

To validate the potential regulatory mechanisms of the FAM134B-mediated reticulophagy in SAHA-induced HCC cell death.

Research methods

The proliferation, apoptosis, and cell cycle of SAHA-treated Huh7 and MHCC97L cells were quantified using cell counting kit-8 and flow cytometry. The migration and invasion of Huh7 and MHCC97L cells were measured using the transwell assay. Proteins related to the reticulophagy pathway, mitochondria-endoplasmic reticulum contact sites, intrinsic mitochondrial apoptosis, and histone H4K16 acetylation were detected using western blotting. ER and lysosome co-localization, and mitochondrial Ca^{2+} levels were observed *via* confocal microscopy. Autophagy-mediated cell death was validated through Hoechst33342 staining and propidium iodide colocalization. The enrichment of histone H4 lysine 16 acetylation in the *FAM134B* promoter region was determined using chromatin immunoprecipitation.

Research results

SAHA treatment augmented the expression of proteins related to the reticulophagy pathway and enhanced the level of reticulophagy in HCC cells. Chromatin immunoprecipitation experiments confirmed that SAHA regulated FAM134B expression by increasing the histone H4 lysine 16 acetylation in the *FAM134B* promoter region. SAHA interfered with Ca^{2+} homeostasis in HCC cells and upregulated the expression of autocrine motility factor receptor-related and mitochondria-endoplasmic reticulum contact sites-related proteins. Furthermore, SAHA reduced mitochondrial membrane potential and aggravated the activation of the reticulophagy-mediated mitochondrial apoptosis pathway and HCC cell death.

Research conclusions

SAHA stimulated excessive reticulophagy and induced autophagy-mediated cell death, which acted synergistically with the mitochondria-dependent apoptotic pathway to facilitate HCC cell death.

Research perspectives

FAM134B-induced reticulophagy may further provide a novel avenue for more effective interventions in HCC treatment. Our results confirmed that reticulophagy participates in SAHA-induced apoptosis and autophagy-mediated cell death in HCC cells, where SAHA-induced regulation of FAM134B expression *via* histone H4 lysine 16 is the key to HCC cell death.

ACKNOWLEDGEMENTS

The authors thank Mr. Yao Mu and Mrs. Yao Ran from the Guizhou Provincial Key Laboratory of Pathogenesis and Drug Research on Common Chronic Diseases, Guizhou Medical University (Guizhou, China) for their technical advice for using the confocal microscope and flow cytometer.

FOOTNOTES

Author contributions: Xie RJ and Yang Q contributed to the experimental conception and design; Li JY, Tian T, and Han B conducted the experiments; Yang T and Guo YX collected and assembled the experimental data; Li JY, Chen YS, and Wu JY contributed to data analysis and interpretation; Li JY and Xie RJ wrote the article; All authors approved the final manuscript. Li JY, Tian T, and Han B contributed equally to this work.

Supported by the National Natural Science Foundation of China, No. 82260127; Guizhou Provincial Science and Technology Projects, No. Qiankehe Jichu-ZK[2021]365 and Qiankehe Jichu-ZK[2021]364; National Natural Science Foundation Cultivation Project of Guizhou Medical University, No. 20NSP016; Guizhou Provincial Natural Science Foundation, No. [2021]4029 and [2022]4017; and Science and Technology Foundation of Guizhou Provincial Health Commission, No. gzwjkj2019-1-102.

Institutional review board statement: This study did not involve human subjects or living animals.

Conflict-of-interest statement: All the authors report having no relevant conflicts of interest for this article.

Data sharing statement: The data used to support the findings of this study are available from the corresponding author at 592153968@qq.com upon request.

Country/Territory of origin: China

ORCID number: Jia-Yao Li 0000-0003-2880-4978; Tian Tian 0000-0002-1926-2639; Bing Han 0000-0002-9577-293X; Ting Yang 0000-0001-5174-7575; Yi-Xin Guo 0000-0001-6789-8669; Jia-Yu Wu 0009-0000-8578-7778; Yu-Si Chen 0000-0003-2566-8878; Qin Yang 0000-0003-1479-6700; Ru-Jia Xie 0000-0001-5991-2678.

S-Editor: Wang JJ
L-Editor: Filipodia
P-Editor: Cai YX

REFERENCES

1 **Wang W**, Wei C. Advances in the early diagnosis of hepatocellular carcinoma. *Genes Dis* 2020; **7**: 308-319 [PMID: 32884985 DOI: 10.1016/j.gendis.2020.01.014]
2 **Santoni M**, Rizzo A, Kucharz J, Mollica V, Rosellini M, Marchetti A, Tassinari E, Monteiro FSM, Soares A, Molina-Cerrillo J, Grande E, Battelli N, Massari F. Complete remissions following immunotherapy or immuno-oncology combinations in cancer patients: the MOUSEION-03 meta-analysis. *Cancer Immunol Immunother* 2023; **72**: 1365-1379 [PMID: 36633661 DOI: 10.1007/s00262-022-03349-4]
3 **Di Federico A**, Rizzo A, Carloni R, De Giglio A, Bruno R, Ricci D, Brandi G. Atezolizumab-bevacizumab plus Y-90 TARE for the treatment of hepatocellular carcinoma: preclinical rationale and ongoing clinical trials. *Expert Opin Investig Drugs* 2022; **31**: 361-369 [PMID: 34798793 DOI: 10.1080/13543784.2022.2009455]
4 **Rizzo A**, Ricci AD, Brandi G. Atezolizumab in advanced hepatocellular carcinoma: good things come to those who wait. *Immunotherapy* 2021; **13**: 637-644 [PMID: 33820447 DOI: 10.2217/imt-2021-0026]
5 **Rizzo A**, Cusmai A, Gadaleta-Caldarola G, Palmiotti G. Which role for predictors of response to immune checkpoint inhibitors in hepatocellular carcinoma? *Expert Rev Gastroenterol Hepatol* 2022; **16**: 333-339 [PMID: 35403533 DOI: 10.1080/17474124.2022.2064273]
6 **He B**, Dai L, Zhang X, Chen D, Wu J, Feng X, Zhang Y, Xie H, Zhou L, Zheng S. The HDAC Inhibitor Quisinostat (JNJ-26481585) Supresses Hepatocellular Carcinoma alone and Synergistically in Combination with Sorafenib by G0/G1 phase arrest and Apoptosis induction. *Int J Biol Sci* 2018; **14**: 1845-1858 [PMID: 30443188 DOI: 10.7150/ijbs.27661]
7 **Ji H**, Zhou Y, Zhuang X, Zhu Y, Wu Z, Lu Y, Li S, Zeng Y, Lu QR, Huo Y, Shi Y, Bu H. HDAC3 Deficiency Promotes Liver Cancer through a Defect in H3K9ac/H3K9me3 Transition. *Cancer Res* 2019; **79**: 3676-3688 [PMID: 31097476 DOI: 10.1158/0008-5472.CAN-18-3767]
8 **Dawson MA**, Kouzarides T. Cancer epigenetics: from mechanism to therapy. *Cell* 2012; **150**: 12-27 [PMID: 22770212 DOI: 10.1016/j.cell.2012.06.013]
9 **Hogg SJ**, Beavis PA, Dawson MA, Johnstone RW. Targeting the epigenetic regulation of antitumour immunity. *Nat Rev Drug Discov* 2020; **19**: 776-800 [PMID: 32929243 DOI: 10.1038/s41573-020-0077-5]
10 **Chianese A**, Santella B, Ambrosino A, Stelitano D, Rinaldi L, Galdiero M, Zannella C, Franci G. Oncolytic Viruses in Combination Therapeutic Approaches with Epigenetic Modulators: Past, Present, and Future Perspectives. *Cancers (Basel)* 2021; **13** [PMID: 34199429 DOI: 10.3390/cancers13112761]
11 **Zhao P**, Malik S, Xing S. Epigenetic Mechanisms Involved in HCV-Induced Hepatocellular Carcinoma (HCC). *Front Oncol* 2021; **11**: 677926 [PMID: 34336665 DOI: 10.3389/fonc.2021.677926]
12 **Shvedunova M**, Akhtar A. Modulation of cellular processes by histone and non-histone protein acetylation. *Nat Rev Mol Cell Biol* 2022; **23**: 329-349 [PMID: 35042977 DOI: 10.1038/s41580-021-00441-y]
13 **Shen Y**, Wei W, Zhou DX. Histone Acetylation Enzymes Coordinate Metabolism and Gene Expression. *Trends Plant Sci* 2015; **20**: 614-621 [PMID: 26440431 DOI: 10.1016/j.tplants.2015.07.005]
14 **Eckschlager T**, Plch J, Stiborova M, Hrabeta J. Histone Deacetylase Inhibitors as Anticancer Drugs. *Int J Mol Sci* 2017; **18** [PMID: 28671573 DOI: 10.3390/ijms18071414]
15 **Yu L**, Xie R, Tian T, Zheng L, Tang L, Cai S, Ma Z, Yang T, Han B, Yang Q. Suberoylanilide hydroxamic acid upregulates histone acetylation and activates endoplasmic reticulum stress to induce apoptosis in HepG2 liver cancer cells. *Oncol Lett* 2019; **18**: 3537-3544 [PMID: 31516571 DOI: 10.3892/ol.2019.10705]
16 **Samata M**, Alexiadis A, Richard G, Georgiev P, Nuebler J, Kulkarni T, Renschler G, Basilicata MF, Zenk FL, Shvedunova M, Semplicio G, Mirny L, Iovino N, Akhtar A. Intergenerationally Maintained Histone H4 Lysine 16 Acetylation Is Instructive for Future Gene Activation. *Cell* 2020; **182**: 127-144.e23 [PMID: 32502394 DOI: 10.1016/j.cell.2020.05.026]
17 **Füllgrabe J**, Lynch-Day MA, Heldring N, Li W, Struijk RB, Ma Q, Hermanson O, Rosenfeld MG, Klionsky DJ, Joseph B. The histone H4 lysine 16 acetyltransferase hMOF regulates the outcome of autophagy. *Nature* 2013; **500**: 468-471 [PMID: 23863932 DOI: 10.1038/nature12313]
18 **Islam F**, Gopalan V, Lam AK. RETREG1 (FAM134B): A new player in human diseases: 15 years after the discovery in cancer. *J Cell Physiol* 2018; **233**: 4479-4489 [PMID: 29226326 DOI: 10.1002/jcp.26384]
19 **Kasem K**, Sullivan E, Gopalan V, Salajegheh A, Smith RA, Lam AK. JK1 (FAM134B) represses cell migration in colon cancer: a functional study of a novel gene. *Exp Mol Pathol* 2014; **97**: 99-104 [PMID: 24927874 DOI: 10.1016/j.yexmp.2014.06.002]
20 **Lee KT**, Islam F, Vider J, Martin J, Chruścik A, Lu CT, Gopalan V, Lam AK. Overexpression of family with sequence similarity 134, member B (FAM134B) in colon cancers and its tumor suppressive properties in vitro. *Cancer Biol Ther* 2020; **21**: 954-962 [PMID: 32857678 DOI: 10.1080/15384047.2020.1810535]

21 **Islam F**, Chaousis S, Wahab R, Gopalan V, Lam AK. Protein interactions of FAM134B with EB1 and APC/beta-catenin *in vitro* in colon carcinoma. *Mol Carcinog* 2018; **57**: 1480-1491 [PMID: 29964340 DOI: 10.1002/mc.22871]

22 **Jiang X**, Wang X, Ding X, Du M, Li B, Weng X, Zhang J, Li L, Tian R, Zhu Q, Chen S, Wang L, Liu W, Fang L, Neculai D, Sun Q. FAM134B oligomerization drives endoplasmic reticulum membrane scission for ER-phagy. *EMBO J* 2020; **39**: e102608 [PMID: 31930741 DOI: 10.15252/embj.2019102608]

23 **Zhu L**, Wang X, Wang Y. Roles of FAM134B in diseases from the perspectives of organelle membrane morphogenesis and cellular homeostasis. *J Cell Physiol* 2021; **236**: 7242-7255 [PMID: 33843059 DOI: 10.1002/jcp.30377]

24 **Chen W**, Ouyang X, Chen L, Li L. FAM134B-mediated ER-phagy regulates ER-mitochondria interaction through MAMs. *Acta Biochim Biophys Sin (Shanghai)* 2022; **54**: 412-414 [PMID: 35130624 DOI: 10.3724/abbs.2021020]

25 **Bao FX**, Shi HY, Long Q, Yang L, Wu Y, Ying ZF, Qin DJ, Zhang J, Guo YP, Li HM, Liu XG. Mitochondrial Membrane Potential-dependent Endoplasmic Reticulum Fragmentation is an Important Step in Neuritic Degeneration. *CNS Neurosci Ther* 2016; **22**: 648-660 [PMID: 27080255 DOI: 10.1111/cns.12547]

26 **Missiroli S**, Patergnani S, Caroccia N, Pedriali G, Perrone M, Previati M, Wieckowski MR, Giorgi C. Mitochondria-associated membranes (MAMs) and inflammation. *Cell Death Dis* 2018; **9**: 329 [PMID: 29491386 DOI: 10.1038/s41419-017-0027-2]

27 **Sterea AM**, El Hiani Y. The Role of Mitochondrial Calcium Signaling in the Pathophysiology of Cancer Cells. *Adv Exp Med Biol* 2020; **1131**: 747-770 [PMID: 31646533 DOI: 10.1007/978-3-030-12457-1_30]

28 **Liang C**, Xie RJ, Wang JL, Zhang YW, Zhang JY, Yang Q, Han B. Roles of C/EBP-homologous protein and histone H3 lysine 4 methylation in arsenic-induced mitochondrial apoptosis in hepatocytes. *Toxicol Ind Health* 2022; **38**: 745-756 [PMID: 36120900 DOI: 10.1177/07482337221127148]

29 **Denton D**, Kumar S. Autophagy-dependent cell death. *Cell Death Differ* 2019; **26**: 605-616 [PMID: 30568239 DOI: 10.1038/s41418-018-0252-y]

30 **Watanabe H**, Carmi P, Hogan V, Raz T, Silletti S, Nabi IR, Raz A. Purification of human tumor cell autocrine motility factor and molecular cloning of its receptor. *J Biol Chem* 1991; **266**: 13442-13448 [PMID: 1649192]

31 **Mo J**, Chen J, Zhang B. Critical roles of FAM134B in ER-phagy and diseases. *Cell Death Dis* 2020; **11**: 983 [PMID: 33199694 DOI: 10.1038/s41419-020-03195-1]

32 **Joshi V**, Upadhyay A, Kumar A, Mishra A. Gp78 E3 Ubiquitin Ligase: Essential Functions and Contributions in Proteostasis. *Front Cell Neurosci* 2017; **11**: 259 [PMID: 28890687 DOI: 10.3389/fncel.2017.00259]

33 **Park SJ**, Kim SM, Moon JH, Kim JH, Shin JS, Hong SW, Shin YJ, Lee DH, Lee EY, Hwang IY, Kim JE, Kim KP, Hong YS, Lee WK, Choi EK, Lee JS, Jin DH, Kim TW. SAHA, an HDAC inhibitor, overcomes erlotinib resistance in human pancreatic cancer cells by modulating E-cadherin. *Tumour Biol* 2016; **37**: 4323-4330 [PMID: 26493999 DOI: 10.1007/s13277-015-4216-2]

34 **Carlisi D**, Lauricella M, D'Anneo A, Emanuele S, Angileri L, Di Fazio P, Santulli A, Vento R, Tesoriere G. The histone deacetylase inhibitor suberoylanilide hydroxamic acid sensitises human hepatocellular carcinoma cells to TRAIL-induced apoptosis by TRAIL-DISC activation. *Eur J Cancer* 2009; **45**: 2425-2438 [PMID: 19643600 DOI: 10.1016/j.ejca.2009.06.024]

35 **Jiang X**, Tsang YH, Yu Q. c-Myc overexpression sensitizes Bim-mediated Bax activation for apoptosis induced by histone deacetylase inhibitor suberoylanilide hydroxamic acid (SAHA) through regulating Bcl-2/Bcl-xL expression. *Int J Biochem Cell Biol* 2007; **39**: 1016-1025 [PMID: 17331788 DOI: 10.1016/j.biocel.2007.01.024]

36 **Chipurupalli S**, Ganesan R, Martini G, Mele L, Reggio A, Esposito M, Kannan E, Namasivayam V, Grumati P, Desiderio V, Robinson N. Cancer cells adapt FAM134B/BiP mediated ER-phagy to survive hypoxic stress. *Cell Death Dis* 2022; **13**: 357 [PMID: 35436985 DOI: 10.1038/s41419-022-04813-w]

37 **Zhong L**. [The Expression Significance and Function of FAM134B in Hepatocellular Carcinoma Tissue]. 2020

38 **Chino H**, Mizushima N. ER-Phagy: Quality Control and Turnover of Endoplasmic Reticulum. *Trends Cell Biol* 2020; **30**: 384-398 [PMID: 32302550 DOI: 10.1016/j.tcb.2020.02.001]

39 **Grumati P**, Dikic I, Stolz A. ER-phagy at a glance. *J Cell Sci* 2018; **131** [PMID: 30177506 DOI: 10.1242/jcs.217364]

40 **Ferro-Novick S**, Reggiori F, Brodsky JL. ER-Phagy, ER Homeostasis, and ER Quality Control: Implications for Disease. *Trends Biochem Sci* 2021; **46**: 630-639 [PMID: 33509650 DOI: 10.1016/j.tibs.2020.12.013]

41 **Hübner CA**, Dikic I. ER-phagy and human diseases. *Cell Death Differ* 2020; **27**: 833-842 [PMID: 31659280 DOI: 10.1038/s41418-019-0444-0]

42 **Wilkinson S**. ER-phagy: shaping up and destressing the endoplasmic reticulum. *FEBS J* 2019; **286**: 2645-2663 [PMID: 31116513 DOI: 10.1111/febs.14932]

43 **Liao Y**, Duan B, Zhang Y, Zhang X, Xia B. Excessive ER-phagy mediated by the autophagy receptor FAM134B results in ER stress, the unfolded protein response, and cell death in HeLa cells. *J Biol Chem* 2019; **294**: 20009-20023 [PMID: 31748416 DOI: 10.1074/jbc.RA119.008709]

44 **Hrzenjak A**, Kremser ML, Strohmeier B, Moinfar F, Zatloukal K, Denk H. SAHA induces caspase-independent, autophagic cell death of endometrial stromal sarcoma cells by influencing the mTOR pathway. *J Pathol* 2008; **216**: 495-504 [PMID: 18850582 DOI: 10.1002/path.2434]

45 **Lee YJ**, Won AJ, Lee J, Jung JH, Yoon S, Lee BM, Kim HS. Molecular mechanism of SAHA on regulation of autophagic cell death in tamoxifen-resistant MCF-7 breast cancer cells. *Int J Med Sci* 2012; **9**: 881-893 [PMID: 23155362 DOI: 10.7150/ijms.5011]

46 **Kania E**, Pająk B, Orzechowski A. Calcium homeostasis and ER stress in control of autophagy in cancer cells. *Biomed Res Int* 2015; **2015**: 352794 [PMID: 25821797 DOI: 10.1155/2015/352794]

47 **Puzianowska-Kuznicka M**, Kuznicki J. The ER and ageing II: calcium homeostasis. *Ageing Res Rev* 2009; **8**: 160-172 [PMID: 19427411 DOI: 10.1016/j.arr.2009.05.002]

48 **Thoudam T**, Ha CM, Leem J, Chanda D, Park JS, Kim HJ, Jeon JH, Choi YK, Liangpunsakul S, Huh YH, Kwon TH, Park KG, Harris RA, Park KS, Rhee HW, Lee IK. PDK4 Augments ER-Mitochondria Contact to Dampen Skeletal Muscle Insulin Signaling During Obesity. *Diabetes* 2019; **68**: 571-586 [PMID: 30523025 DOI: 10.2337/db18-0363]

49 **Means RE**, Katz SG. Yes, MAM! *Mol Cell Oncol* 2021; **8**: 1919473 [PMID: 34616865 DOI: 10.1080/23723556.2021.1919473]

50 **Zhang SS**, Zhou S, Crowley-McHattan ZJ, Wang RY, Li JP. A Review of the Role of Endo/Sarcoplasmic Reticulum-Mitochondria Ca(2+) Transport in Diseases and Skeletal Muscle Function. *Int J Environ Res Public Health* 2021; **18** [PMID: 33917091 DOI: 10.3390/ijerph18083874]

51 **Xu H**, Guan N, Ren YL, Wei QJ, Tao YH, Yang GS, Liu XY, Bu DF, Zhang Y, Zhu SN. IP(3)R-Grp75-VDAC1-MCU calcium regulation axis

antagonists protect podocytes from apoptosis and decrease proteinuria in an Adriamycin nephropathy rat model. *BMC Nephrol* 2018; **19**: 140 [PMID: 29907098 DOI: 10.1186/s12882-018-0940-3]

World Journal of Gastroenterology

Submit a Manuscript: https://www.f6publishing.com

World J Gastroenterol 2023 September 14; 29(34): 5054-5074

DOI: 10.3748/wjg.v29.i34.5054

ISSN 1007-9327 (print) ISSN 2219-2840 (online)

ORIGINAL ARTICLE

Basic Study

Green tea polyphenols alleviate di-(2-ethylhexyl) phthalate-induced liver injury in mice

Heng Shi, Xin-Hai Zhao, Qin Peng, Xian-Ling Zhou, Si-Si Liu, Chuan-Chuan Sun, Qiu-Yu Cao, Shi-Ping Zhu, Sheng-Yun Sun

Specialty type: Gastroenterology and hepatology

Provenance and peer review: Unsolicited article; Externally peer reviewed.

Peer-review model: Single blind

Peer-review report's scientific quality classification

Grade A (Excellent): 0
Grade B (Very good): B, B
Grade C (Good): 0
Grade D (Fair): 0
Grade E (Poor): 0

P-Reviewer: Kuznietsova H, Ukraine; Scarfi S, Italy

Received: May 16, 2023
Peer-review started: May 16, 2023
First decision: July 10, 2023
Revised: July 19, 2023
Accepted: August 21, 2023
Article in press: August 21, 2023
Published online: September 14, 2023

Heng Shi, Xin-Hai Zhao, Xian-Ling Zhou, Chuan-Chuan Sun, Qiu-Yu Cao, Shi-Ping Zhu, Sheng-Yun Sun, Department of Traditional Chinese Medicine, The First Affiliated Hospital of Jinan University, Guangzhou 522000, Guangdong Province, China

Heng Shi, Qin Peng, Department of Gastroenterology, The Central Hospital of Shaoyang, Shaoyang 422000, Hunan Province, China

Si-Si Liu, Department of Pathology, The Central Hospital of Shaoyang, Shaoyang 422000, Hunan Province, China

Corresponding author: Sheng-Yun Sun, MD, PhD, Chief Doctor, Department of Traditional Chinese Medicine, The First Affiliated Hospital of Jinan University, No. 613 Huangpu Avenue West, Tianhe District, Guangzhou 522000, Guangdong Province, China.
shengyunsun2020@163.com

Abstract

BACKGROUND

Di (2-ethylhexyl) phthalate (DEHP) is a common plasticizer known to cause liver injury. Green tea is reported to exert therapeutic effects on heavy metal exposure-induced organ damage. However, limited studies have examined the therapeutic effects of green tea polyphenols (GTPs) on DEHP-induced liver damage.

AIM

To evaluate the molecular mechanism underlying the therapeutic effects of GTPs on DEHP-induced liver damage.

METHODS

C57BL/6J mice were divided into the following five groups: Control, model [DEHP (1500 mg/kg bodyweight)], treatment [DEHP (1500 mg/kg bodyweight) + GTP (70 mg/kg bodyweight), oil, and GTP (70 mg/kg bodyweight)] groups. After 8 wk, the liver function, blood lipid profile, and liver histopathology were examined. Differentially expressed micro RNAs (miRNAs) and mRNAs in the liver tissues were examined using high-throughput sequencing. Additionally, functional enrichment analysis and immune infiltration prediction were performed. The miRNA-mRNA regulatory axis was elucidated using the starBase database. Protein expression was evaluated using immunohistochemistry.

RESULTS

GTPs alleviated DHEP-induced liver dysfunction, blood lipid dysregulation, fatty liver disease, liver fibrosis, and mitochondrial and endoplasmic reticulum lesions in mice. The infiltration of macrophages, mast cells, and natural killer cells varied between the model and treatment groups. mmu-miR-141-3p (a differentially expressed miRNA), *Zcchc24* (a differentially expressed mRNA), and Zcchc24 (a differentially expressed protein) constituted the miRNA-mRNA-protein regulatory axis involved in mediating the therapeutic effects of GTPs on DEHP-induced liver damage in mice.

CONCLUSION

This study demonstrated that GTPs mitigate DEHP-induced liver dysfunction, blood lipid dysregulation, fatty liver disease, and partial liver fibrosis, and regulate immune cell infiltration. Additionally, an important miRNA-mRNA-protein molecular regulatory axis involved in mediating the therapeutic effects of GTPs on DEHP-induced liver damage was elucidated.

Key Words: Green tea polyphenols; Di(2-ethylhexyl) phthalate; Liver fibrosis; Fatty liver disease; Mitochondria; Immune

Core Tip: Green tea polyphenols (GTPs) alleviated Di (2-ethylhexyl) phthalate (DEHP)-induced liver dysfunction, blood lipid dysregulation, fatty liver disease, liver fibrosis, and mitochondrial and endoplasmic reticulum lesions in mice. The infiltration of macrophages, mast cell, and natural killer cells varied between the model and treatment groups. mmu-miR-141-3p (a differentially expressed miRNA), *Zcchc24* (a differentially expressed mRNA), and Zcchc24 (a differentially expressed protein) constituted the miRNA-mRNA-protein regulatory axis involved in mediating the therapeutic effects of GTPs on DEHP-induced liver damage in mice.

Citation: Shi H, Zhao XH, Peng Q, Zhou XL, Liu SS, Sun CC, Cao QY, Zhu SP, Sun SY. Green tea polyphenols alleviate di-(2-ethylhexyl) phthalate-induced liver injury in mice. *World J Gastroenterol* 2023; 29(34): 5054-5074
URL: https://www.wjgnet.com/1007-9327/full/v29/i34/5054.htm
DOI: https://dx.doi.org/10.3748/wjg.v29.i34.5054

INTRODUCTION

Di (2-ethylhexyl) phthalate (DEHP), which is the most widely used representative phthalic acid ester, can non-covalently bind to polyolefin plastics and predominantly serves as a plasticizer, increasing the flexibility, transparency, durability, and longevity of plastics. Additionally, DEHP is extensively detected in various daily-life products (including baby toys, food packaging, and cosmetics) and several surgical and medical devices[1]. Furthermore, DEHP can be continuously released into the environment (air, soil, water, food, *etc.*), enter living organisms *via* ingestion, inhalation, or skin contact, and subsequently exert toxic effects on health[2]. A previous study reported that DEHP and its metabolites were detected in 100% of tested human urine samples, indicating persistent exposure to DEHP[3]. The DEHP exposure range of the general population is estimated to be 5.8-19 μg/kg/d, while DEHP exposure in medical environments may exceed 167.9 mg/d[4]. The development of modern chemical agriculture has increased the severity of DEHP pollution. DEHP exposure in the Pearl River Delta region of Guangdong Province, China, can reach up to 61 μg/kg/d, which is higher than the tolerable intake of DEHP[5]. Additionally, DEHP undergoes rapid degradation upon ingestion in humans. According to the United States Environmental Protection Agency, the average half-life of DEHP in the human body is 12 h. DEHP and its active metabolite mono-(2-ethylhexyl) phthalate have been detected in various human tissues, including the liver, blood, placenta, amniotic fluid, and early-pregnancy chorionic villus sample[6]. Therefore, evaluating the effect of DEHP on the environment and human health has piqued the interest of the scientific community.

The liver, an important organ involved in the synthesis, metabolism, and detoxification processes, is highly susceptible to acute or chronic damage induced by various drugs[7]. Recent studies have demonstrated that DEHP adversely affects multiple systems in the body. In particular, epidemiological and animal studies have demonstrated the hepatoxicity of DEHP[8]. The mechanism underlying the hepatotoxic effects of DEHP mainly involves oxidative stress, cell apoptosis, and signaling pathway activation. DEHP induces apoptosis in healthy human liver cells through the mitochondrial signaling pathway and/or the caspase-mediated death receptor pathway[9]. Additionally, DEHP may adversely affect gap junctional intercellular communication, peroxisome beta-oxidation activity, and DNA replication synthesis, leading to the formation of liver tumors[10]. Currently, the most extensively studied mechanism of DEHP-induced liver damage is oxidative stress in which the regulation of reactive oxygen species (ROS) production plays a critical role[11]. Excessive ROS production leads to peroxidation of the polyunsaturated fatty acids in the cell membrane. DEHP promotes lipid peroxidation in the liver, primarily through the downregulation of superoxide dismutase and catalase activity and the upregulation of malondialdehyde (MDA) concentrations[12]. Additionally, DEHP mediates the pathogenesis of non-alcoholic fatty liver disease in a high-fat diet-fed animal model by promoting lipid peroxidation[8].

Green tea is the second most widely consumed beverage worldwide after water[13]. The harvested tea leaves are steamed at high temperatures to inactivate the polyphenol oxidase in green tea, preserving most of the vitamins in tea leaves. Thus, green tea exhibits enhanced antioxidant activity. Epidemiological and clinical studies have reported that phenol compounds in tea extracts, such as green tea polyphenols (GTPs), exert a wide range of beneficial effects on human health, including anti-aging, neuroprotective[14], and therapeutic or preventive effects on various diseases, such as cancer[15], cardiovascular disease[16], and obesity[17]. Moreover, GTPs mitigate the adverse effects of poisoning with various heavy metals[18]. However, limited studies have examined the therapeutic effects of GTPs on DEHP-induced liver diseases.

Micro RNAs (miRNAs), a class of endogenous non-coding small RNAs encoded by mRNA, regulate gene expression by modulating mRNA stability. Several miRNAs are reported to play important roles in the pathogenesis of liver fibrosis [19], cirrhosis[20], and hepatocellular carcinoma[21]. Some miRNAs are diagnostic markers for drug-induced liver injury [22]. This study aimed to identify key protein nodes that may affect the expression level of miRNAs in the regulatory network of miRNA and target genes by analyzing the miRNA regulation network. Hence, this study will provide a theoretical basis for future studies on the functions and regulatory mechanisms underlying the therapeutic effects of GTPs on DEHP exposure-induced liver damage.

MATERIALS AND METHODS

Regents

DEHP was purchased from Shanghai Aladdin Biochemical Technology Co., Ltd. (Shanghai, China). GTPs were purchased from Shanghai Yuanye Bio-Technology Co., Ltd. (Shanghai, China). Corn oil was purchased from Hebei Pin Research Biotechnology Co., Ltd. (Baoding, China). Anti-ZCCHC24 antibodies were purchased from Biorbyt Ltd. (Cambridge, United Kingdom).

Animal experiments

Animal experiments were performed at the specific pathogen-free grade animal laboratory of the Medical College of Jinan University. C57BL/6J mice (n = 50) were purchased from Guangdong Yaokang Biotechnology Co., Ltd. And allowed to acclimatize to the laboratory environment for 1 wk. The animals were maintained under the following conditions: Room temperature, 20 ℃-24 ℃; relative humidity, 50%-65%; circadian cycle, 12-h light-dark cycle; access to food and water, ad libitum; diet, regular mouse chow. This study was approved by the Institutional Animal Care and Use Committee of Jinan University (ethics approval number: IACUC-20210630-15). All experimental procedures were performed according to the regulations established by the ethical committee.

Previous studies[23,24] have reported that DEHP is soluble in corn oil. Hence, this study used corn oil as the solvent for DEHP. After 1 wk of acclimatization, 50 mice were randomly assigned into the following five groups (10 mice/group): Control group, administered with 0.2 mL distilled water; model group, administered with 0.2 mL corn oil and DEHP (1500 mg/kg bodyweight); treatment group, administered with 0.2 mL corn oil and DEHP (1500 mg/kg bodyweight), followed by administration of 0.2 mL GTPs (70 mg/kg bodyweight) after 1 h; oil group, administered with 0.2 mL corn oil; GTP group, administered with 0.2 mL GTP (70 mg/kg bodyweight). Based on our previous study, DEHP [25] and GTPs[26] were gavaged. The doses were adjusted weekly based on the bodyweight of the mice. The mice were subjected to daily gavage for 8 wk. At the end of the experimental period, the blood and liver samples were obtained under anesthesia after the mice were allowed to fast overnight. Liver index = (liver weight/bodyweight) × 100%.

Evaluation of liver function and blood lipid profile

The blood from mice was collected using the retro-orbital venous plexus method. Next, the whole blood was placed in a 1.5-mL centrifuge tube and left undisturbed at room temperature for 2 h. The sample was centrifuged at 5 °C and 3000 rpm for 15 min using a high-speed refrigerated centrifuge to obtain the serum. The serum levels of liver function markers [aspartate aminotransferase (AST), alanine aminotransferase (ALT), and total bilirubin (TBIL)] and lipids [low-density lipoprotein (LDL), total cholesterol, and triglycerides (TGs)] were analyzed using a fully automated biochemical analyzer.

Hematoxylin and eosin staining

The tissue sections were fixed in 4% neutral buffered formalin, embedded in paraffin, and sectioned into 4 μm-thick sections. The sections were deparaffinized using xylene, rehydrated using a series of graded ethanol solutions, stained with hematoxylin for 5–10 min, washed with distilled water, and stained with eosin for 2-7 min. Next, the sections were dehydrated using a series of graded ethanol solutions, cleared with xylene, mounted with mounting medium, and covered with a cover slip.

Oil red O staining

The frozen sections were fixed in 4% neutral buffered formalin, rinsed with 60% isopropanol, and allowed to dry. The sections were then stained with oil red O for 15-30 min, rinsed with 60% isopropanol, counterstained with hematoxylin for 1-2 min, washed with distilled water, dehydrated, mounted with a mounting medium, and covered with a coverslip.

Periodic acid-Schiff staining

The tissue sections were deparaffinized using xylene, rehydrated using a series of graded ethanol solutions, and oxidized

with a periodic acid solution for 10-15 min. Next, the sections were rinsed with distilled water, stained with Schiff reagent for 30-60 min in the dark, counterstained with hematoxylin, washed with distilled water, dehydrated, mounted using a mounting medium, and covered with a cover slip.

Masson's trichrome staining

The tissue sections were deparaffinized using xylene, rehydrated using a series of graded ethanol solutions, stained with Weigert's iron hematoxylin for 10 min, rinsed with distilled water, stained with Biebrich scarlet-acid fuchsin solution for 5-10 min, washed with distilled water, and incubated with phosphotungstic-phosphomolybdic acid solution for 5-10 min. Next, the sections were counterstained with aniline blue for 5-10 min, washed with distilled water, dehydrated, mounted with a mounting medium, and covered with a cover slip.

Sirius red staining

The tissue sections were deparaffinized using xylene, rehydrated using a series of graded ethanol solutions, stained with Sirius red solution for 1 h, washed with distilled water, dehydrated, and cleared with xylene. Finally, the sections were mounted with a mounting medium and covered with a cover slip.

Transmission electron microscopy

One mouse from the control, treatment, and model groups was randomly selected for electron microscopy. Liver sections with a size of approximately 1 mm were treated with 2.5% glutaraldehyde (Scientific Phygene, Fuzhou, China) and rinsed thrice with phosphate-buffered saline (PBS) (PH = 7.4). The samples were fixed with 1% osmium tetroxide (Ted Pella, Redding, United States) for 2 h, rinsed thrice with PBS, and dehydrated using alcohol and acetone gradients as follows: 50% ethanol for 30 min, 70% ethanol for 30 h, 80% acetone for 30 min, and 90% acetone for 30 h. Next, the samples were washed thrice with 100% acetone and embedded in epoxy resin (Ted Pella, Redding, United States). Ultrathin sections (7 nm) were prepared using a microtome (LKB, Bromma, Sweden). The sections were stained with uranyl acetate (EMS, Hatfield, United States) for 30 min and 3% lead citrate (Ted Pella, Redding, United States) for 15 min. The target structures were observed using a transmission electron microscope (JEM-1400, Japan Electron Optics Laboratory Co., Ltd. Tokyo, Japan).

High-throughput sequencing

Liver samples (n = 3 per group) from the control, treatment, and model groups stored in liquid nitrogen were randomly selected and sent to Huada Genomics (Wuhan, China, http://www.genomics.cn) for high-throughput sequencing. For specific sequencing steps, refer to the Supplementary material.

Differentially expressed mRNAs and miRNAs

The mRNA and miRNA expression levels were measured using fragments per kilobase of transcript per million mapped reads (FPKM) values. Sequencing data were subjected to quality control. Differential expression between groups was estimated using the Limma R package (version: 3.52.2) based on the generalized linear model. To comparatively analyze the expression levels between multiple groups, the control-model and model-treatment expression profiles were regressed using the Limma package in R software (version: 4.2.1, https://posit.co/). A loose threshold was set to avoid excessive filtering of differentially expressed mRNAs and miRNAs (log fold-change > 1; P < 0.05). Differentially expressed mRNAs and miRNAs were identified.

Enrichment analysis

The mRNA expression data were subjected to Gene Ontology (GO) and Kyoto Encyclopedia of Genes and Genomes (KEGG) pathway analyses to identify the enrichment of mRNAs in the GO terms biological process (BP), cellular component (CC), and molecular function (MF) and the KEGG signaling pathways. The clusterprofiler R package (version: 4.4.4) was used for enrichment analyses with the reference files based on the org.Mm.eg.db R package (version 3.1.0) for mouse enrichment analysis. Enrichment was considered significant at P < 0.05.

Immune infiltration analysis

CIBERSORT is a gene expression-based algorithm for the accurate detection of immune cell infiltration. The "CIBERSORT" R package (CIBERSORTR script v1.03; http://cibersort.stanford.edu/) developed by Newman *et al*[27] was used to successfully quantify 22 types of immune cells, including B cells, regulatory T cells, CD4+ T, CD8+ T, natural killer (NK) cells, mast cells, plasma cells, dendritic cells, neutrophils, eosinophils, and macrophages. The reference dataset of mouse immune cells was obtained from Chen *et al*[28]. The mRNA expression data of the control, model, and treatment groups were examined using the CIBERSORT algorithm with a perm of the deconvolution algorithm set to 1000.

Regulatory network of miRNA-mRNA

miRNA, a type of non-coding RNA, negatively regulates gene expression at the posttranscriptional level. To generate a preliminary regulatory network of miRNA-mRNA in the model and treatment groups, the upregulated miRNAs or mRNAs and downregulated mRNAs or miRNAs were selected and analyzed using Cytoscape software (version: 3.7.1, https://cytoscape.org/).

The Sun Yat-sen University research team developed the starBase database (https://starbase.sysu.edu.cn/starbase2/) to analyze interaction networks between long non-coding RNA, miRNA, competitive endogenous RNAs, RNA-binding proteins, and mRNAs using cross-linked immunoprecipitation sequencing (CLIP-seq) (high-throughput sequencing of RNA using CLIP, photoactivable ribonucleoside-enhanced CLIP, individual nucleotide resolution ultraviolet CLIP, and cross-linking ligation and sequencing of hybrids) data. To obtain the final miRNA-mRNA regulatory network, the initially selected network was intersected with the mouse interaction network obtained from the starBase database. Gene expression was verified using immunohistochemical analyses. This study aimed to establish the miRNA-mRNA-protein regulatory axis.

Immunohistochemistry

The paraffin sections (4 μm) of mouse liver tissue were deparaffinized, rehydrated, and subjected to antigen retrieval in a buffer solution (pH 9.0). After blocking endogenous peroxidase activity and non-specific binding, the sections were incubated with anti-ZCCHC24 antibodies (1:100) at 4 °C overnight. The sections were then washed and incubated with horseradish peroxidase-conjugated secondary antibodies at room temperature for 1 h. Immunoreactive signals were developed using diaminobenzidine. The sections were counterstained with hematoxylin and observed under a microscope.

Statistical analyses

The average optical density (AOD) (integrated optical density/area) of positive reactions was calculated using Image-Pro Plus 6.0 software. Data were analyzed using the dplyr R package (v. 1.0.10) and visualized using the ggplot2 R package (v. 3.3.6). Categorical variables were analyzed using the Chi-squared test. Continuous variables were represented as mean ± SD. Continuous variables between two groups were compared using the Wilcoxon signed-rank test, while those between more than two groups were compared using the Kruskal-Wallis test. Differences were considered significant at $P < 0.05$.

RESULTS

Effect of GTPs on bodyweight and liver index

The flowchart of the study is shown in Figure 1. Mice in all groups survived during the experiment and did not exhibit aberrant behaviors in urination, defecation, food intake, or water consumption. As shown in Supplementary Table 1 and Figure 2A, the bodyweight of mice in all groups increased with time and was not significantly different between the groups. The liver index (Supplementary Table 2 and Figure 2B) values in the model group were significantly higher than those in the control group ($P = 0.016$) but were not significantly different between the treatment and model groups ($P = 0.51$). Additionally, the liver index values in the oil and GTP groups were not significantly different from those in the control group ($P > 0.05$).

Effect of GTPs on the serum levels of liver function markers and lipids

The serum levels of ALT, AST, TBIL, LDL, and TGs were analyzed. As shown in Figure 2C-G, the serum levels of ALT, AST, TBIL, LDL, and TGs in the model group were significantly higher than those in the control group ($P < 0.001$). Compared with those in the model group, the serum levels of liver function markers and lipids were significantly downregulated in the treatment group ($P < 0.001$). The ALT, AST, and LDL levels were not significantly different between the oil, control, and GTP groups ($P > 0.05$).

Effect of GTPs on hepatic histological characteristics

The results of liver hematoxylin and eosin staining are shown in Figure 3A. Mice in the model group exhibited significant hepatocyte ballooning degeneration, whereas those in the control, oil, and GTP groups did not exhibit hepatocyte ballooning degeneration.

Effect of GTPs on fat deposition

Oil red O staining was performed to further analyze the severity of fatty liver in different groups. As shown in Figure 3A, the model group exhibited the highest red color staining intensity in the liver, followed by the oil and control groups. Meanwhile, the liver of the treatment and GTP groups exhibited the lowest red staining intensity. Five positive staining sites in the liver of the model and treatment groups were selected to calculate the AOD. As shown in Figure 3B, the AOD in the model group (7.270 ± 1.120%) was significantly higher than that in the treatment (0.185 ± 0.061%) ($P = 0.037$) and control groups (5.760 ± 0.586%) ($P < 0.001$).

Effect of GTPs on polysaccharide accumulation

The results of Periodic acid-Schiff staining (Figure 3A) revealed the lack of red-stained areas in the liver of the model group, while the red-stained areas were upregulated in the control, oil, treatment, and GTP groups. Five positive staining sites in the liver of the model and treatment groups were selected to calculate the AOD. As shown in Figure 3C, the AOD in the model group (0.431 ± 0.083%) was significantly lower than that in the treatment (1.170 ± 0.099%) and control groups (1.360 ± 0.148%) ($P < 0.001$).

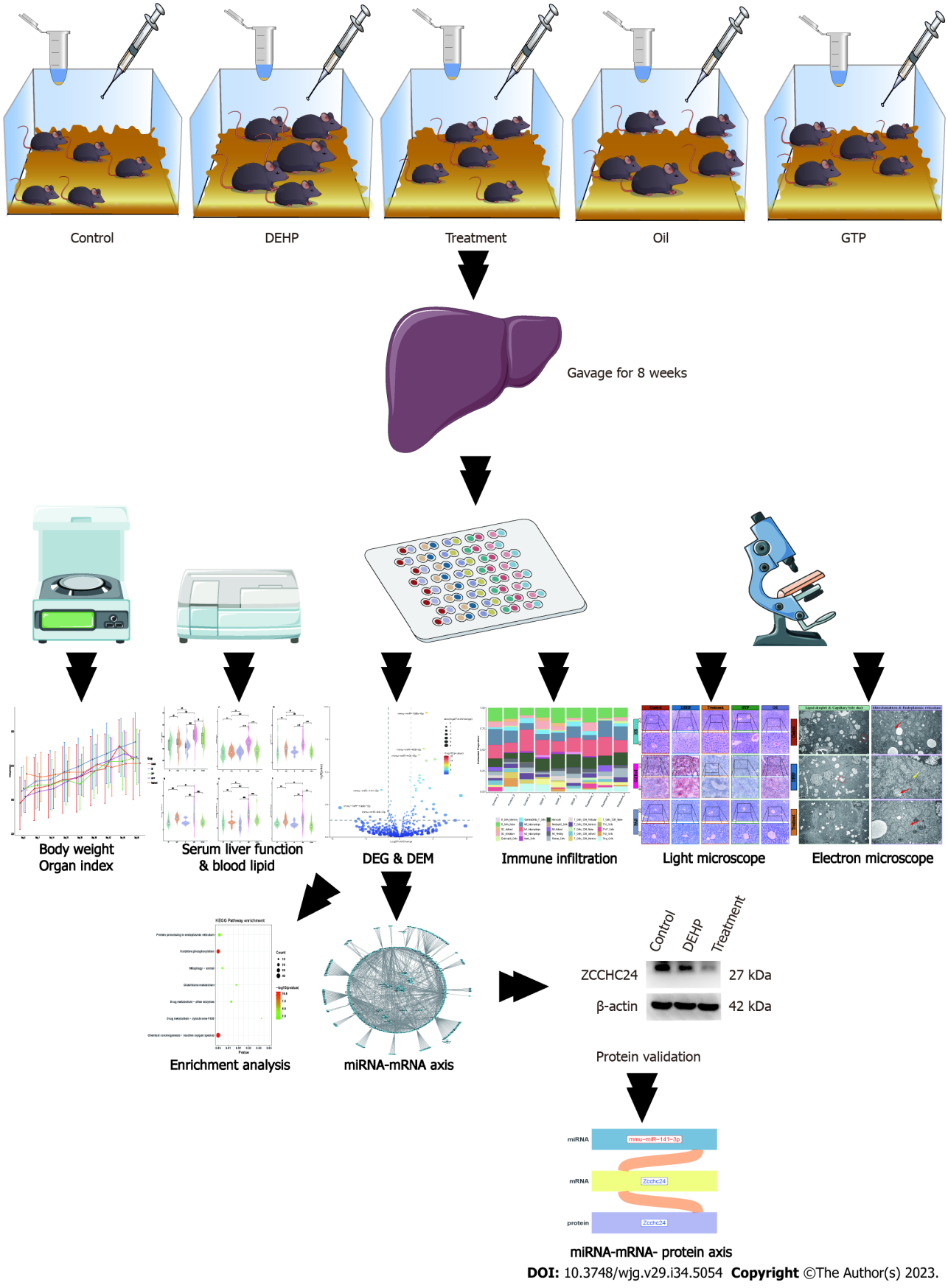

DOI: 10.3748/wjg.v29.i34.5054

Figure 1 Flowchart of the study. DEG: Differentially expressed gene; DEM: Differentially expressed microRNA (miRNA).

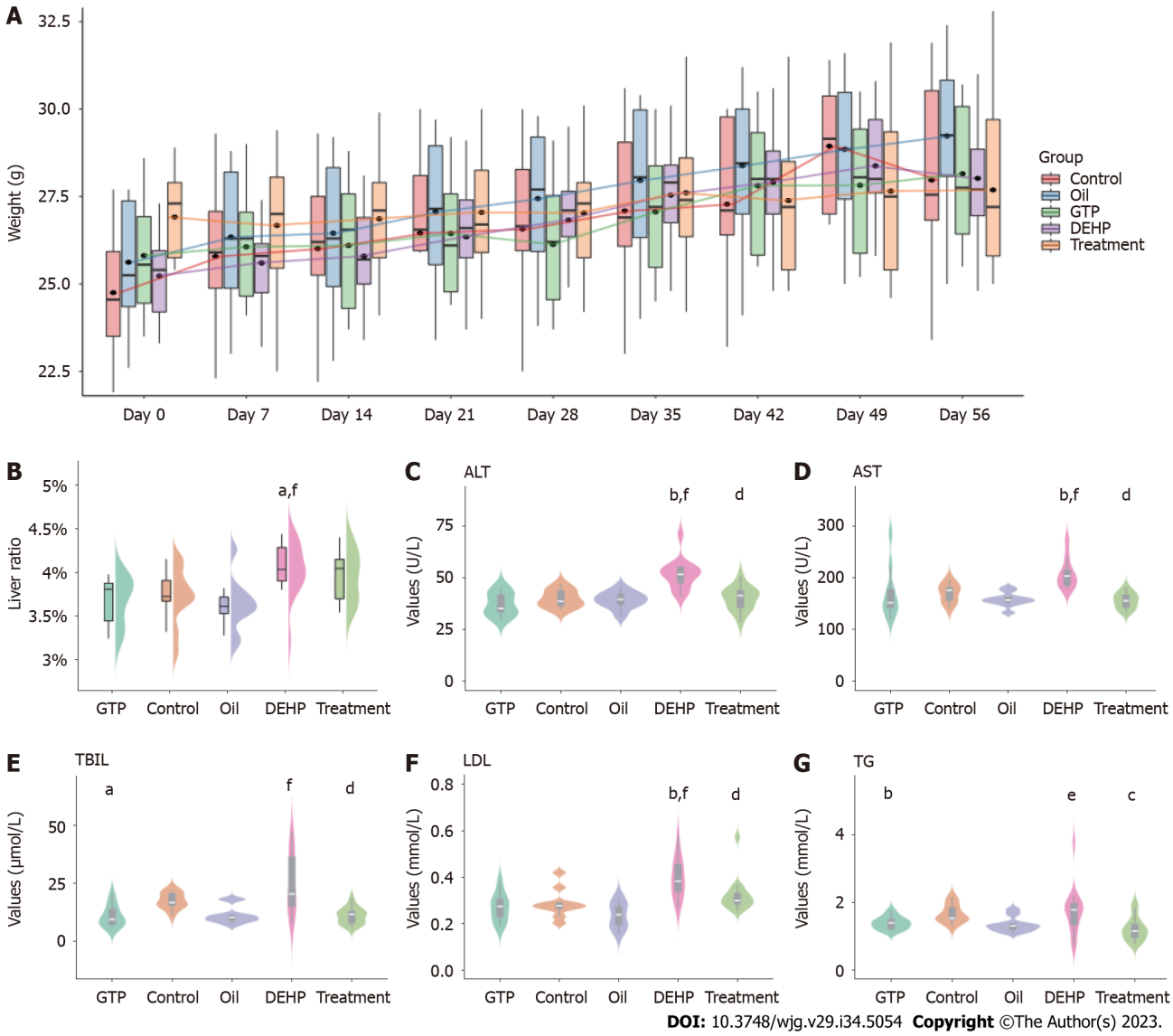

DOI: 10.3748/wjg.v29.i34.5054

Figure 2 Mouse bodyweight and liver index and serum levels of liver function markers and lipids. A: Bodyweight changes in different groups within 8 wk; B-G: Comparative analysis of organ indices (B) and serum levels of alanine aminotransferase (C), glutamate aminotransferase (D), total bilirubin (E), low-density lipoprotein (F), and triglyceride (G) in different groups. $^{a}P < 0.05$ and $^{b}P < 0.01$ (compared to the Control group); $^{c}P < 0.05$ and $^{d}P < 0.01$ (compared to Di (2-ethylhexyl) phthalate group); $^{e}P < 0.05$ and $^{f}P < 0.01$ (compared to Oil group). ALT: Alanine aminotransferase; AST: Glutamate aminotransferase; TBIL: Total bilirubin; LDL: Low-density lipoprotein; TG: Triglyceride; DEHP: Di (2-ethylhexyl) phthalate.

Effect of GTPs on collagen fibers

The results of Masson's trichrome staining (Figure 4A) revealed blue-stained fibrous tissue around the liver blood vessels in the model group. In contrast, the area of blue-stained fibrous tissue around the liver blood vessels in the treatment group was lower than that in the model group. Fibrous tissue was not detected around the liver blood vessels in the control, oil, and GTP groups. Five positive staining sites in the liver of the model and treatment groups were selected to calculate the AOD. As shown in Figure 4B, the AOD in the model group (0.337 ± 0.113%) was significantly higher than that in the treatment group (0.183 ± 0.014%) ($P = 0.02$).

Effect of GTPs on collagen network

In Sirius red staining, type I collagen fibers exhibit strong orange-yellow or bright red colors under a polarized light microscope, whereas type III collagen fibers exhibit green color. In this study, the results of Sirius red staining (Figure 4A) revealed red-stained fibrous tissue around the blood vessels in the model group. The red-stained area around the blood vessels in the treatment group was significantly lower than that in the model group. Red-stained fibrous tissue was not detected around the blood vessels of the control, oil, and GTP groups. Next, semiquantitative analysis was performed by selecting five positive staining sites in the liver of the model and treatment groups to calculate the AOD. The AOD in the model group (1.240 ± 0.125%) was significantly higher than that in the treatment group (0.080 ± 0.025%) ($P = 0.012$) (Figure 4C).

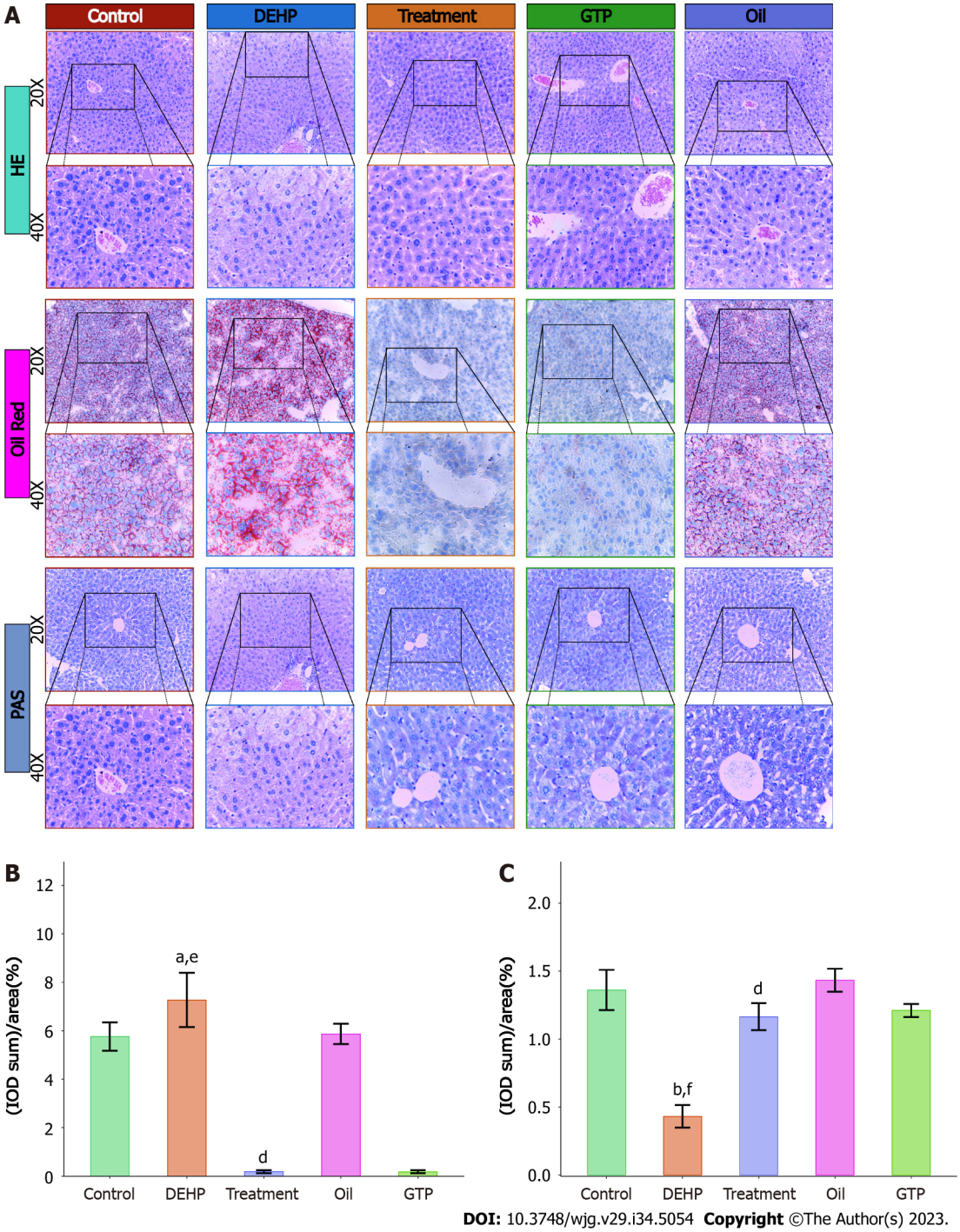

DOI: 10.3748/wjg.v29.i34.5054

Figure 3 Hematoxylin and eosin, oil red O, and periodic acid-Schaff staining of liver sections and semiquantitative analysis of liver pathologies in mice from different groups. A: Hematoxylin and eosin-stained, oil red O-stained, and periodic acid-Schaff (PAS)-stained liver sections of different groups; B and C: Comparative analysis of average optical density of oil red O staining (B) and PAS staining (C) intensities between different groups. $^{a}P < 0.05$ and $^{b}P < 0.01$ (compared to the Control group); $^{d}P < 0.01$ (compared to Di (2-ethylhexyl) phthalate group); $^{e}P < 0.05$ and $^{f}P < 0.01$ (compared to Oil group). DEHP: Di (2-ethylhexyl) phthalate; HE: Hematoxylin and eosin; PAS: Periodic acid-Schaff.

Effect of GTPs on the liver microstructures

The liver tissues of the control, model, and treatment groups were subjected to transmission electron microscopy. The number and size of lipid droplets in the liver were upregulated and the capillary bile ducts were significantly dilated in the model group (Figure 5A). Additionally, the mitochondria were slightly swollen, and the arrangement of the rough endoplasmic reticulum was disordered. In contrast, the number of lipid droplets in the liver was downregulated in the treatment group, while the capillary bile ducts exhibited physiological structure. Additionally, the swelling of the mitochondria was alleviated. The results of quantitative analysis of the diameter of small bile ducts (Figure 5B) were consistent with the observations in Figure 5A. However, these findings must be carefully interpreted. Additionally, further studies with large sample sizes are needed to confirm and generalize the results.

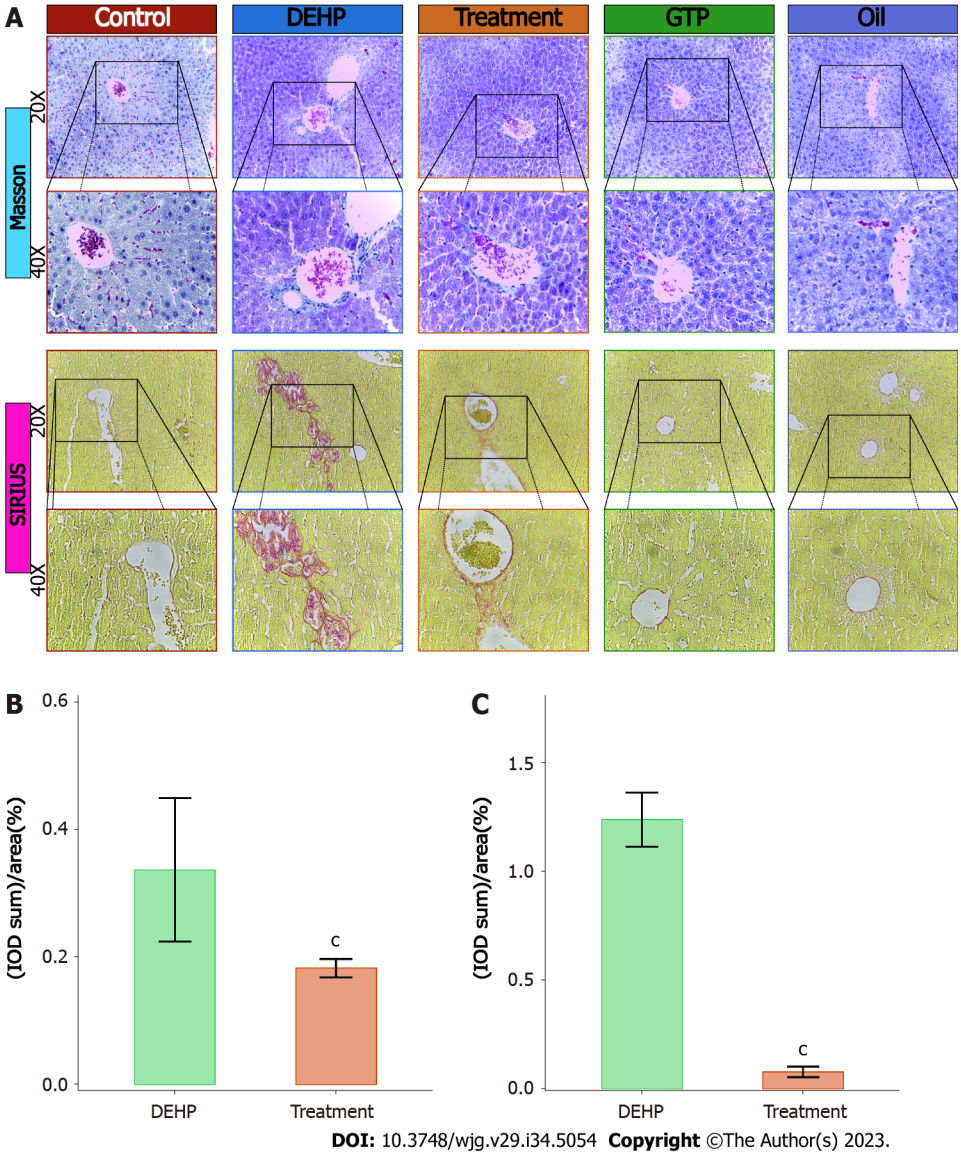

DOI: 10.3748/wjg.v29.i34.5054

Figure 4 Masson's trichrome and Sirius red staining and semiquantitative analysis of hepatic pathologies in mice from different groups.
A: Masson's trichrome and Sirius red staining of liver samples from different groups; B and C: Comparative analysis of average optical density of Masson's trichrome staining (B) and Sirius red staining (C) intensities between the model and treatment groups. °$P < 0.05$ (compared to Di (2-ethylhexyl) phthalate group). DEHP: Di (2-ethylhexyl) phthalate.

Effect of GTPs on mRNA and miRNA expression levels

The liver samples from the control, treatment, and model groups were subjected to high-throughput screening with 3 replicate samples for each group. The mRNA and miRNA expression data were subjected to quality control analysis. The differences in the expression levels of miRNA and mRNA were minimal between the groups (Supplementary Figure 1A and B). Next, principal component analysis was performed (Supplementary Figure 1C and D). The mRNA and miRNA profiles of the control, model, and treatment groups exhibited distinct separation. Differential analysis revealed that compared with those in the model group, the number of upregulated mRNAs and miRNAs was 377 and 33, respectively, while the number of downregulated mRNAs and miRNAs was 583 and 7, respectively (Figure 6A and B). The expression levels of the significantly upregulated and downregulated mRNAs and miRNAs are shown in Figure 6C and D.

Enrichment analyses

Compared with those in the control group, the differentially expressed mRNAs in the model group were enriched in the following GO terms: BP term: Fatty acid metabolic process, small molecule catabolic process, organic acid catabolic process, and carboxylic acid catabolic process (Figure 7A); CC term: Mitochondrial protein-containing complex, mitochondrial inner membrane, ribosome subunit, and ribosome (Figure 7B); MF term: Ribosome structure, electron transfer activity, oxidoreductase activity, and ubiquitin protein ligase binding (Figure 7C). Additionally, the differentially expressed mRNAs in the model group were enriched in the following KEGG pathways: Fatty acid metabolism, ferroptosis, glutathione metabolism, and PPAR signaling pathway (Figure 7D). Compared with those in the model group, the differentially expressed mRNAs in the treatment group were enriched in the following GO terms: BP term:

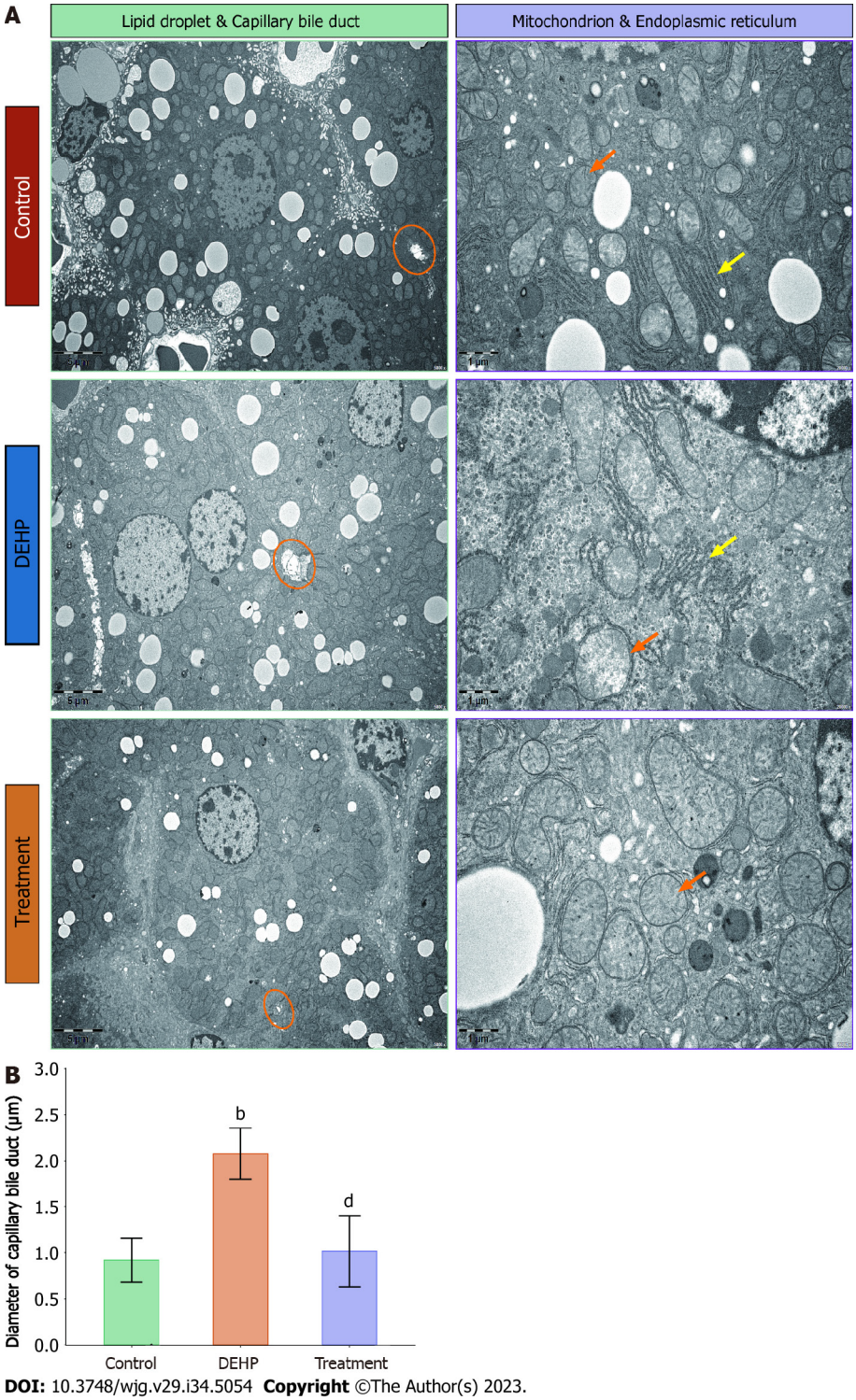

DOI: 10.3748/wjg.v29.i34.5054

Figure 5 Comparative quantitative analysis of transmission electron microscopy results between the control, model, and treatment groups. A: Comparison of transmission electron microscopy results between the control, model, and treatment groups. In the model and control groups, increased numbers of fat droplets with enhanced size were visible. Expanded capillary bile ducts (indicated with orange circles), mildly swollen mitochondria (indicated with orange arrows), and disordered rough endoplasmic reticulum (indicated with yellow arrows) were observed in the model group. In the treatment group, the number of fat droplets decreased, capillary bile ducts appeared mostly healthy (indicated with orange circles), and mitochondrial swelling was reduced (indicated with orange arrows); B: Quantitative analysis of small bile duct diameter in mice from the control, model, and treatment groups. $^{b}P < 0.01$ (compared to the Control group); $^{d}P < 0.01$ (compared to Di (2-ethylhexyl) phthalate group). DEHP: Di (2-ethylhexyl) phthalate.

Mitochondrial organization, proteasome protein catabolic process, and oxidative phosphorylation (Figure 8A); CC term: Ribosome, ribosomal subunit, and large ribosomal subunit (Figure 8B); MF term: Structural constituent of ribosome and molecular carrier activity (Figure 8C). Additionally, the differentially expressed mRNAs in the treatment group were enriched in the following KEGG pathways: Mitochondrial autophagy, glutathione metabolism, oxidative phosphorylation, and drug metabolism (Figure 8D).

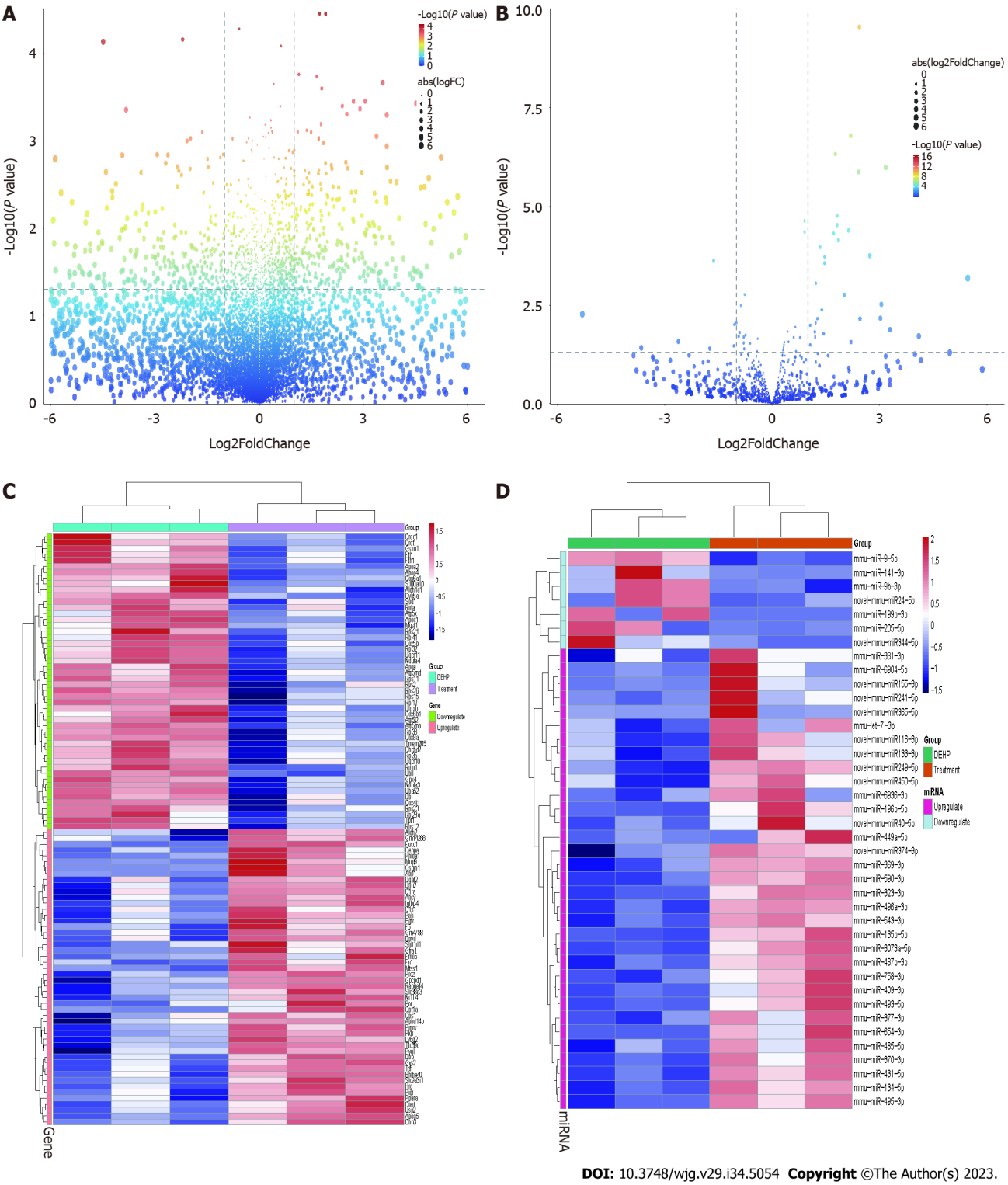

DOI: 10.3748/wjg.v29.i34.5054

Figure 6 Differential expression of mRNAs and microRNAs between the treatment and model groups. A: The volcano plot of differentially expressed mRNAs between the treatment and model groups. The upper left quadrant and the upper right quadrant in the figure represent downregulated and upregulated mRNAs, respectively; B: The volcano plot of differentially expressed microRNAs (miRNAs) between the treatment and model groups. The upper left quadrant and the upper right quadrant in the figure represent downregulated and upregulated miRNAs, respectively; C: Heatmap shows the 50 mRNAs that exhibited the highest upregulation and downregulation in the treatment group relative to the model group; D: Heatmap shows the miRNAs that exhibited the highest upregulation and downregulation in the treatment group relative to the model group.

Immune infiltration analysis

The proportions and infiltration levels of immune cells in the control, model, and treatment groups are shown in Figure 9A and B. Compared with those in the control group, the infiltration levels of monocytes and immature CD8+ T cells were significantly upregulated and the infiltration levels of immature CD4+ T cells were significantly downregulated in the model group (Figure 9C). Meanwhile, compared with those in the model group, the infiltration levels of

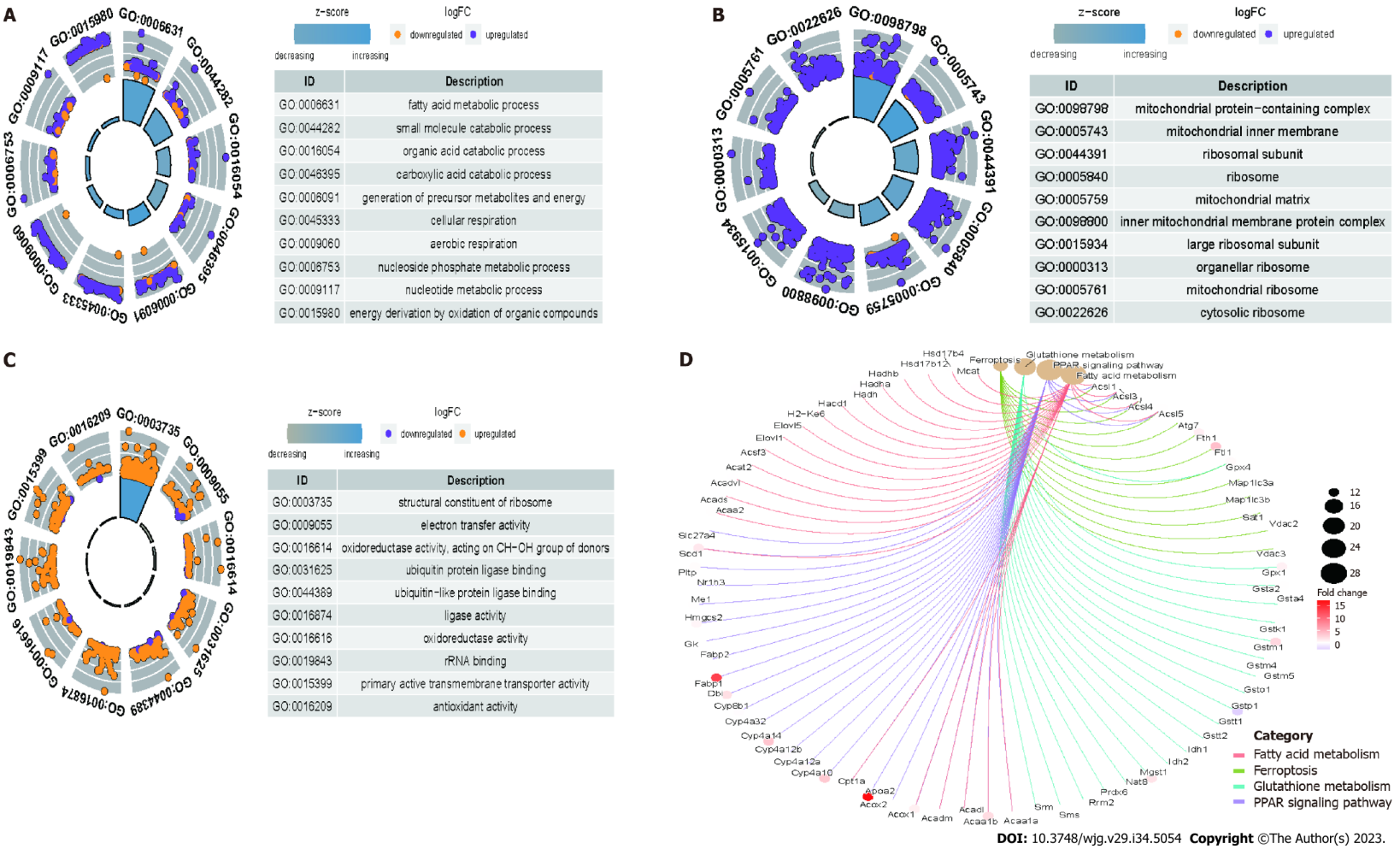

ID	Description
GO:0006631	fatty acid metabolic process
GO:0044282	small molecule catabolic process
GO:0016054	organic acid catabolic process
GO:0046395	carboxylic acid catabolic process
GO:0006091	generation of precursor metabolites and energy
GO:0045333	cellular respiration
GO:0009060	aerobic respiration
GO:0006753	nucleoside phosphate metabolic process
GO:0009117	nucleotide metabolic process
GO:0015980	energy derivation by oxidation of organic compounds

ID	Description
GO:0098798	mitochondrial protein-containing complex
GO:0005743	mitochondrial inner membrane
GO:0044391	ribosomal subunit
GO:0005840	ribosome
GO:0005759	mitochondrial matrix
GO:0098800	inner mitochondrial membrane protein complex
GO:0015934	large ribosomal subunit
GO:0000313	organellar ribosome
GO:0005761	mitochondrial ribosome
GO:0022626	cytosolic ribosome

ID	Description
GO:0003735	structural constituent of ribosome
GO:0009055	electron transfer activity
GO:0016614	oxidoreductase activity, acting on CH-OH group of donors
GO:0031625	ubiquitin protein ligase binding
GO:0044389	ubiquitin-like protein ligase binding
GO:0016874	ligase activity
GO:0016618	oxidoreductase activity
GO:0019843	rRNA binding
GO:0015399	primary active transmembrane transporter activity
GO:0016209	antioxidant activity

DOI: 10.3748/wjg.v29.i34.5054

Figure 7 The differentially expressed mRNAs between the model and control groups were enriched in different Gene Ontology terms and Kyoto Encyclopedia of Genes and Genomes pathways. A: Biological processes; B: Cellular components; C: Molecular function; D: Kyoto Encyclopedia of Genes and Genomes pathways.

mast cells and active NK cells were significantly upregulated and the infiltration levels of M2 macrophages were significantly downregulated in the treatment group (Figure 9D). The correlation analysis results of various immune cells are shown in Figure 9E.

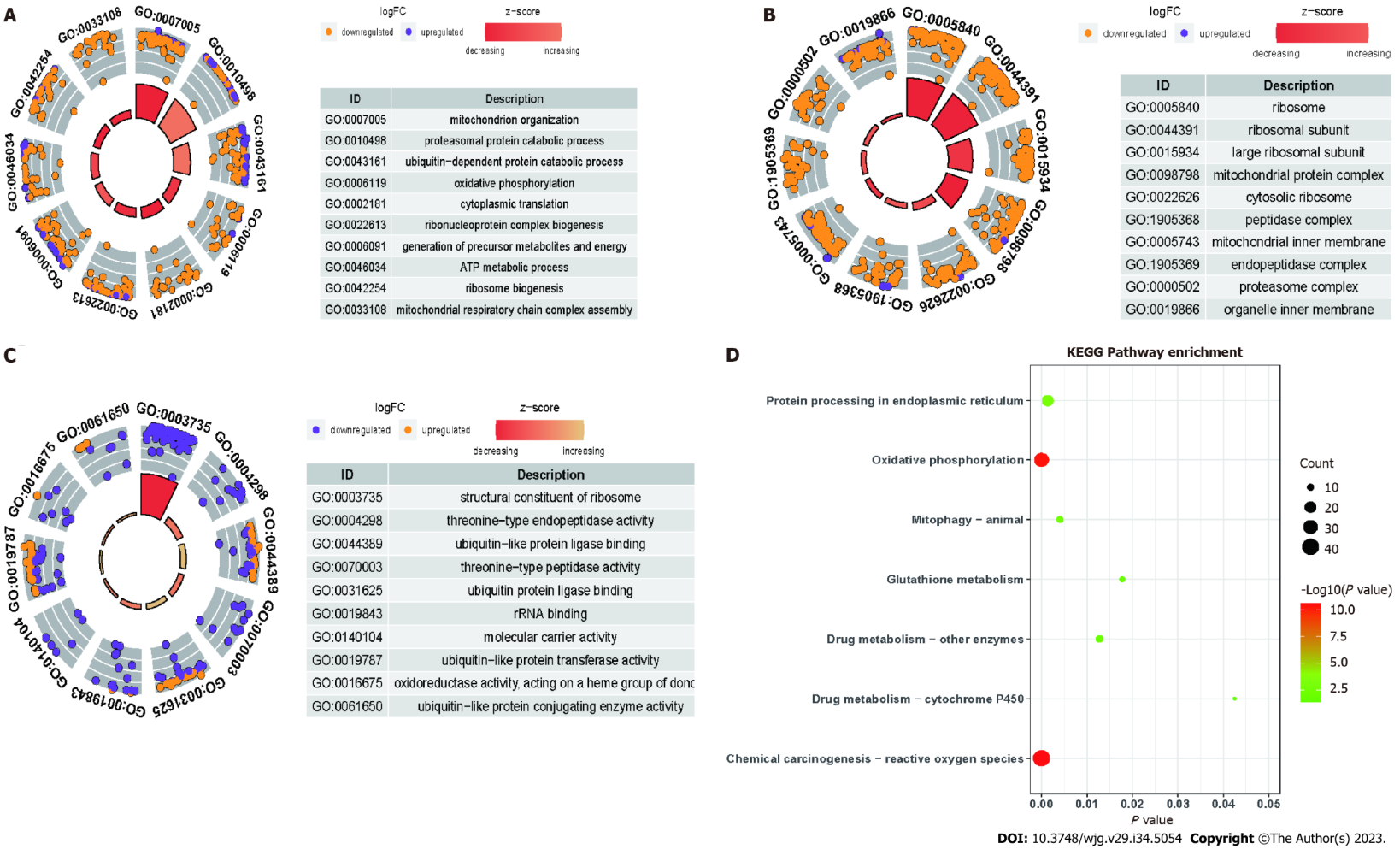

DOI: 10.3748/wjg.v29.i34.5054

Figure 8 The differentially expressed mRNAs between the treatment and model groups were enriched in different Gene Ontology terms and Kyoto Encyclopedia of Genes and Genomes pathways. A: Biological processes; B: Cellular components; C: Molecular function; D: Kyoto Encyclopedia of Genes and Genomes pathways.

Construction of miRNA-mRNA-protein regulatory axis

Network diagrams (Figure 10A) of upregulated miRNAs and downregulated mRNAs, as well as that of downregulated miRNAs and upregulated mRNAs, in the treatment group were constructed. The data were matched with the miRNA-mRNA regulatory axis in the starBase database to obtain the mmu-miR-141-3p/Zcchc24 and mmu-miR-9-5p/Zbtb7a axes (Figure 10B). Correlation analysis (Figure 10C and D) revealed that the correlation coefficients of mmu-miR-141-3p/

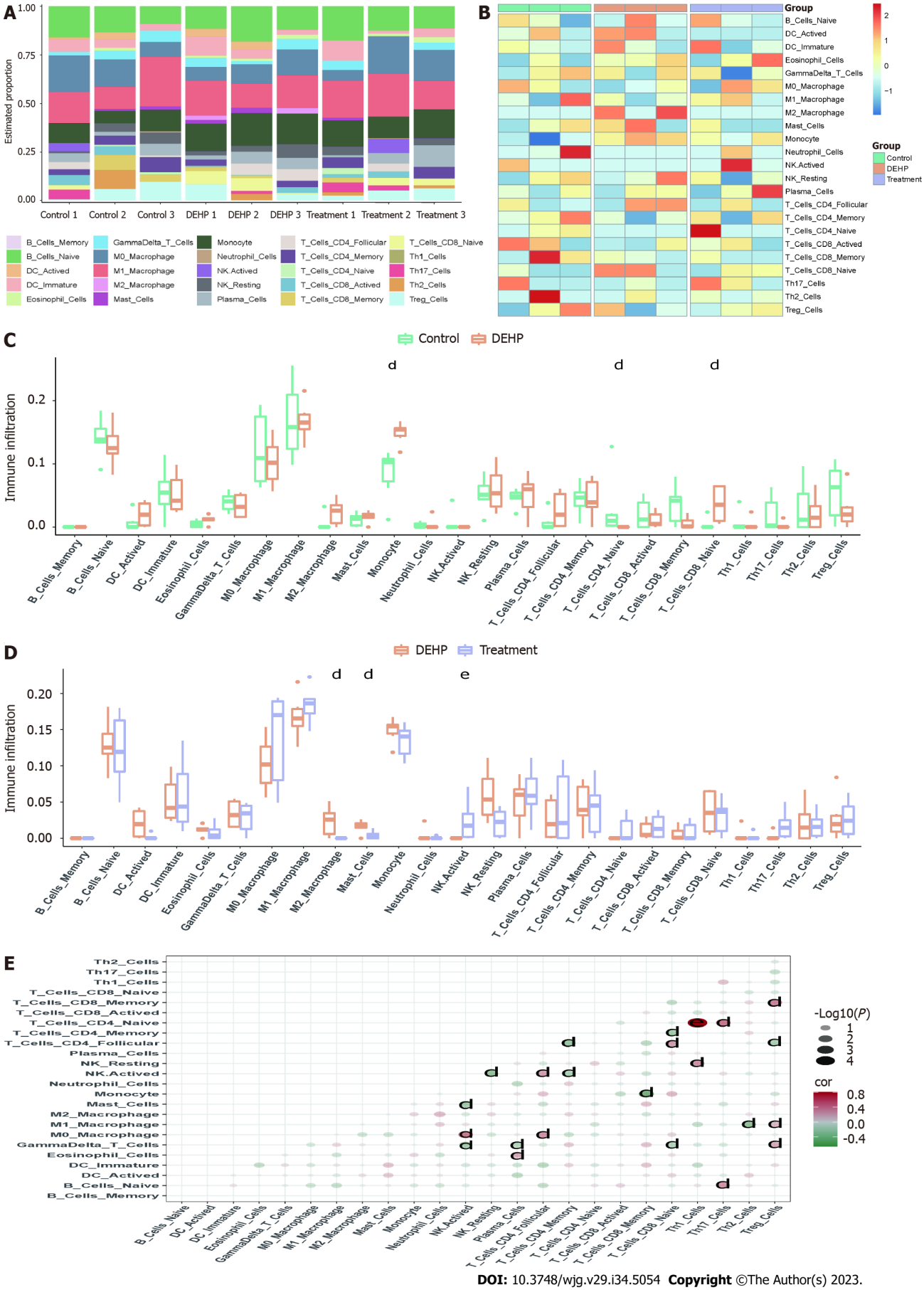

DOI: 10.3748/wjg.v29.i34.5054

Figure 9 Immune infiltration analyses. A and B: Histograms (A) and heatmaps (B) of the proportions of immune cells in the control, model, and treatment groups; C and D: Analyses of differential immune cell infiltration between the model and control groups (C), as well as between the treatment and model groups (D); E:

Correlation analyses of immune cells in different groups. [d]*P* < 0.01 (compared to Di (2-ethylhexyl) phthalate group); [e]*P* < 0.05 (compared to Oil group). DEHP: Di (2-ethylhexyl) phthalate.

Zcchc24 and mmu-miR-9-5p/Zbtb7a axes were -0.44 and -0.87, respectively. To validate these regulatory axes, the liver tissues of the control, model, and treatment groups were subjected to western blotting (Figure 10E). Compared with that in the model group, the average gray value of Zcchc24 protein was significantly downregulated in the treatment group (Figure 10F), indicating that protein expression changes were consistent with mRNA expression changes. However, Zbtb7a protein expression could not be validated using western blotting or immunohistochemical analysis due to low expression levels. These findings indicate that the mmu-miR-141-3p/*Zcchc24* (mRNA)/Zcchc24 (protein) regulatory axis plays an important role in the protective effects of GTPs on DEHP-induced liver injury in mice (Figure 10G).

DISCUSSION

This study aimed to investigate the therapeutic mechanism of GTPs in alleviating DEHP-induced liver dysfunction, blood lipid dysregulation, non-alcoholic fatty liver, and liver fibrosis. Additionally, the role of a miRNA-mRNA-protein regulatory axis in the therapeutic effects of GTPs on DEHP-induced liver damage was elucidated (Figure 11). Thus, the findings of this study provide valuable insights into the potential therapeutic application of GTPs in DEHP-induced liver damage.

Histopathological analysis revealed that GTPs are effective in mitigating DEHP-induced non-alcoholic fatty liver disease and liver fibrosis in mice. This finding is consistent with that of previous studies, which reported the beneficial effects of GTP on liver health. For example, a meta-analysis[29] of 20 randomized controlled trials with 1536 participants revealed that green tea decreases the levels of total cholesterol and LDL. Zhao *et al*[30] reported that DEHP exposure significantly promotes inflammation, necrosis, and fibrosis in the liver and upregulates the expression of proteins associated with the development of liver inflammation and fibrosis. Kim *et al*[31] suggested that GTPs downregulate the expression of collagen content and type 1 collagen, and consequently alleviate liver fibrosis. Additionally, animal studies [32] have indicated that supplementation of green tea effectively prevented excessive accumulation of visceral and liver lipids, elevated blood glucose levels, and alleviated aberrant blood lipid levels, liver dysfunction, and hepatic steatosis in male C57BL/6 mice fed on a high-fat diet for six weeks as evidenced by the analysis of serum biochemical parameters, histological changes, lipid accumulation, inflammatory cytokines, and related indices. These findings further indicated the therapeutic potential of GTPs in liver-related conditions.

In this study, GTPs were found to ameliorate the DEHP-induced pathological damage to the liver microstructures, including the mitochondria, endoplasmic reticulum, and capillary bile ducts. These findings are consistent with those of previous studies, which reported the adverse effects of DEHP on liver microstructures. For instance, an animal study[33] indicated that DEHP induced mitochondrial and endoplasmic reticulum ultrastructural damages, characterized by increased fission and decreased fusion. Furthermore, Sun *et al*[34] suggested that DEHP promoted mitochondrial-associated endoplasmic reticulum membrane disruption, potentially through endoplasmic reticulum unfolded protein response, to induce endoplasmic reticulum stress. Consistent with the results of this study, in vitro and *in vivo* experimental studies[35] have demonstrated that GTPs effectively alleviate acetaminophen-induced liver damage and mitochondrial dysfunction. These studies have shown that GTPs possess antioxidant capacity and can prevent liver mitochondrial damage. Specifically, GTPs have been found to enhance the membrane potential and activity of liver mitochondrial respiratory chain complexes, thereby protecting against mitochondrial dysfunction. However, further research is needed to fully elucidate the underlying mechanisms and to explore the clinical applications of GTPs in protecting liver microstructures from DEHP-induced damage.

In this study, we aimed to analyze the signaling pathways involved in DEHP-induced liver damage and the hepatoprotective effects of GTPs using high-throughput sequencing. Ferroptosis, a recently discovered non-apoptotic cell death process, is induced by intracellular iron-dependent lipid peroxidation damage. Consistent with the findings of this study, Yin *et al*[36] investigated the acute toxicity of DEHP exposure in marine medaka. They conducted transcriptome analysis on the liver of DEHP-exposed medaka and reported that females were more sensitive to the immune response than males under acute DEHP exposure conditions. Furthermore, they found that DEHP exposure promoted iron depletion, leading to iron overload, increased levels of MDA and lipid peroxidation, and decreased levels of glutathione. These findings suggest that DEHP can rapidly alter certain molecular regulatory patterns and induce cell death through ferroptosis. In addition, we discussed the PPAR signaling pathway, which is a classic pathway associated with hyperlipidemia, regulates lipid metabolism and blood lipid levels by mediating various biological functions, such as the synthesis and decomposition of cholesterol and the oxidation of fatty acids[37]. Previous studies[38,39] have revealed that DEHP exposure dysregulates blood lipid levels and hepatic lipid metabolism in mice through the PPAR signaling pathway.

In this study, we utilized the CIBERSORT algorithm to identify specific alterations in immune cells. Consistent with the findings of this study, Yang *et al*[40] investigated the effect of DEHP on the immune system of male C57Bl/6 mice and reported significant atrophy of the thymus and spleen with the proportions of immature CD4+ and CD8+ populations exhibiting the highest downregulation. Additionally, they found a downregulation in the number of T and B cells in the spleen. A previous study[41] reported that green tea extract promotes macrophage phagocytic activity at a dosage of 5 mg/kg bodyweight and enhances NK cell activity and T cell proliferation at a dosage of 40 mg/kg bodyweight, supporting the potential immunomodulatory effects of GTPs demonstrated in this study.

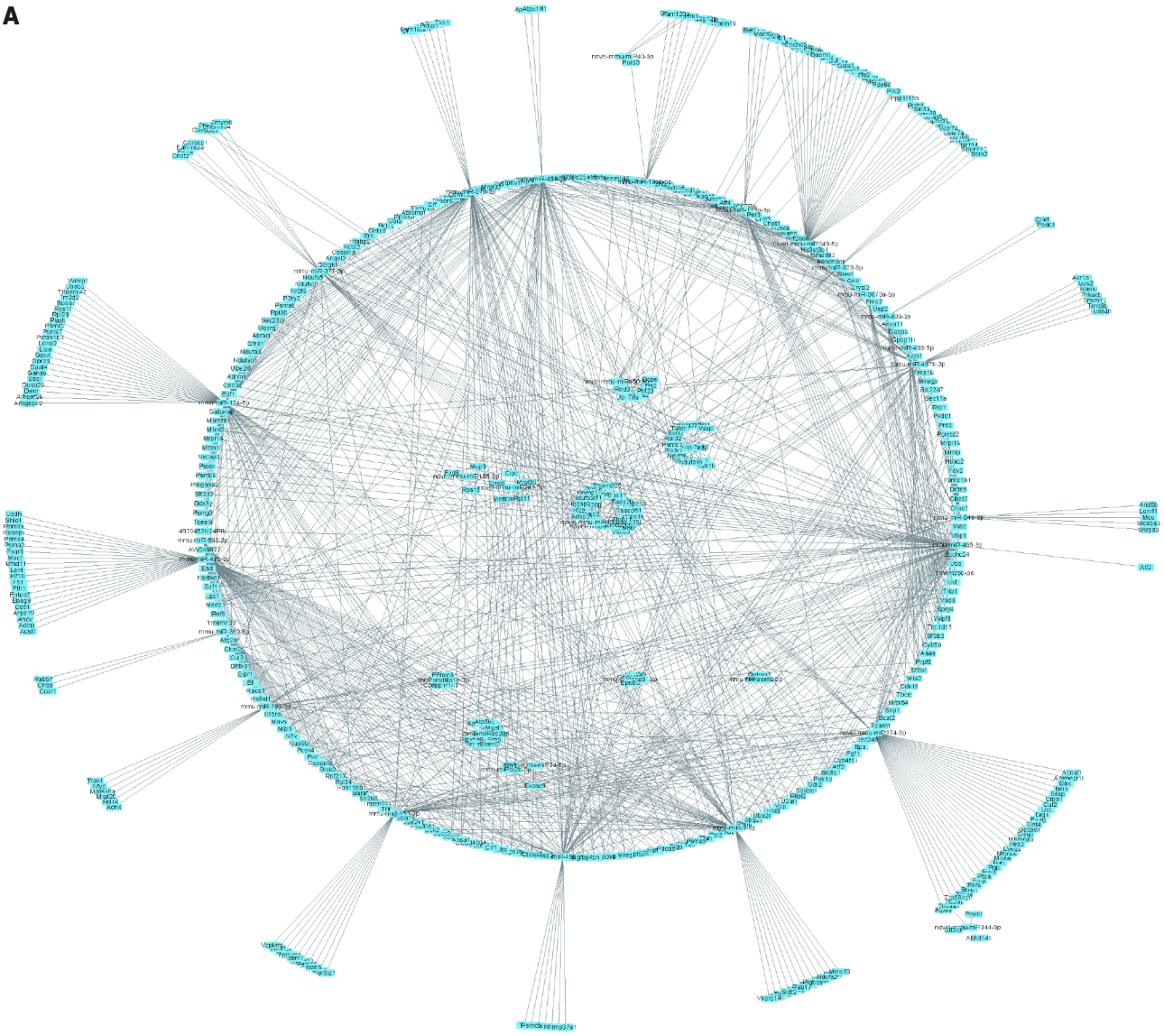
A

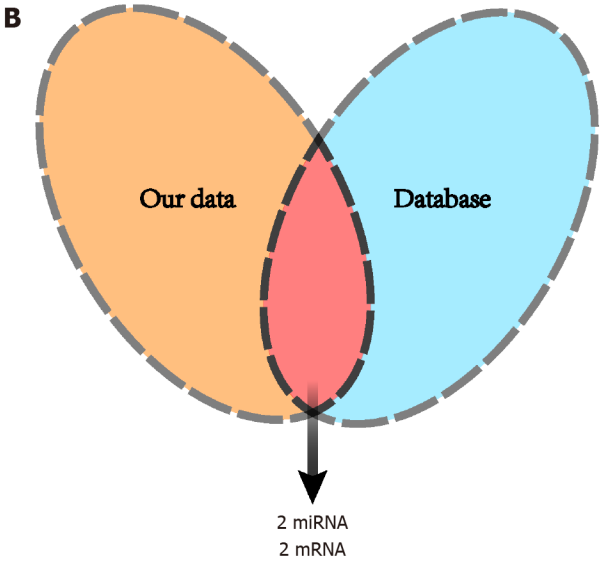
B
Our data
Database
2 miRNA
2 mRNA

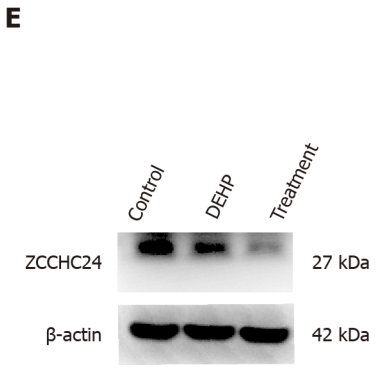
E
Control
DEHP
Treatment
ZCCHC24
27 kDa
β-actin
42 kDa

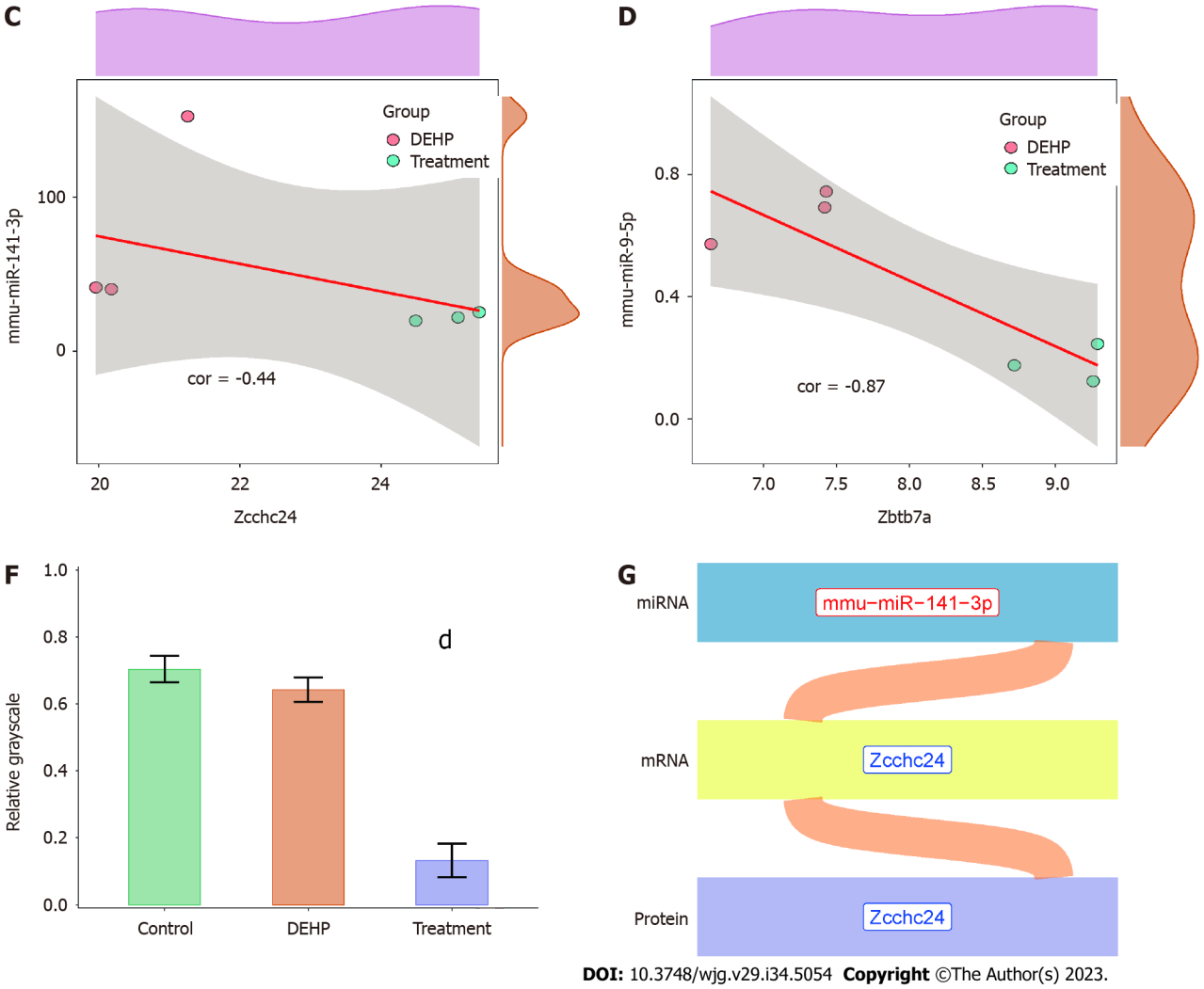

DOI: 10.3748/wjg.v29.i34.5054

Figure 10 Construction of the microRNA-mRNA-protein regulatory axis. A: The network diagram was constructed using differentially expressed mRNAs and microRNAs (miRNAs); B: Wayne diagram indicating the intersection of the miRNA-mRNA regulatory axis and mouse interaction network from the starBase database; C: Correlation analyses of mmu-miR-141-3p and Zcchc24; D: Correlation analyses of mmu-miR-9-5p and Zbtb7a; E: Western blotting validation of Zcchc24 protein expression in the control, model, and treatment groups; F: Semiquantitative analysis of Zcchc24 protein levels in the control, model, and treatment groups; G: The Sankey plot of the miRNA-mRNA-protein regulatory axes mediating the suppressive effects of green tea polyphenols (GTPs) on di-(2-ethylhexyl) phthalate (DEHP)-induced liver damage in mice. Red and blue fonts indicate upregulated and downregulated expression, respectively. $^{d}P < 0.01$ (compared to DEHP group). DEHP: Di (2-ethylhexyl) phthalate; GTPs: Green tea polyphenols.

This study identified the mmu-miR-141-3p/*Zcchc24* (mRNA)/Zcchc24 (protein) regulatory axis, which exerted its function through Zcchc24. *Zcchc24* is reported to be involved in cell differentiation in mice. Previous studies[42] have suggested that *Zcchc24* can serve as a key gene in liver cancer prediction models, which are used to predict patient survival time. Additionally, *Zcchc24* is one of the major selective splicing factors that plays a critical role in cell fate transition, development, and disease progression.

This study has several limitations. In this study, three samples per group were analyzed using high-throughput sequencing, which may have yielded biased results. Additionally, the levels of immune cells in each group were determined using the CIBERSORT algorithm. However, immune cell infiltration was not verified using alternate methods, such as single-cell sequencing. Furthermore, the importance of *Zcchc24* was not verified using knockdown or overexpression experiments.

CONCLUSION

In conclusion, this study demonstrated that GTPs can alleviate the DEHP-induced changes in liver function and lipid profiles, improve fatty liver disease and partial liver fibrosis, and regulate immune cell infiltration. Additionally, an important miRNA-mRNA-protein molecular regulation axis that plays a crucial role in the therapeutic effects of GTPs on DEHP-induced liver damage was validated.

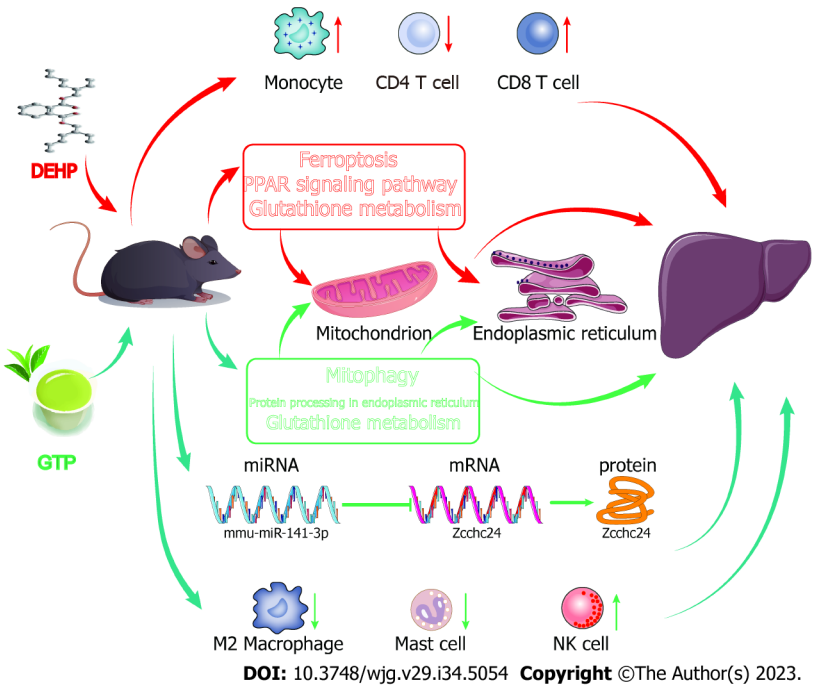

Figure 11 Mechanisms underlying di-(2-ethylhexyl) phthalate exposure-induced liver injury and the therapeutic effects of green tea polyphenols on Di (2-ethylhexyl) phthalate-indued liver injury. DEHP: Di (2-ethylhexyl) phthalate; GTPs: Green tea polyphenols.

ARTICLE HIGHLIGHTS

Research background

Di (2-ethylhexyl) phthalate (DEHP) is a widely used plasticizer that has been shown to cause liver injury. Previous studies have reported the therapeutic effects of green tea on organ damage caused by heavy metal exposure. However, there is limited research on the therapeutic effects of green tea polyphenols (GTPs) specifically on DEHP-induced liver damage.

Research motivation

Despite the known therapeutic effects of green tea on heavy metal exposure-induced organ damage, there is a lack of studies investigating the specific therapeutic effects of GTPs on DEHP-induced liver damage.

Research objectives

The research objectives of this study were to evaluate the molecular mechanism underlying the therapeutic effects of GTPs on DEHP-induced liver damage.

Research methods

In this study, C57BL/6J mice were divided into different groups and treated with DEHP and GTPs. After 8 wk, various assessments were conducted, including examination of liver function, blood lipid profile, and liver histopathology. High-throughput sequencing was used to analyze differentially expressed miRNAs and mRNAs in the liver tissues. Functional enrichment analysis and immune infiltration prediction were performed, and the miRNA-mRNA regulatory axis was elucidated using the starBase database. Protein expression was evaluated using immunohistochemistry.

Research results

The results of this study showed that GTPs had beneficial effects on DEHP-induced liver damage in mice. GTPs alleviated liver dysfunction, blood lipid dysregulation, fatty liver disease, liver fibrosis, and mitochondrial and endoplasmic reticulum lesions. The infiltration of immune cells, such as macrophages, mast cells, and natural killer cells, varied between the model and treatment groups. Furthermore, the study identified specific miRNAs, mRNAs, and proteins that constituted a regulatory axis involved in mediating the therapeutic effects of GTPs on DEHP-induced liver damage.

Research conclusions

The findings of this study indicate that GTPs have a therapeutic effect on DEHP-induced liver damage. GTPs were shown to alleviate liver dysfunction, blood lipid dysregulation, fatty liver disease, and partial liver fibrosis. Additionally, GTPs were found to regulate immune cell infiltration. The study also identified a significant miRNA-mRNA-protein regulatory axis involved in mediating the therapeutic effects of GTPs on DEHP-induced liver damage.

Research perspectives

Further studies are needed to investigate the long-term effects of GTPs on DEHP-induced liver damage and to explore the potential mechanisms underlying the regulation of immune cell infiltration. Additionally, future research should focus on optimizing the dosage and administration of GTPs to maximize their therapeutic effects and minimize potential side effects. Furthermore, clinical trials are warranted to evaluate the efficacy and safety of GTPs as a potential therapeutic intervention for DEHP-induced liver damage in humans.

ACKNOWLEDGEMENTS

We thank Bullet Edits Limited for the linguistic editing and proofreading of the manuscript. We also thank Figraw (www.figdraw.com) for the materials provided in the scientific research drawing.

FOOTNOTES

Author contributions: Shi H performed the conceptualization, software, data curation, software, writing; Zhao XH, Zhou XL, Sun CC, Cao QY, and Zhu SP contributed to the supervision and writing; Liu SS contributed to the pathology and analysis; Sun SY performed the review, editing, and supervision; all authors approved the final version of the article.

Supported by Guangdong Provincial Department of Science and Technology, Science and Technology Plan Project, Journal of Jinan University High-Level Science and Technology Journal Construction Project, No. 2021B121020012; and Guangdong Provincial Administration of Traditional Chinese Medicine, Traditional Chinese Medicine Research Project, No. 20213005.

Institutional review board statement: The study does not include Human subject research.

Institutional animal care and use committee statement: All animal experiments conformed to the internationally accepted principles for the care and use of laboratory animals (licence No. IACUC-20210630-15; protocol no. 2021621-01, The Laboratory Animal Welfare and Ethic Commettee, Jinan University, Guangzhou, China).

Conflict-of-interest statement: The authors declare no competing financial interest.

Data sharing statement: The data that support the findings of this study are openly available in the NCBI GEO database at https://www.ncbi.nlm.nih.gov/geo/ with the accession number: GSE232128.

ARRIVE guidelines statement: The authors have read the ARRIVE guidelines, and the manuscript was prepared and revised according to the ARRIVE guidelines.

Country/Territory of origin: China

ORCID number: Qin Peng 0000-0001-6243-3416; Sheng-Yun Sun 0000-0002-0374-8482.

S-Editor: Fan JR
L-Editor: A
P-Editor: Yuan YY

REFERENCES

1 **Liu Y**, Guo Z, Zhu R, Gou D, Jia PP, Pei DS. An insight into sex-specific neurotoxicity and molecular mechanisms of DEHP: A critical review. *Environ Pollut* 2023; **316**: 120673 [PMID: 36400143 DOI: 10.1016/j.envpol.2022.120673]

2 **Erythropel HC**, Maric M, Nicell JA, Leask RL, Yargeau V. Leaching of the plasticizer di(2-ethylhexyl)phthalate (DEHP) from plastic containers and the question of human exposure. *Appl Microbiol Biotechnol* 2014; **98**: 9967-9981 [PMID: 25376446 DOI: 10.1007/s00253-014-6183-8]

3 **Silva MJ**, Wong LY, Samandar E, Preau JL, Calafat AM, Ye X. Exposure to di-2-ethylhexyl terephthalate in a convenience sample of U.S. adults from 2000 to 2016. *Arch Toxicol* 2017; **91**: 3287-3291 [PMID: 28314884 DOI: 10.1007/s00204-017-1956-3]

4 **Kavlock R**, Boekelheide K, Chapin R, Cunningham M, Faustman E, Foster P, Golub M, Henderson R, Hinberg I, Little R, Seed J, Shea K, Tabacova S, Tyl R, Williams P, Zacharewski T. NTP Center for the Evaluation of Risks to Human Reproduction: phthalates expert panel report on the reproductive and developmental toxicity of di-n-octyl phthalate. *Reprod Toxicol* 2002; **16**: 721-734 [PMID: 12406498 DOI: 10.1016/s0890-6238(02)00031-x]

5 **Chen L**, Zhao Y, Li L, Chen B, Zhang Y. Exposure assessment of phthalates in non-occupational populations in China. *Sci Total Environ* 2012; **427-428**: 60-69 [PMID: 22578696 DOI: 10.1016/j.scitotenv.2012.03.090]

6 **Matsumoto M**, Hirata-Koizumi M, Ema M. Potential adverse effects of phthalic acid esters on human health: a review of recent studies on reproduction. *Regul Toxicol Pharmacol* 2008; **50**: 37-49 [PMID: 17983696 DOI: 10.1016/j.yrtph.2007.09.004]

7 **Jadeja RN**, Urrunaga NH, Dash S, Khurana S, Saxena NK. Withaferin-A Reduces Acetaminophen-Induced Liver Injury in Mice. *Biochem Pharmacol* 2015; **97**: 122-132 [PMID: 26212553 DOI: 10.1016/j.bcp.2015.07.024]

8 **Chen H**, Zhang W, Rui BB, Yang SM, Xu WP, Wei W. Di(2-ethylhexyl) phthalate exacerbates non-alcoholic fatty liver in rats and its potential mechanisms. *Environ Toxicol Pharmacol* 2016; **42**: 38-44 [PMID: 26773359 DOI: 10.1016/j.etap.2015.12.016]

9 **Yang G**, Zhang W, Qin Q, Wang J, Zheng H, Xiong W, Yuan J. Mono(2-ethylhexyl) phthalate induces apoptosis in p53-silenced L02 cells *via* activation of both mitochondrial and death receptor pathways. *Environ Toxicol* 2015; **30**: 1178-1191 [PMID: 24706461 DOI: 10.1002/tox.21990]

10 **Isenberg JS**, Kamendulis LM, Smith JH, Ackley DC, Pugh G Jr, Lington AW, Klaunig JE. Effects of Di-2-ethylhexyl phthalate (DEHP) on gap-junctional intercellular communication (GJIC), DNA synthesis, and peroxisomal beta oxidation (PBOX) in rat, mouse, and hamster liver. *Toxicol Sci* 2000; **56**: 73-85 [PMID: 10869455 DOI: 10.1093/toxsci/56.1.73]

11 **Ray PD**, Huang BW, Tsuji Y. Reactive oxygen species (ROS) homeostasis and redox regulation in cellular signaling. *Cell Signal* 2012; **24**: 981-990 [PMID: 22286106 DOI: 10.1016/j.cellsig.2012.01.008]

12 **Santhosh A**, Nair KG, Arun P, Deepadevi KV, Manojkumar V, Lakshmi LR, Kurup PA. Effect of DEHP [di-(2-ethyl hexyl) phthalate] on lipid peroxidation in liver in rats and in primary cultures of rat hepatocytes. *Indian J Med Res* 1998; **108**: 17-23 [PMID: 9745214]

13 **Ghosh J**, Das J, Manna P, Sil PC. Hepatotoxicity of di-(2-ethylhexyl)phthalate is attributed to calcium aggravation, ROS-mediated mitochondrial depolarization, and ERK/NF-κB pathway activation. *Free Radic Biol Med* 2010; **49**: 1779-1791 [PMID: 20854900 DOI: 10.1016/j.freeradbiomed.2010.09.011]

14 **Afzal M**, Safer AM, Menon M. Green tea polyphenols and their potential role in health and disease. *Inflammopharmacology* 2015; **23**: 151-161 [PMID: 26164000 DOI: 10.1007/s10787-015-0236-1]

15 **Mukhtar H**, Ahmad N. Tea polyphenols: prevention of cancer and optimizing health. *Am J Clin Nutr* 2000; **71**: 1698S-702S; discussion 1703S [PMID: 10837321 DOI: 10.1093/ajcn/71.6.1698S]

16 **Nagao T**, Hase T, Tokimitsu I. A green tea extract high in catechins reduces body fat and cardiovascular risks in humans. *Obesity (Silver Spring)* 2007; **15**: 1473-1483 [PMID: 17557985 DOI: 10.1038/oby.2007.176]

17 **Huang J**, Wang Y, Xie Z, Zhou Y, Zhang Y, Wan X. The anti-obesity effects of green tea in human intervention and basic molecular studies. *Eur J Clin Nutr* 2014; **68**: 1075-1087 [PMID: 25074392 DOI: 10.1038/ejcn.2014.143]

18 **Zwolak I**. Epigallocatechin Gallate for Management of Heavy Metal-Induced Oxidative Stress: Mechanisms of Action, Efficacy, and Concerns. *Int J Mol Sci* 2021; **22** [PMID: 33919748 DOI: 10.3390/ijms22084027]

19 **Zhao Z**, Lin CY, Cheng K. siRNA- and miRNA-based therapeutics for liver fibrosis. *Transl Res* 2019; **214**: 17-29 [PMID: 31476281 DOI: 10.1016/j.trsl.2019.07.007]

20 **El-Maraghy SA**, Adel O, Zayed N, Yosry A, El-Nahaas SM, Gibriel AA. Circulatory miRNA-484, 524, 615 and 628 expression profiling in HCV mediated HCC among Egyptian patients; implications for diagnosis and staging of hepatic cirrhosis and fibrosis. *J Adv Res* 2020; **22**: 57-66 [PMID: 31956442 DOI: 10.1016/j.jare.2019.12.002]

21 **Lin Q**, Zhou CR, Bai MJ, Zhu D, Chen JW, Wang HF, Li MA, Wu C, Li ZR, Huang MS. Exosome-mediated miRNA delivery promotes liver cancer EMT and metastasis. *Am J Transl Res* 2020; **12**: 1080-1095 [PMID: 32269736]

22 **Sanjay S**, Girish C. Role of miRNA and its potential as a novel diagnostic biomarker in drug-induced liver injury. *Eur J Clin Pharmacol* 2017; **73**: 399-407 [PMID: 28028586 DOI: 10.1007/s00228-016-2183-1]

23 **Hou P**, Dai W, Jin Y, Zhao F, Liu J, Liu H. Maternal exposure to di-2-ethylhexyl phthalate (DEHP) depresses lactation capacity in mice. *Sci Total Environ* 2022; **837**: 155813 [PMID: 35550907 DOI: 10.1016/j.scitotenv.2022.155813]

24 **XueXia L**, YaNan L, Zi T, YuSheng Z, ZeLin W, Peng Z, MeiNa X, FuJun L. Di-2-ethylhexyl phthalate (DEHP) exposure induces sperm quality and functional defects in mice. *Chemosphere* 2023; **312**: 137216 [PMID: 36372335 DOI: 10.1016/j.chemosphere.2022.137216]

25 **Zhou X**, Zhang Z, Shi H, Liu Q, Chang Y, Feng W, Zhu S, Sun S. Effects of Lycium barbarum glycopeptide on renal and testicular injury induced by di(2-ethylhexyl) phthalate. *Cell Stress Chaperones* 2022; **27**: 257-271 [PMID: 35362893 DOI: 10.1007/s12192-022-01266-0]

26 **Abdelrazek HM**, Helmy SA, Elsayed DH, Ebaid HM, Mohamed RM. Ameliorating effects of green tea extract on cadmium induced reproductive injury in male Wistar rats with respect to androgen receptors and caspase- 3. *Reprod Biol* 2016; **16**: 300-308 [PMID: 27840064 DOI: 10.1016/j.repbio.2016.11.001]

27 **Newman AM**, Liu CL, Green MR, Gentles AJ, Feng W, Xu Y, Hoang CD, Diehn M, Alizadeh AA. Robust enumeration of cell subsets from tissue expression profiles. *Nat Methods* 2015; **12**: 453-457 [PMID: 25822800 DOI: 10.1038/nmeth.3337]

28 **Chen Z**, Huang A, Sun J, Jiang T, Qin FX, Wu A. Inference of immune cell composition on the expression profiles of mouse tissue. *Sci Rep* 2017; **7**: 40508 [PMID: 28084418 DOI: 10.1038/srep40508]

29 **Onakpoya I**, Spencer E, Heneghan C, Thompson M. The effect of green tea on blood pressure and lipid profile: a systematic review and meta-analysis of randomized clinical trials. *Nutr Metab Cardiovasc Dis* 2014; **24**: 823-836 [PMID: 24675010 DOI: 10.1016/j.numecd.2014.01.016]

30 **Zhao ZB**, Ji K, Shen XY, Zhang WW, Wang R, Xu WP, Wei W. Di(2-ethylhexyl) phthalate promotes hepatic fibrosis by regulation of oxidative stress and inflammation responses in rats. *Environ Toxicol Pharmacol* 2019; **68**: 109-119 [PMID: 30884453 DOI: 10.1016/j.etap.2019.03.008]

31 **Kim HK**, Yang TH, Cho HY. Antifibrotic effects of green tea on in vitro and in vivo models of liver fibrosis. *World J Gastroenterol* 2009; **15**: 5200-5205 [PMID: 19891020 DOI: 10.3748/wjg.15.5200]

32 **Zhou J**, Yu Y, Ding L, Xu P, Wang Y. Matcha Green Tea Alleviates Non-Alcoholic Fatty Liver Disease in High-Fat Diet-Induced Obese Mice by Regulating Lipid Metabolism and Inflammatory Responses. *Nutrients* 2021; **13** [PMID: 34204055 DOI: 10.3390/nu13061950]

33 **Zhao Y**, Cui JG, Zhang H, Li XN, Li MZ, Talukder M, Li JL. Role of mitochondria-endoplasmic reticulum coupling in lycopene preventing DEHP-induced hepatotoxicity. *Food Funct* 2021; **12**: 10741-10749 [PMID: 34608470 DOI: 10.1039/d1fo00478f]

34 **Sun X**, Lin Y, Huang Q, Shi J, Qiu L, Kang M, Chen Y, Fang C, Ye T, Dong S. Di(2-ethylhexyl) phthalate-induced apoptosis in rat INS-1 cells is dependent on activation of endoplasmic reticulum stress and suppression of antioxidant protection. *J Cell Mol Med* 2015; **19**: 581-594 [PMID: 25418486 DOI: 10.1111/jcmm.12409]

35 **Lin Y**, Huang J, Gao T, Wu Y, Huang D, Yan F, Weng Z. Preliminary Study on Hepatoprotective Effect and Mechanism of (-)-

Epigallocatechin-3-gallate against Acetaminophen-induced Liver Injury in Rats. *Iran J Pharm Res* 2021; **20**: 46-56 [PMID: 34903968 DOI: 10.22037/ijpr.2020.112727.13918]

36 **Yin X**, Zeb R, Wei H, Cai L. Acute exposure of di(2-ethylhexyl) phthalate (DEHP) induces immune signal regulation and ferroptosis in oryzias melastigma. *Chemosphere* 2021; **265**: 129053 [PMID: 33272674 DOI: 10.1016/j.chemosphere.2020.129053]

37 **Giordano Attianese GM**, Desvergne B. Integrative and systemic approaches for evaluating PPARβ/δ (PPARD) function. *Nucl Recept Signal* 2015; **13**: e001 [PMID: 25945080 DOI: 10.1621/nrs.13001]

38 **Zhang Y**, Ge S, Yang Z, Li Z, Gong X, Zhang Q, Dong W, Dong C. Disturbance of di-(2-ethylhexyl) phthalate in hepatic lipid metabolism in rats fed with high fat diet. *Food Chem Toxicol* 2020; **146**: 111848 [PMID: 33166671 DOI: 10.1016/j.fct.2020.111848]

39 **Xu M**, Li Y, Wang X, Zhang Q, Wang L, Zhang X, Cui W, Han X, Ma N, Li H, Fang H, Tang S, Li J, Liu Z, Yang H, Jia X. Role of Hepatocyte- and Macrophage-Specific PPARγ in Hepatotoxicity Induced by Diethylhexyl Phthalate in Mice. *Environ Health Perspect* 2022; **130**: 17005 [PMID: 35019730 DOI: 10.1289/EHP9373]

40 **Yang Q**, Xie Y, Depierre JW. Effects of peroxisome proliferators on the thymus and spleen of mice. *Clin Exp Immunol* 2000; **122**: 219-226 [PMID: 11091278 DOI: 10.1046/j.1365-2249.2000.01367.x]

41 **Huang AC**, Cheng HY, Lin TS, Chen WH, Lin JH, Lin JJ, Lu CC, Chiang JH, Hsu SC, Wu PP, Huang YP, Chung JG. Epigallocatechin gallate (EGCG), influences a murine WEHI-3 leukemia model in vivo through enhancing phagocytosis of macrophages and populations of T- and B-cells. *In Vivo* 2013; **27**: 627-634 [PMID: 23988898]

42 **Apizi A**, Wang L, Wusiman L, Song E, Han Y, Jia T, Zhang W. Establishment and verification of a prognostic model of liver cancer by RNA-binding proteins based on the TCGA database. *Transl Cancer Res* 2022; **11**: 1925-1937 [PMID: 36249884 DOI: 10.21037/tcr-21-2820]

World Journal of Gastroenterology

Submit a Manuscript: https://www.f6publishing.com

World J Gastroenterol 2023 September 14; 29(34): 5075-5081

DOI: 10.3748/wjg.v29.i34.5075

ISSN 1007-9327 (print) ISSN 2219-2840 (online)

ORIGINAL ARTICLE

Retrospective Study

Role of biochemical markers and autoantibodies in diagnosis of early-stage primary biliary cholangitis

Yu-Jin Zhu, Jing Li, Yong-Gang Liu, Yong Jiang, Xiao-Jing Cheng, Xu Han, Chun-Yan Wang, Jia Li

Specialty type: Gastroenterology and hepatology

Provenance and peer review: Unsolicited article; Externally peer reviewed.

Peer-review model: Single blind

Peer-review report's scientific quality classification

Grade A (Excellent): 0
Grade B (Very good): B, B
Grade C (Good): 0
Grade D (Fair): 0
Grade E (Poor): 0

P-Reviewer: Filipec Kanizaj T, Croatia; Granito A, Italy

Received: June 4, 2023
Peer-review started: June 4, 2023
First decision: June 21, 2023
Revised: July 15, 2023
Accepted: August 25, 2023
Article in press: August 25, 2023
Published online: September 14, 2023

Yu-Jin Zhu, Jing Li, Graduate School, Tianjin Medical University, Tianjin 300041, China

Yong-Gang Liu, Department of Pathology, Clinical School of the Second People's Hospital, Tianjin 300110, China

Yong Jiang, Department of Gastroenterology, The Second Hospital of Tianjin Medical University, Tianjin 300211, China

Xiao-Jing Cheng, Xu Han, Chun-Yan Wang, Jia Li, Department of Gastroenterology, Clinical School of the Second People's Hospital, Tianjin 300110, China

Corresponding author: Chun-Yan Wang, Doctor, Chief Doctor, Department of Gastroenterology, Clinical School of the Second People's Hospital, No. 7 Sudi South Road, Nankai District, Tianjin 300110, China. wangchunyan123@tmu.edu.cn

Abstract

BACKGROUND

Primary biliary cholangitis (PBC) is a chronic progressive autoimmune cholestatic disease. The main target organ of PBC is the liver, and nonsuppurative inflammation of the small intrahepatic bile ducts may eventually develop into cirrhosis or liver fibrosis.

AIM

To explore the clinical characteristics of early-stage PBC, identify PBC in the early clinical stage, and promptly treat and monitor PBC.

METHODS

The data of 82 patients with PBC confirmed by pathology at Tianjin Second People's Hospital from January 2013 to November 2021 were collected, and the patients were divided into stage I, stage II, stage III, and stage IV according to the pathological stage. The general data, serum biochemistry, immunoglobulins, and autoimmune antibodies of patients in each stage were retrospectively analyzed.

RESULTS

In early-stage (stages I + II) PBC patients, 50.0% of patients had normal alanine aminotransferase (ALT) levels, and 37.5% had normal aspartate aminotransferase (AST) levels. For the remaining patients, the ALT and AST levels were mildly elevated; all of these patients had levels of < 3 times the upper limit of normal

values. The AST levels were significantly different among the three groups (stages I + II *vs* stage III *vs* stage IV, $P < 0.05$). In the early stage, 29.2% of patients had normal alkaline phosphatase (ALP) levels. The remaining patients had different degrees of ALP elevation; 6.3% had ALP levels > 5 times the upper limit of normal value. Moreover, γ-glutamyl transferase (GGT) was more robustly elevated, as 29.2% of patients had GGT levels of > 10 times the upper limit of normal value. The ALP values among the three groups were significantly different ($P < 0.05$). In early stage, the jaundice index did not increase significantly, but it gradually increased with disease progression. However, the above indicators were significantly different ($P < 0.05$) between the early-stage group and the stage IV group. With the progression of the disease, the levels of albumin and albumin/globulin ratio tended to decrease, and the difference among the three groups was statistically significant ($P < 0.05$). In early-stage patients, IgM and IgG levels as well as cholesterol levels were mildly elevated, but there were no significant differences among the three groups. Triglyceride levels were normal in the early-stage group, and the differences among the three groups were statistically significant ($P < 0.05$). The early detection rates of anti-mitochondria antibody (AMA) and AMA-M2 were 66.7% and 45.8%, respectively. The positive rate of anti-sp100 antibodies was significantly higher in patients with stage IV PBC. When AMA and AMA-M2 were negative, in the early stage, the highest autoantibody was anti-nuclear antibody (ANA) (92.3%), and in all ANA patterns, the highest was ANA centromere (38.5%).

CONCLUSION

In early-stage PBC patients, ALT and AST levels are normal or mildly elevated, GGT and ALP levels are not elevated in parallel, GGT levels are more robustly elevated, and ALP levels are normal in some patients. When AMA and AMA-M2 are negative, ANA especially ANA centromere positivity suggests the possibility of early PBC. Therefore, in the clinic, significantly elevated GGT levels with or without normal ALP levels and with ANA (particularly ANA centromere) positivity (when AMA and AMA-M2 are negative) may indicate the possibility of early PBC.

Key Words: Primary biliary cholangitis; Early stage; Biochemical makers; Autoantibodies; Pathology

Core Tip: This is a retrospective study of the characteristics of early-stage primary biliary cholangitis (PBC) patients, in which we found the suggestive role of γ-glutamyl transferase as an indicator of cholestasis in the early diagnosis of PBC. We also found that when anti-mitochondria antibody (AMA) and AMA-M2 were negative, positivity for anti-nuclear antibody (ANA) especially ANA centromere indicates early-stage PBC.

Citation: Zhu YJ, Li J, Liu YG, Jiang Y, Cheng XJ, Han X, Wang CY, Li J. Role of biochemical markers and autoantibodies in diagnosis of early-stage primary biliary cholangitis. *World J Gastroenterol* 2023; 29(34): 5075-5081
URL: https://www.wjgnet.com/1007-9327/full/v29/i34/5075.htm
DOI: https://dx.doi.org/10.3748/wjg.v29.i34.5075

INTRODUCTION

Primary biliary cholangitis (PBC) is a chronic progressive autoimmune cholestatic disease. The main target organ of PBC is the liver, and nonsuppurative inflammation of the small intrahepatic bile ducts may eventually develop into cirrhosis or liver fibrosis[1]. Currently, patients who are diagnosed and treated early respond well to ursodeoxycholic acid (UDCA) and have an estimated survival rate similar to that of the general population. Based on this, we retrospectively analyzed the data of patients with PBC in our hospital, aiming to analyze the biochemical parameters and autoimmune antibody characteristics of patients with early PBC to help identify early-stage PBC, actively treat this condition, and delay disease progression.

MATERIALS AND METHODS

Study design and sample collection

This retrospective observational study was conducted at the Clinical School of the Second People's Hospital. Patients were included if they met the following criteria: (1) Confirmed PBC (detected by "APASL clinical practice guidance: The diagnosis and management of patients with primary biliary cholangitis"). The diagnosis of PBC can be established when two or more of the following three criteria are met: (a) Biochemical evidence of cholestasis based mainly on the elevation of alkaline phosphatase (ALP) and gamma glutamyl transferase (GGT) with the exclusion of extrahepatic biliary

obstruction by imaging studies; (b) presence of anti-mitochondria antibody (AMA) or other PBC-specific anti-nuclear antibodies (ANAs) including anti-sp100 or anti-gp210; and (c) histologic evidence of non-suppurative destructive cholangitis mainly affecting the interlobular bile ducts; (2) underwent liver pathology biopsy and had a clear pathological stage; (3) initially diagnosed with PBC; and (4) were not previously treated with UDCA. Exclusion was based on the following criteria: (1) Various liver tumors; (2) other autoimmune diseases; (3) alcoholic liver disease, nonalcoholic fatty liver disease, and drug-induced liver injury; (4) active viral hepatitis; (5) obstructive cholestasis; (6) repeated liver biopsy; (7) incomplete information; (8) no defined pathological stage; (9) long-term application of UDCA; and (10) rejected liver biopsy (Figure 1).

Serological analysis

For the detection of ANA, a Hep-2 kit was used, according to standard indirect immunofluorescence (IIF) protocols. Each serum sample was investigated at a starting dilution of 1:100 and titrated to zero positive; samples with positive IIF at a titer ≥ 1:100 were deemed positive. Line immunoassay was used to detect AMA (M2), anti-sp100, and anti-gp210. According to Hep-2 cell patterns, ANAs were divided into nuclear (including homogeneous, cytoplasmic speckled, nucleolar, centromere, discrete, and nuclear) and cytoplasmic (including fibrillar, cytoplasmic speckled, and reticular)[2]. Pathology readings were performed by two experienced pathologists and at least one chief pathologist.

Statistical analysis

The data were analyzed with SPSS 25.0 software. Normally distributed data were analyzed by ANOVA and are expressed as the mean ± SD. Nonnormally distributed data were analyzed by the rank sum test and are expressed as medians and ranges. Count data are expressed as the number of subjects and percentages and were compared using the chi-square test. A difference was considered statistically significant at $P < 0.05$.

RESULTS

Comparison of general information among different groups

The age distribution of PBC patients ranged from 33-71 years, with an average age of 53.7 ± 8.9 years. The mean age in the three stage groups (stages I + II, stage III, and stage IV) was 52.4 ± 9.2 years, 57.7 ± 7.3 years, and 51.5 ± 8.7 years, respectively. The 82 patients with PBC were predominantly female (68/82), and the number of females in the three stage groups was 38, 20 and 10, respectively. There were no statistically significant differences in the mean age or sex proportion among the groups ($P > 0.05$).

In early-stage patients ($n = 48$), 18 (37.5%) patients did not have significant symptoms. The major symptoms of patients were gastrointestinal symptoms (including abdominal discomfort, pain, bloating, and nausea), fatigue, yellow urine, and pruritus.

Comparison of biochemical and immunological indicators among the three groups

The alanine aminotransferase (ALT) and aspartate aminotransferase (AST) levels were normal or mildly increased in the early-stage PBC patients, and an increasing trend with the progression of the pathological stage was observed. Furthermore, the AST levels were significantly different among the three groups ($P < 0.05$). There were significant differences in total bilirubin (TBIL), direct bilirubin (DBIL), and total bile acid (TBA) levels among the three groups of PBC patients ($P < 0.05$), and the difference between the early stage group and stage IV group was statistically significant ($P = 0.002$, 0.003, and 0.009, respectively). With pathological progression, a decreasing trend for albumin and albumin/globulin levels was observed, and there were statistically significant differences among the three groups and between the early stage group and stage IV group ($P = 0.005$ and 0.001, respectively). ALP and GGT levels were trending toward an increase. While 29.2% of patients had normal ALP levels, the remaining patients had different degrees of elevation. For 6.3% of the patients, the ALP levels were elevated to > 5 times the upper limit of normal value. The elevation in GGT levels was more robust, as 29.2% of patients had elevated GGT levels of > 10 times the upper limit of normal value. The difference of ALP levels among the three groups was statistically significant ($P < 0.05$), and there was a statistically significant difference between the early stage group and stage IV group ($P = 0.006$). Triglyceride levels gradually decreased with the progression of the disease, and the differences among the different groups were statistically significant ($P < 0.05$). Cholesterol (CHO) levels showed an increasing tendency. CHO levels gradually increased but were not significantly different among the three groups. IgG, IgA, and IgM all showed an increasing trend with disease progression. IgG and IgM were predominantly elevated, while IgA and complement (C)3 and C4 were normal in the early stage. The IgA levels were significantly different among the three groups ($P < 0.05$) (Table 1).

Autoantibody levels in different groups of patients with PBC

The positive rates of AMA, AMA-M2, anti-sp100, and anti-gp210 were 52 (63.4%), 40 (48.8%), 16 (19.5%), and 13 (15.9%), respectively. The positive rate of ANA was 62 (75.6%). Cytoplasmic speckled pattern had the highest rate of 48.8%, and this was followed by nuclear pattern at 23.2% and centromere pattern at 15.9%. The positive rate of AMA-M2 significantly differed among the three groups ($P = 0.045$), but the remaining autoantibodies were not significantly different ($P > 0.05$). In early-stage PBC patients, 32 patients were positive for AMA, 22 positive for AMA-M2, 8 positive for anti-sp100, and 9 positive for anti-gp210 (Table 2). Thirty-four patients were positive for ANA, of which 24 had cytoplasmic speckled pattern, 10 had nuclear pattern, and 6 had centromere pattern (Table 3).

Table 1 Clinical and laboratory data of patients with primary biliary cholangitis

	Early-stage (stages I + II; *n* = 48)	Stage III (*n* = 22)	Stage IV (*n* = 12)	*P* value
ALT	53.5 (29.5-124.5)	54.0 (30.0-127.6)	80.0 (42.8-127.4)	0.639
AST	53.5 (34.0-97.3)[a]	68.5 (39.6-114.1)	112.2 (81.1-136.3)	0.009
TBA	9.0 (3.6-36.4)[a]	18.0 (7.0-45.1)	28.2 (18.0-111.5)	0.011
TBIL	15.4 (11.2-27.8)[a]	16.7 (13.7-24.2)[a]	61.2 (28.1-114.3)	0.002
DBIL	5.2 (3.7-16.0)[a]	8.7 (2.5-12.4)[a]	42.3 (15.8-67.3)	0.003
ALB	42.1 (38.3-44.8)[a]	39.3 (36.5-42.5)	35.8 (30. 5-41.0)	0.005
A/G	1.2 (1.1-1.4)[a]	1.0 (0.9-1.3)	0.9 (0.7-1.1)	0.001
ALP	200.4 (117.8-414.0)[a]	292.5 (162.0-421.3)	463.5 (329.6-770.5)	0.008
GGT	289.0 (133.0-668.8)	532.0 (326. 5-764.3)	336.5 (264.0-648.0)	0.070
CHO	5.8 (4.6-6.9)	6.2 (5.1-7.5)	6.8 (4.9-7.0)	0.509
TG	1.3 (1.0-1.8)	1.6 (1.2-2.1)[a]	1.1 (0.8-1.5)	0.019
IgG	16.7 ± 4.6	17.6 ± 6.7	20.6 ± 7.9	0.056
IgA	2.9 (2.1-3.3)	3.5 (2.5-4.7)	3.4 (2.4-4.4)	0.031
IgM	3.4 (1.8-5.1)	3.7 (2.1-5.0)	3.7 (1.9-6.8)	0.967
C3	1.4 (1.2-1.6)	1.6 (1.3-1.8)	1.2 (1.0-1.7)	0.126
C4	0.2 (0.2-0.3)	0.2 (0.2-0.3)	0.2 (0.2-0.3)	0.963

[a]$P < 0.05$ indicates statistically significant difference compared to stage IV.
ALT: Alanine aminotransferase; AST: Aspartate aminotransferase; TBA: Total bile acid; ALP: Alkaline phosphatase; GGT: γ-glutamyl transferase; ALB: Albumin; A/G: Albumin/globulin; TBIL: Total bilirubin, DBIL: Direct bilirubin; CHO: Cholesterol; TG: Triglycerides; IgG: Immunoglobulin G; IgM: Immunoglobulin M; IgA: Immunoglobulin A; C3: Complement 3; C4: Complement 4.

Table 2 Autoantibody positive rate in patients with early-stage primary biliary cholangitis

Autoantibody	AMA	AMA-M2	Anti-sp100	Anti-gp210	Anti-SSA/Ro52	Anti-SSA/Ro60	ANA
n	32	22	8	9	8	2	34
%	66.7	45.8	16.7	18.8	16.7	4.2	70.8

AMA: Anti-mitochondria antibody; ANA: Anti-nuclear antibody.

Table 3 Anti-nuclear antibody subtype positive rate in patients with early-stage primary biliary cholangitis

ANA	Cytoplasmic speckled	Fibrillar	Reticular	Discrete	Homogeneous	Centromere	Nuclear speckled	Nucleolar	Nuclear
n	24	2	6	7	1	6	5	0	10
%	50	4.2	12.5	14.6	2.1	12.5	10.4	0	20.8

ANA: Anti-nuclear antibody.

Analysis of other autoantibodies detected when AMA and AMA-M2 are negative

There were 25 PBC patients negative for both AMA and AMA-M2. These included 13 patients in the early stage, 6 patients in stage III, and 6 patients in stage IV. The autoantibody positive rates among the three groups were not significantly different ($P > 0.05$). In early-stage AMA- and AMA-M2-negative patients, the positive rate was highest for ANA (92.3%), followed by anti-SSA/RO52 (23.1%) and anti-sp100 (15.3%). In all ANA patterns, the highest was ANA centromere (38.5%).

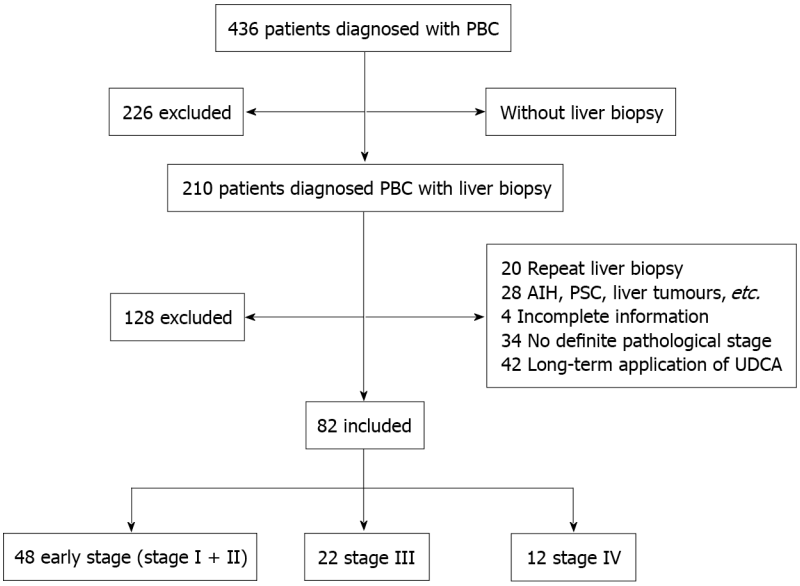

DOI: 10.3748/wjg.v29.i34.5075

Figure 1 Participant flow in the study. AIH: Autoimmune hepatitis; PSC: Primary sclerosing cholangitis; PBC: Primary biliary cholangitis; UDCA: Ursodeoxycholic acid.

DISCUSSION

PBC occurs mainly in middle-aged women, and the common clinical presentations are fatigue, splenomegaly, jaundice, and pruritus[1]. PBC may take 10-15 years to develop from the onset of illness to the symptomatic stage. Early diagnosis and treatment can improve the survival and quality of life of patients. In the early stage of PBC, patients have no obvious symptoms, but most patients have liver fibrosis or cirrhosis when they are diagnosed. Therefore, to improve PBC patient prognosis, early diagnosis and treatment are essential.

In this study, we found that GGT levels were significantly elevated in early-stage patients (29.2% of patients had elevated levels of > 10 times the upper limit of normal value) and tended to increase with the progression of illness. A study from Switzerland found elevated GGT levels in 15 of 24 PBC patients with normal ALP levels and liver biopsy results, and GGT levels were elevated in 13 patients who had early Nakanura stage histology. These findings suggest that elevated GGT levels have potential diagnostic value in PBC patients with normal ALP levels[3]. Reportedly, elevated GGT levels are closely related to the inflammation caused by fat deposition[4]. GGT is a key factor in maintaining the activity of reduced glutathione (GSH), which is an important antioxidant in the body. GGT is also involved in the production of GSH, which plays a cytoprotective role in inflammation and when an inflammatory response occurs[5]. In contrast to the levels of GGT, the levels of the cholestasis indicator ALP are not significantly elevated, and some PBC patients have normal ALP levels. Elevated ALP levels may be due to increased intracapillary pressure or to bile acids dissolving ALP from the lipid membrane into the blood[6]. A study of 67 patients with normal ALP levels and AMA positivity who underwent liver puncture biopsies found that 55 of these cases had pathology consistent with characteristic PBC presentation. Of these 55 patients, 50 were in the early stage[7]. In our study, we found that the elevation of GGT levels was more pronounced in patients with early-stage disease, which may be related to early chronic inflammation, excessive GSH depletion, and a compensatory increase in GGT.

We found that most patients had normal or mildly elevated ALT and AST levels in the early stage, and these levels increased with disease progression. These findings suggest that the degree of hepatocellular damage gradually increases. Alternatively, TBA, TBIL, and DBIL levels were not significantly elevated in the early stage but gradually increased with disease progression. In stage IV, TBIL and DBIL levels were significantly elevated, and DBIL levels were robustly elevated. This may be due to most of the hepatic parenchyma being damaged. In this study, IgM levels were predominantly elevated in early-stage PBC patients, which is consistent with previous studies[8]. A rise in IgM levels may be caused by a strong IgM secretory capacity and cellular autophagy[9].

AMA and AMA-M2 may be detectable in serum when patients are symptom-free and liver tests are normal, and they are highly specific autoantibodies for PBC. In recent years, with the development of detection methods, anti-sp100 and anti-gp210 have already been identified as PBC-specific autoantibodies. In a retrospective study of 4371 patients from Italy, the specificity of anti-sp100 and anti-gp210 for PBC was confirmed, especially in AMA-negative patients[10]. However, the reported positive rates vary widely across regions. The differences in antibody positive rates among regions could be due to different patient selection criteria and differences in technical and genetic backgrounds. In our study, the autoantibody rates of all patients were as follows: AMA, 63.4%; AMA-M2, 48.8%; and anti-gp210, 15.9%. These rates are lower than those reported in previous studies[11,12]. We found that the positive rate of anti-sp100 was 19.5%, and the positive rate of ANA was 75.6%. These rates are higher than those in other reports. One possible explanation for this is that our study did not adopt random sampling, but only patients with PBC confirmed by liver biopsy were included. This may be the main reason why the autoantibody positive rates in this study are lower than those in other

studies. The positive rates of AMA, AMA-M2, and anti-gp210 in early-stage patients with PBC were 66.7%, 45.8%, and 18.8%, respectively, which were similar to the rates of all PBC patients. The positive rate of anti-sp100 was significantly higher in stage IV PBC patients.

The number of AMA- and AMA-M2-negative PBC patients was 25, of which 13 (86.7%) were in the early stage. In early-stage AMA- and AMA-M2-negative patients, the positive rate of ANA was highest (92.3%). In all ANA patterns, the highest was ANA centromere (38.5%), which decreased with the progression of the disease. However, there were no significant differences in this parameter among the three groups ($P > 0.05$). In this article, we summarized available data on the characteristics of ANA patterns. We should be aware of the possibility of unexplained elevations in serum markers for cholestasis in AMA(M2)-negative patients, but ANA, especially centromere pattern, was positive in early-stage patients. Although those ANAs are not specific for PBC diagnostic purposes, they can still be used as auxiliary markers to reduce the rate of missed diagnoses when AMA(M2) is negative. A previous study reported that ANA centromere was almost exclusively limited to PBC patients. Thus, this antibody can still be used as an auxiliary marker to reduce the rate of missed diagnoses when AMA(M2) is negative[12].

CONCLUSION

In summary, in early-stage PBC patients, ALT and AST levels are normal or mildly elevated, GGT and ALP levels are not elevated in parallel, GGT levels are more robustly elevated, and ALP levels are normal in some patients. When AMA and AMA-M2 are negative, ANA (especially ANA centromere) positivity suggests the possibility of early PBC. Therefore, in the clinic, significantly elevated GGT levels with or without normal ALP levels and with ANA (particularly ANA centromere) positivity (when AMA and AMA-M2 are negative) may indicate the possibility of early PBC.

This study is a retrospective study with limited inclusion. Thus, it adopted nonrandom sampling with some bias. Further studies should be conducted in the future to expand the sample size and to follow up on the prognosis of patients with early-stage PBC after treatment with UDCA.

ARTICLE HIGHLIGHTS

Research background

The long course and insidious symptoms of primary biliary cholangitis (PBC) make it difficult to diagnose in the early stage.

Research motivation

To analyze clinical features and autoantibodies in patients with early-stage PBC.

Research objectives

To improve the diagnosis rates of early-stage PBC.

Research methods

We included 82 patients with PBC diagnosed by liver pathology with clear pathologic stage and divided them into three groups to compare their laboratory parameters and autoantibody positivity.

Research results

In early-stage PBC patients, alanine aminotransferase and aspartate aminotransferase levels were normal or mildly elevated, gamma glutamyl transferase (GGT) and alkaline phosphatase (ALP) levels were not elevated in parallel, GGT levels were more robustly elevated, and ALP levels were normal in some patients. When anti-mitochondria antibody (AMA) and AMA-M2 were negative, anti-nuclear antibody (ANA) (especially ANA centromere) positivity suggests the possibility of early-stage PBC.

Research conclusions

We found that GGT is elevated significantly and earlier in the early-stage PBC group. ANA and associated-ANA subtypes can be used as second-line markers for the diagnosis of early-stage PBC (particularly when specific autoantibodies are negative).

Research perspectives

We hope that this study will increase the rates of diagnosis of early-stage PBC by clinicians.

FOOTNOTES

Author contributions: Zhu YJ wrote the manuscript; Zhu YJ, Cheng XJ, and Han X contributed to data collation; Zhu YJ and Li J

contributed to statistical analysis; Liu YG contributed to liver pathology reading; Jiang Y, Wang CY, and Li J contributed to manuscript revision; Wang CY and Li J contributed to research supervision; Wang CY contributed to project design.

Institutional review board statement: The study protocol conforms to the ethical guidelines of the 1975 Declaration of Helsinki and was approved by the local Ethics Committee (Clinical School of the Second People's Hospital of Tianjin).

Informed consent statement: Patients were not required to give informed consent to the study because the analysis used anonymous clinical data that were obtained after each patient agreed to treatment by written consent.

Conflict-of-interest statement: All authors have no conflict of interest to disclose.

Data sharing statement: The data underlying this article can be available in this article and in its online supplementary material or from the first author.

Country/Territory of origin: China

ORCID number: Yu-Jin Zhu 0000-0003-3332-9606; Jing Li 0000-0001-5308-4146; Yong-Gang Liu 0000-0001-6165-564X; Yong Jiang 0000-0001-7402-5129; Xiao-Jing Cheng 0009-0008-8088-0103; Chun-Yan Wang 0000-0002-1074-1537; Jia Li 0000-0003-0100-417X.

S-Editor: Yan JP
L-Editor: Wang TQ
P-Editor: Yan JP

REFERENCES

1 **You H**, Ma X, Efe C, Wang G, Jeong SH, Abe K, Duan W, Chen S, Kong Y, Zhang D, Wei L, Wang FS, Lin HC, Yang JM, Tanwandee T, Gani RA, Payawal DA, Sharma BC, Hou J, Yokosuka O, Dokmeci AK, Crawford D, Kao JH, Piratvisuth T, Suh DJ, Lesmana LA, Sollano J, Lau G, Sarin SK, Omata M, Tanaka A, Jia J. APASL clinical practice guidance: the diagnosis and management of patients with primary biliary cholangitis. *Hepatol Int* 2022; **16**: 1-23 [PMID: 35119627 DOI: 10.1007/s12072-021-10276-6]

2 **Chan EK**, Damoiseaux J, Carballo OG, Conrad K, de Melo Cruvinel W, Francescantonio PL, Fritzler MJ, Garcia-De La Torre I, Herold M, Mimori T, Satoh M, von Mühlen CA, Andrade LE. Report of the First International Consensus on Standardized Nomenclature of Antinuclear Antibody HEp-2 Cell Patterns 2014-2015. *Front Immunol* 2015; **6**: 412 [PMID: 26347739 DOI: 10.3389/fimmu.2015.00412]

3 **Terziroli Beretta-Piccoli B**, Stirnimann G, Mertens J, Semela D, Zen Y, Mazzucchelli L, Voreck A, Kolbus N, Merlo E, Di Bartolomeo C, Messina P, Cerny A, Costantini S, Vergani D, Mieli-Vergani G; Swiss PBC Cohort Study Group. Primary biliary cholangitis with normal alkaline phosphatase: A neglected clinical entity challenging current guidelines. *J Autoimmun* 2021; **116**: 102578 [PMID: 33229138 DOI: 10.1016/j.jaut.2020.102578]

4 **Haring R**, Baumeister SE, Völzke H, Dörr M, Kocher T, Nauck M, Wallaschofski H. Prospective inverse associations of sex hormone concentrations in men with biomarkers of inflammation and oxidative stress. *J Androl* 2012; **33**: 944-950 [PMID: 22207707 DOI: 10.2164/jandrol.111.015065]

5 **Chen LW**, Huang MS, Shyu YC, Chien RN. Gamma-glutamyl transpeptidase elevation is associated with metabolic syndrome, hepatic steatosis, and fibrosis in patients with nonalcoholic fatty liver disease: A community-based cross-sectional study. *Kaohsiung J Med Sci* 2021; **37**: 819-827 [PMID: 34002481 DOI: 10.1002/kjm2.12395]

6 **Poupon R**. Liver alkaline phosphatase: a missing link between choleresis and biliary inflammation. *Hepatology* 2015; **61**: 2080-2090 [PMID: 25603770 DOI: 10.1002/hep.27715]

7 **Sun C**, Xiao X, Yan L, Sheng L, Wang Q, Jiang P, Lian M, Li Y, Wei Y, Zhang J, Chen Y, Li B, Huang B, Peng Y, Chen X, Fang J, Qiu D, Hua J, Tang R, Leung P, Gershwin ME, Miao Q, Ma X. Histologically proven AMA positive primary biliary cholangitis but normal serum alkaline phosphatase: Is alkaline phosphatase truly a surrogate marker? *J Autoimmun* 2019; **99**: 33-38 [PMID: 30709684 DOI: 10.1016/j.jaut.2019.01.005]

8 **Lleo A**, Liao J, Invernizzi P, Zhao M, Bernuzzi F, Ma L, Lanzi G, Ansari AA, Coppel RL, Zhang P, Li Y, Zhou Z, Lu Q, Gershwin ME. Immunoglobulin M levels inversely correlate with CD40 ligand promoter methylation in patients with primary biliary cirrhosis. *Hepatology* 2012; **55**: 153-160 [PMID: 21898485 DOI: 10.1002/hep.24630]

9 **Lian C**, Zhao Y, Sun J, Zhao L, Zhang F. Role of cell autophagy in the generation of IgM and hepatic fibrosis in primary biliary cholangitis. *Clin Rheumatol* 2020; **39**: 3499-3506 [PMID: 32382831 DOI: 10.1007/s10067-020-05111-6]

10 **Granito A**, Muratori P, Muratori L, Pappas G, Cassani F, Worthington J, Guidi M, Ferri S, DE Molo C, Lenzi M, Chapman RW, Bianchi FB. Antinuclear antibodies giving the 'multiple nuclear dots' or the 'rim-like/membranous' patterns: diagnostic accuracy for primary biliary cirrhosis. *Aliment Pharmacol Ther* 2006; **24**: 1575-1583 [PMID: 17206945 DOI: 10.1111/j.1365-2036.2006.03172.x]

11 **Lindor KD**, Bowlus CL, Boyer J, Levy C, Mayo M. Primary Biliary Cholangitis: 2018 Practice Guidance from the American Association for the Study of Liver Diseases. *Hepatology* 2019; **69**: 394-419 [PMID: 30070375 DOI: 10.1002/hep.30145]

12 **Granito A**, Muratori P, Quarneti C, Pappas G, Cicola R, Muratori L. Antinuclear antibodies as ancillary markers in primary biliary cirrhosis. *Expert Rev Mol Diagn* 2012; **12**: 65-74 [PMID: 22133120 DOI: 10.1586/erm.11.82]

World Journal of Gastroenterology

Submit a Manuscript: https://www.f6publishing.com

World J Gastroenterol 2023 September 14; 29(34): 5082-5090

DOI: 10.3748/wjg.v29.i34.5082

ISSN 1007-9327 (print) ISSN 2219-2840 (online)

CASE REPORT

Simultaneous rectal neuroendocrine tumors and pituitary adenoma: A case report and review of literature

Jing-Yi Li, Jie Chen, Jun Liu, Su-Zhen Zhang

Specialty type: Gastroenterology and hepatology

Provenance and peer review: Unsolicited article; Externally peer reviewed.

Peer-review model: Single blind

Peer-review report's scientific quality classification
Grade A (Excellent): 0
Grade B (Very good): B, B
Grade C (Good): 0
Grade D (Fair): 0
Grade E (Poor): 0

P-Reviewer: Hasan A, Egypt; Lykoudis PM, United Kingdom

Received: April 19, 2023
Peer-review started: April 19, 2023
First decision: May 27, 2023
Revised: June 9, 2023
Accepted: August 18, 2023
Article in press: August 18, 2023
Published online: September 14, 2023

Jing-Yi Li, Su-Zhen Zhang, Department of Gastroenterology, Cancer Hospital Affiliated to Shanxi Medical University, Taiyuan 030000, Shanxi Province, China

Jie Chen, Department of Neuroendocrine Tumor, Fudan University Shanghai Cancer Center, Shanghai 200032, China

Jun Liu, Department of Gastroenterology, Shanxi Bethune Hospital, Taiyuan 030032, Shanxi Province, China

Corresponding author: Su-Zhen Zhang, MM, Chief Physician, Department of Gastroenterology, Cancer Hospital Affiliated to Shanxi Medical University, No. 3 Gongxin Street, Xinghualing District, Taiyuan 030000, Shanxi Province, China. zhangsuzhen209@163.com

Abstract

BACKGROUND

Neuroendocrine tumors (NET) are rare heterogeneous tumors that arise from neuroendocrine cells throughout the body. Acromegaly, a rare and slowly progressive disorder, usually results from a growth hormone (GH)-secreting pituitary adenoma.

CASE SUMMARY

We herein describe a 38-year-old patient who was initially diagnosed with diabetes. During colonoscopy, two bulges were identified and subsequently removed through endoscopic submucosal dissection. Following the surgical intervention, the excised tissue samples were examined and confirmed to be grade 2 NET. ^{18}F-ALF-NOTATATE positron emission tomography-computed tomography (PET/CT) and ^{68}Ga-DOTANOC PET/CT revealed metastases in the peri-intestinal lymph nodes, prompting laparoscopic low anterior resection with total mesorectal excision. The patient later returned to the hospital because of hyperglycemia and was found to have facial changes, namely a larger nose, thicker lips, and mandibular prognathism. Laboratory tests and magnetic resonance imaging (MRI) suggested a GH-secreting pituitary adenoma. The pituitary adenoma shrunk after treatment with octreotide and was neuroendoscopically resected *via* a trans-sphenoidal approach. Whole-exome sequencing analysis revealed no genetic abnormalities. The patient recovered well with no evidence of recurrence during follow-up.

CONCLUSION

^{18}F-ALF-NOTATE PET/CT and MRI with pathological analysis can effectively

diagnose rare cases of pituitary adenomas complicated with rectal NET.

Key Words: Neuroendocrine neoplasm; Pituitary adenoma; Rectum; Diagnosis; Case report

Core Tip: We herein present a rare case of rectal dual-source grade 2 neuroendocrine tumors with a pituitary growth hormone-secreting tumor that caused acromegaly and diabetes. The rarity of this combination makes an accurate diagnosis difficult to achieve. The correct diagnosis can be obtained by using ^{18}F-ALF-NOTATATE-positron emission tomography–computed tomography and magnetic resonance imaging combined with pathological analysis.

Citation: Li JY, Chen J, Liu J, Zhang SZ. Simultaneous rectal neuroendocrine tumors and pituitary adenoma: A case report and review of literature. *World J Gastroenterol* 2023; 29(34): 5082-5090
URL: https://www.wjgnet.com/1007-9327/full/v29/i34/5082.htm
DOI: https://dx.doi.org/10.3748/wjg.v29.i34.5082

INTRODUCTION

Neuroendocrine tumors (NETs) are a heterogeneous group of rare tumors that exhibit complex clinical behaviors. They typically originate from peptidergic neurons and neuroendocrine cells throughout the body, with gastroenteropancreatic NETs being the predominant form. The rectum is the most common location of these tumors, accounting for 37.4% of cases[1,2]. Acromegaly, another rare disorder that often goes undiagnosed, is a chronic, progressive endocrine and metabolic disease with an inconspicuous onset. The main cause of acromegaly is excessive production of growth hormone (GH), and > 95% of patients with enlarged limbs have pituitary adenomas that secrete GH[3]. GH stimulates the liver to produce insulin-like growth factor-1 (IGF-1), and excessive proliferation of soft tissue, bone, and cartilage can occur secondary to long-term excessive secretion of GH and IGF-1. This results in the typical symptom of enlarged limbs and can have a significant impact on various organ systems, such as the respiratory, cardiovascular, digestive, and glucose metabolism systems. Compression or invasion of pituitary adenomas can result in headaches, visual impairment, and adenohypophysis. The median age at diagnosis of acromegaly ranges from 40.5 years to 47.0 years, with delays in diagnosis lasting from 4.5 years to 9.0 years. Delayed diagnosis can significantly increase the incidence of complications and difficulty in treating patients with large limbs. In this case report, we describe a 38-year-old woman who was diagnosed with two concurrent grade 2 (G2) rectal NETs and a pituitary adenoma on the basis of ^{18}F-ALF-NOTATATE positron emission tomography-computed tomography (PET/CT) and ^{18}F-fluorodeoxyglucose (^{18}F-FDG) PET/CT findings. To the best of our knowledge, the combination of simultaneous rectal NETs and a GH-secreting pituitary adenoma has not been previously reported. To diagnose this disorder, patients may undergo both ^{18}F-ALF-NOTATATE PET/CT and ^{18}F-FDG PET/CT scans, which can reveal small lesions that cannot be detected through conventional imaging. However, routine imaging examination by CT may fail to identify pelvic metastatic lymph nodes. Because of an abnormal blood glucose concentration, a patient may initially be suspected of having diabetes and given hypoglycemic treatment. However, if the patients' blood glucose control remains poor, their clinical manifestations may be hidden, and changes in their limbs and face may only be detected long after the onset of symptoms. A multidisciplinary approach involving various specialists in the fields of endocrinology, neurosurgery, imaging, pathology, oncology, and others is required for the diagnosis and treatment of NETs. Multidisciplinary diagnosis and treatment can significantly enhance the standardization, accuracy, and individualization of patient management. Collaborative diagnosis and treatment can lead to improvement of patients' quality of life, early diagnosis of diseases, better symptom management, prevention of complications, and reduced psychological distress.

CASE PRESENTATION

Chief complaints

A 38-year-old woman was admitted to our hospital for evaluation of long-standing chronic constipation and polydipsia.

History of present illness

Upon admission to the hospital, the patient underwent colonoscopy, which revealed two masses. The masses were confirmed to be G2 NETs after endoscopic submucosal dissection and pathological examination. Peri-intestinal lymph node metastasis was detected using ^{18}F-ALF-NOTATATE PET/CT and ^{18}F-FDG PET/CT, leading to treatment by laparoscopic low anterior resection with total mesenterectomy. After surgery, the patient exhibited symptoms of poor blood glucose control, and further examination revealed the presence of a pituitary macroadenoma. The patient received three cycles of octreotide acetate before undergoing surgical intervention for the pituitary macroadenoma.

History of past illness
The patient was diagnosed with diabetes on the basis of polydipsia and abnormal blood glucose concentrations.

Personal and family history
She had no family history of NETs or psychological or genetic disorders.

Physical examination
All vital signs were stable and physical examination revealed no notable abnormalities.

Laboratory examinations
Laboratory examinations showed that the patient had a high GH concentration at 47.79 ng/mL (reference range, 0.126-9.88 ng/mL) and high IGF-1 concentration at 497 ng/mL (reference range, 111-284 ng/mL). However, she had normal serum concentrations of sex hormones, adrenocorticotropic hormone (ACTH), thyrotropin, free thyroid hormone, and prolactin. Blood samples were collected at Peking Union Medical College Hospital 0, 30, 60, 120, and 180 min after a standard 75-g glucose test; at each of these time points, her plasma GH concentration was 29.1, 20.9, 19.2, 23.2, and 28.4 ng/mL, respectively.

Imaging examinations
^{18}F-ALF-NOTATATE PET/CT and ^{18}F-FDG PET/CT were performed to detect metastases (Figure 1A and B). ^{18}F-ALF-NOTATATE PET/CT clearly revealed metastases and high uptake in three peri-rectal and pre-sacral lymph nodes with a maximum standardized uptake value (SUV) of 13.24, 7.31, and 5.55, respectively, whereas these findings were not depicted on ^{18}F-FDG PET/CT. The patient then underwent ^{68}Ga-DOTANOC PET/CT at the First Affiliated Hospital of Sun Yat-Sen University. The ^{68}Ga-DOTANOC PET/CT findings were consistent with the ^{18}F-ALF-NOTATATE PET/CT findings, showing that the largest affected lymph node had a maximum SUV of 4.8 (Figure 1C and D).

FINAL DIAGNOSIS
The patient was diagnosed with rectal NETs with peripheral lymph node metastasis. The final pathology report listed rectal NETs, G2, stage T1N1M0 with 4/15 lymph node metastases. The patient also had acromegaly and secondary diabetes caused by a GH-secreting pituitary adenoma.

TREATMENT
Because of chronic constipation, colonoscopy was performed and revealed two lesions of 1.0 cm and 1.8 cm in diameter located 3.0 cm from the anus (Figure 2). These rectal lesions were resected by minimally invasive endoscopic submucosal dissection on 27 June 2019. Pathological examination of the two rectal specimens suggested histologic G2 NETs that were positive for synaptophysin and CD56 but negative for chromogranin A (Figure 3). The Ki67 index was 7% for the 1.8-cm-diameter tumor and 4% for the 1.0-cm-diameter tumor. Strong expression of SSTR2 (+++) suggested a predominance of the SSTR2 subtype. Only a few scattered cells were phosphorylated histone H3-positive. The larger lesion was 0.1 cm from the circumferential margin, whereas the smaller lesion was adjacent to the excision edge. ^{18}F-ALF-NOTATATE PET/CT and ^{18}F-FDG PET/CT scans in our hospital showed metastasis and high uptake in three perirectal and presacral lymph nodes. Laparoscopic low anterior resection with total mesorectal excision was performed 5 mo after diagnosis of the rectal lesions. Histological analysis of the operative specimens showed that the lymph nodes contained neuroendocrine cells. Immunohistochemical staining was positive for synaptophysin and CD56 but negative for chromogranin A. The Ki67 index was 3% (Figure 4). Four months after the rectal lesion was diagnosed by pathological examination, the patient returned to the local hospital because of hyperglycemia, and examination revealed facial changes including an enlarged nose, thickened lips, and mandibular kyphosis. A 2.4 cm × 1.3 cm × 1.3 cm pituitary adenoma was revealed by contrast-enhanced magnetic resonance imaging (MRI) (Figure 5). The GH-secreting pituitary macroadenoma was diagnosed by pathological examination. The patient was treated with long-acting octreotide (20 mg) at an interval of 28 d, and the lesion was reduced to 1.16 cm × 0.61 cm × 1.27 cm after three courses of treatment. The patient then underwent successful neuroendoscopic pituitary surgery *via* a trans-sphenoidal approach with sellar base reconstruction. Postoperative pathological examination confirmed the diagnosis of a pituitary adenoma, which was positive for GH and CAM5.2, was negative for ACTH, and had a Ki67 index of < 1%. The patients' skin condition significantly improved, becoming smoother and more refined after undergoing neuroendoscopic pituitary gland surgery. Moreover, her biochemical indicators consistently remained within the reference range postoperatively, especially with regard to her blood glucose control, which normalized without the need for hypoglycemic drugs. Given that the patients' GH-secreting pituitary tumor was a macroadenoma, direct surgery was challenging and complete removal was difficult. However, the tumor gradually decreased in size with the three cycles of octreotide acetate microsphere treatment, allowing successful R0 resection through timely surgical intervention. Thereafter, follow-up head MRI findings remained normal and the serum GH and IGF-1 concentrations consistently stayed within the reference range.

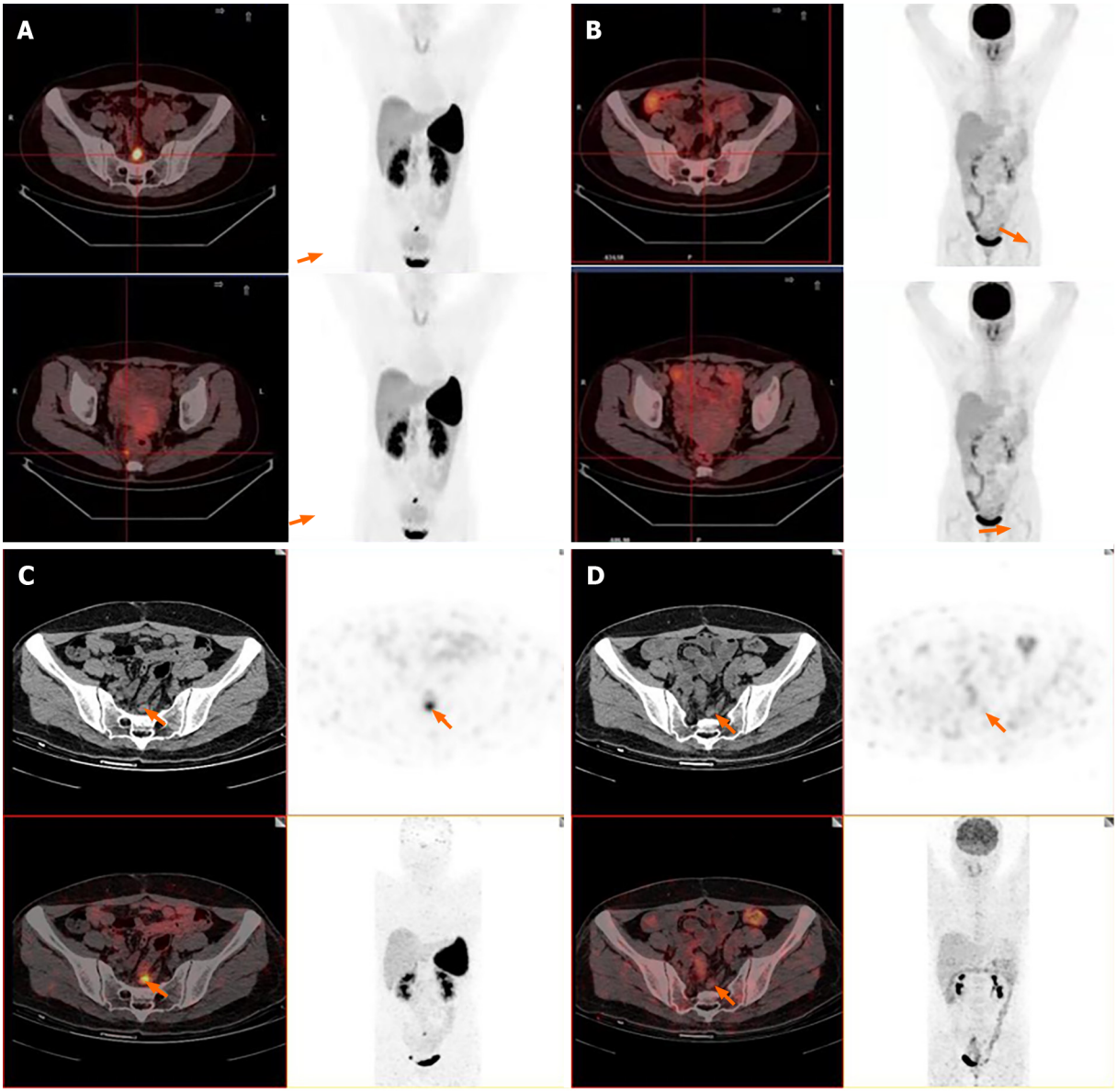

DOI: 10.3748/wjg.v29.i34.5082

Figure 1 Images. A and B: ^{18}F-ALF-NOTATATE positron emission tomography-computed tomography (PET/CT) images and corresponding ^{18}F-fluorodeoxyglucose (^{18}F-FDG) PET/CT images in a patient with rectal neuroendocrine tumors in our hospital; C and D: ^{68}Ga-DOTANOC PET/CT and ^{18}F-FDG PET/CT images in the First Affiliated Hospital of Sun Yat-sen University.

OUTCOME AND FOLLOW-UP

The patient returned for follow-up at 4, 13, and 16 mo after her pituitary surgery. No evidence of recurrence was found, and she remained asymptomatic.

DISCUSSION

Rectal NETs can cause symptoms such as bleeding or changes in bowel habits; however, many patients are asymptomatic. The incidence of gastrointestinal NETs, including rectal NETs, is increasing, with a reported incidence of 1.04 per 100000 individuals per year according to the surveillance, epidemiology and end results database[4]. This increase is likely due to improved diagnostic endoscopy rather than a genuine increase in incidence.

Approximately 80% of rectal NETs are small (< 1 cm). There is typically no invasion or metastasis at the time of initial diagnosis. A strong correlation reportedly exists between the tumor size and spread, with only 2% of tumors under 1 cm having metastasized. The incidence of metastasis of rectal NETs ranges from 10% to 15% for 1- to 2-cm tumors but increases to 60% to 80% for tumors larger than 2 cm[5-7]. Treatment for localized G1 and G2 rectal NETs can be purely endoscopic, whereas low anterior resection of the rectum and removal of lymph nodes is necessary for advanced, localized rectal NETs. Most rectal NETs are located in the mid-section of the rectum, approximately 5 cm to 10 cm from

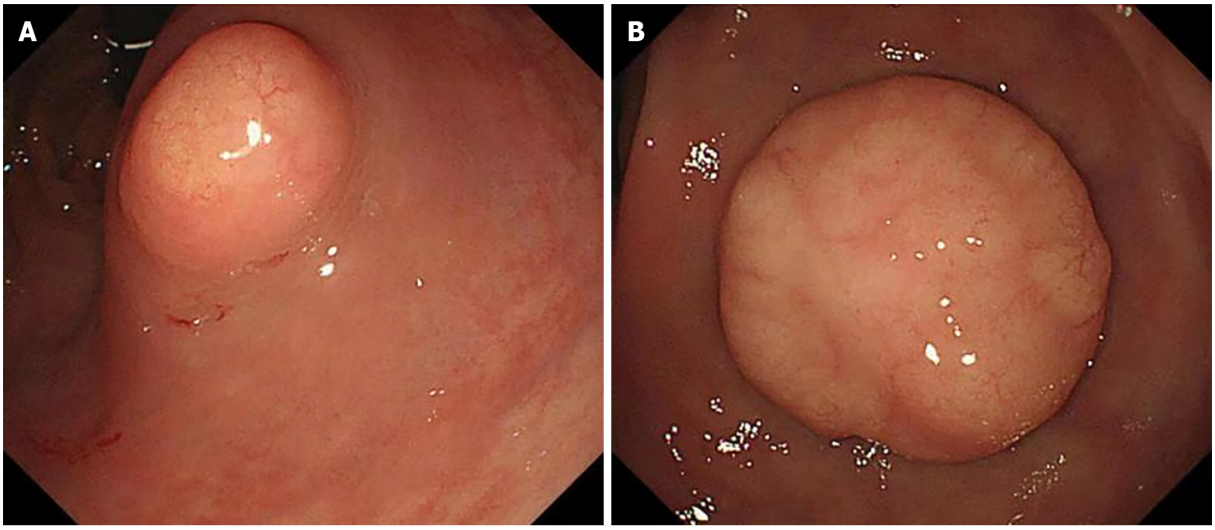

DOI: 10.3748/wjg.v29.i34.5082

Figure 2 Two lesions. A: The one lesion at the lower rectum under colonoscopy; B: The second lesion at the lower rectum under colonoscopy.

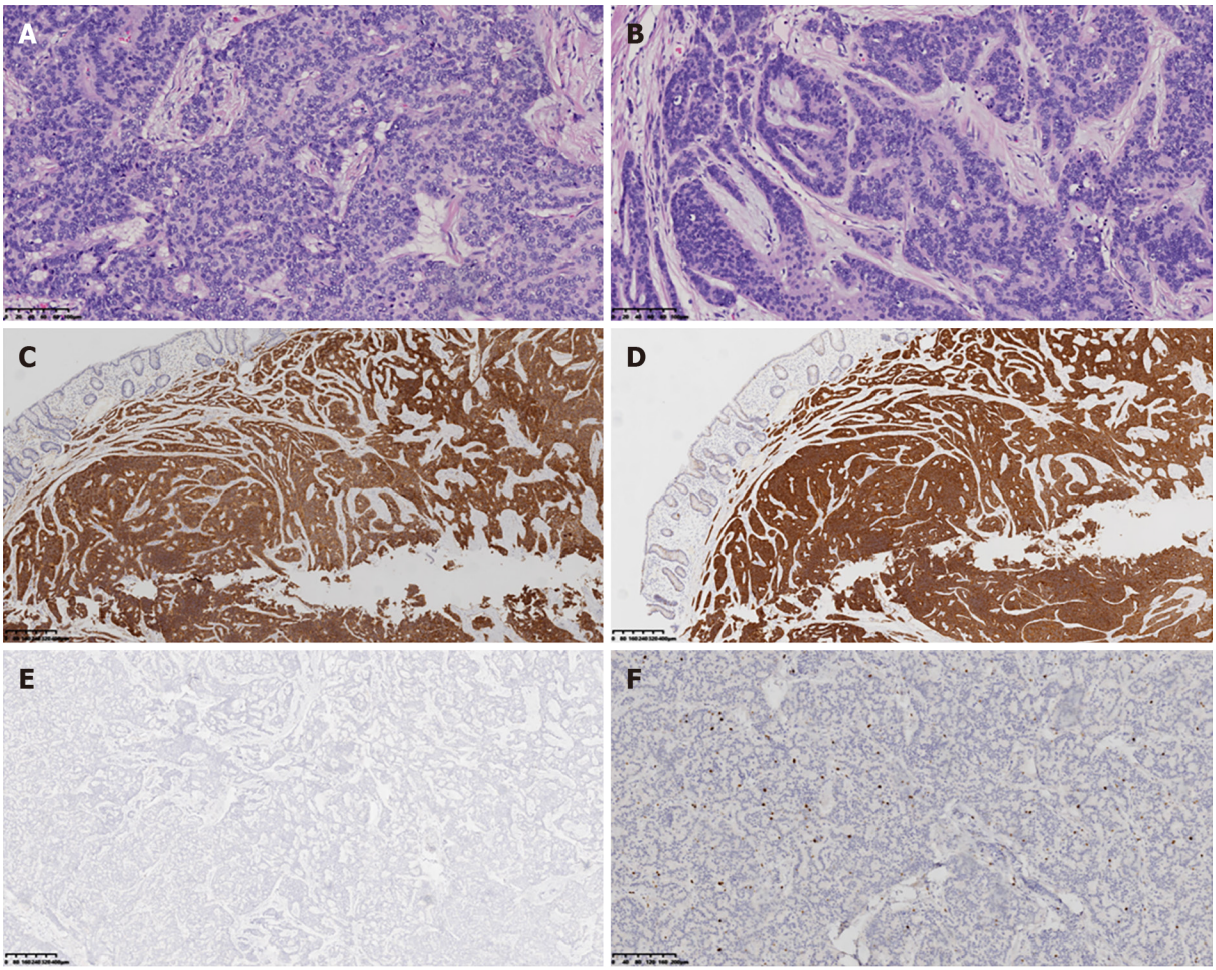

DOI: 10.3748/wjg.v29.i34.5082

Figure 3 Hematoxylin-eosin staining and immunohistochemical staining. A and B: Hematoxylin-eosin staining shows the pathological features of rectal neuroendocrine tumors in the larger and smaller tumor tissue specimens (20 ×); C-E: Immunohistochemical staining of neuroendocrine markers CD56, Syn, and CgA in representative tumor tissue selected by the physician (4 ×); F: Ki-67 expression in the neuroendocrine tumor at the rectum by immunohistochemistry (10 ×). Brown nuclear stain highlights Ki-67-positive tumor cells.

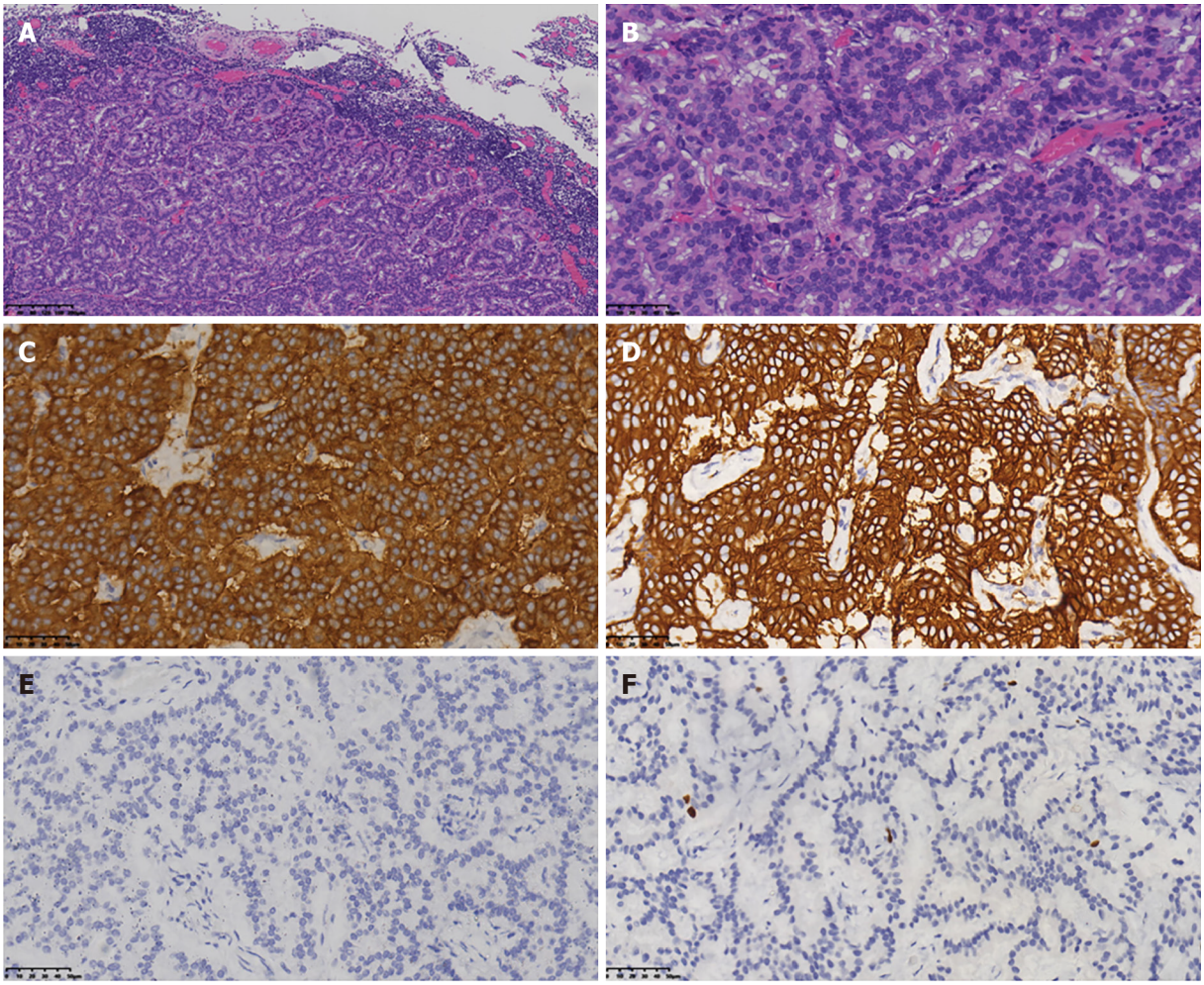

DOI: 10.3748/wjg.v29.i34.5082

Figure 4 Tumor metastasis was observed in the peri-intestinal lymph nodes (4/15). A and B: Laparoscopic low anterior resection with total mesorectal excision was performed 5 mo after diagnosis of the rectal lesions. Central lymph nodes were selected from the lesion for hematoxylin–eosin staining to evaluate the metastasis of neuroendocrine cells (A: 100 ×, B: 400 ×); C-E: Immunohistochemical detection to evaluate the expression and distribution of neuroendocrine markers SSTR2, syn, and CgA in central lymph nodes (400 ×); F: Ki-67 expression in central lymph nodes by immunohistochemistry (400 ×).

the anus[5,8]. In the present case, concurrent rectal G2 NETs were detected in the distal rectum approximately 3 cm from the anus. ^{18}F-ALF-NOTATATE PET/CT showed evidence of lymph node metastases, making this the first patient to be diagnosed with NETs by a combination of ^{18}F-ALF-NOTATATE PET/CT and ^{18}F-FDG PET/CT in our hospital. To confirm these findings, we referred the patient to the First Affiliated Hospital of Sun Yat-Sen University for a ^{68}Ga-DOTANOC PET/CT scan, the results of which were consistent with our initial findings. The ^{18}F-based method is promising, with ^{18}F-octreotide being a potential alternative to ^{68}Ga-DOTA peptides. ^{18}F-AlF-NOTA-octreotide (^{18}F-OC) is a peptide imaging agent that can be rapidly synthesized and demonstrates strong uptake by tumors[9,10]. The combination of ^{18}F-FDG and ^{18}F-OC PET/CT has the potential to enhance the staging and management of neuroendocrine neoplasms [11]. At our hospital, more than 200 patients have undergone combined ^{18}F-ALF-NOTATATE PET/CT and ^{18}F-FDG PET/CT scanning to detect rectal NETs.

Pituitary adenomas are among the most common primary central nervous system tumors; their estimated prevalence is 17% of all such tumors[12-14]. Approximately half (46%-64%) of these tumors are hormone-secreting (*i.e.* functional). Frequently secreted hormones include prolactin, GH, thyrotropin, and ACTH. GH-secreting adenomas account for 13% to 20% of hormone-secreting pituitary adenomas. They cause gigantism before and acromegaly after closure of the epiphyseal growth plates[15-17]. GH hypersecretion leads to acral enlargement (77%), coarse facial features (54%), profuse sweating (52%), and insulin resistance (15%). A diagnosis of acromegaly is often confirmed by a high serum concentration of IGF-1. When the IGF-1 concentration is equivocal, an oral glucose tolerance test may be performed, and the absence of GH suppression to < 1 ng/mL is indicative of acromegaly[18]. MRI of the pituitary gland is used to assess the size and location of an adenoma. Our patient was diagnosed with a pituitary adenoma resulting in acromegaly and diabetes mellitus. Despite being histologically benign, hormone-secreting pituitary adenomas are associated with significant morbidity resulting from their direct impact on surrounding neurovascular structures and/or excessive hormone secretion, both of which may lead to a shortened lifespan[19-21]. Early diagnosis and effective management are critical for reducing morbidity and minimizing mortality.

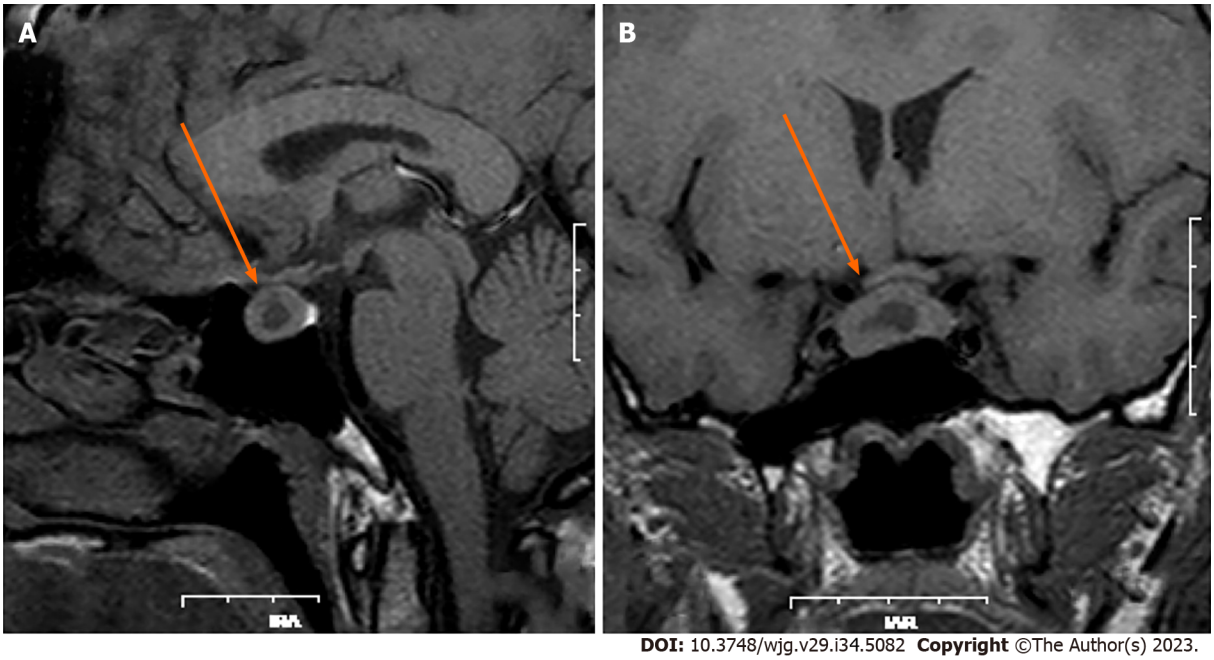

DOI: 10.3748/wjg.v29.i34.5082

Figure 5 Magnetic resonance imaging for pituitary adenoma. A: Pretreatment with long-acting octreotide (20 mg); B: Pretreatment with long-acting octreotide (20 mg) for 28 d.

The global prevalence of acromegaly, a rare and slowly progressive disorder, is approximately 60 per million. Acromegaly occurs when the pituitary gland produces too much GH[22-24]. Pituitary adenomas, which are responsible for approximately 90% of cases of acromegaly, are often very large at the time of detection because of delays in diagnosis. We have herein reported a very rare case. Although familial hereditary syndromes can be linked to the disease, our patient had no known family history of NETs, and whole-exome sequencing with an illumina genome analyzer (Illumina, San Diego, CA, United States) at Jinyu Medicine revealed no genetic abnormalities.

Krug *et al*[25] described a patient with acromegaly that was caused not by a pituitary adenoma but instead by a sporadic pulmonary NET[26]. Here, we have reported the simultaneous occurrence of rectal NETs with a GH-secreting pituitary adenomas; to the best of our knowledge, this combination of tumors has not been previously reported. The increased risk of colonic polyposis in individuals with acromegaly is well-recognized[21]. Several studies have shown that patients with acromegaly have a 2 to 14-fold increased risk of colon cancer compared with the normal population[27-30]. Furthermore, nodular thyroid disease is frequently seen in patients with acromegaly[31], some of whom have thyroid malignancies. The co-occurrence of rectal NETs and a GH-secreting pituitary adenoma in the present patient may have been coincidental. There is emerging evidence of an association between the GH/IGF-1 endocrine axis and cancer progression[32]. Excessive secretion of GH and IGF-1 by the pituitary adenoma may have stimulated the growth of our patients' rectal NETs. Surgical resection of the adenoma is the preferred treatment option for patients diagnosed with a GH-secreting pituitary adenoma. This approach can effectively eliminate or reduce the adenoma and decrease the levels of GH and IGF-1. The transsphenoidal approach is the primary method utilized to perform surgical interventions on pituitary adenomas, whereas craniotomy is only required in rare cases. Despite significant advancements in surgical techniques, there are still inherent risks associated with major extremity surgery, such as olfactory disturbance; hypopituitarism; temporary or permanent central diabetes insipidus; damage to vital nerves, blood vessels, brain tissue, and the blood supply of the skull base, resulting in postoperative cranial nerve dysfunction such as optic nerve impairment; cerebrospinal fluid rhinorrhea; meningitis; bacteremia; sepsis; hypothalamic syndrome; and even death. Patients with GH-secreting pituitary adenomas are at significantly higher risk when undergoing general anesthesia than are patients with other types of pituitary adenomas. These risks include abnormal cardiopulmonary function, increased perioperative risk, and difficulty in tracheal intubation and extubation because of soft tissue hyperplasia, making the operation more challenging for surgeons. The incidence and risk of rectal NETs in patients with acromegaly resulting from GH-secreting pituitary adenomas are unknown. Further research is necessary to elucidate the underlying mechanisms and to determine the clinical significance of this association.

CONCLUSION

We have herein presented a rare case of concurrent rectal G2 NETs combined with a pituitary adenoma. Pituitary adenomas lead to acromegaly and diabetes mellitus. Accurate diagnosis of this patients' condition was difficult. ^{18}F-ALF-NOTATATE PET/CT and pathological analysis achieved the correct diagnoses in this case.

ACKNOWLEDGEMENTS

We sincerely appreciate the patient and her family for their cooperation in information acquisition, treatment, and follow-up.

FOOTNOTES

Author contributions: Li JY drafted the manuscript and collected the data; Chen J and Liu J analyzed and collated the data; Zhang SZ guided the operation and revised the manuscript.

Informed consent statement: Informed written consent was obtained from the patient and her parents for the publication of this report and any accompanying images.

Conflict-of-interest statement: All the authors report having no relevant conflicts of interest for this article.

CARE Checklist (2016) statement: The authors have read the CARE Checklist (2016), and the manuscript was prepared and revised according to the CARE Checklist (2016).

Country/Territory of origin: China

ORCID number: Jing-Yi Li 0000-0002-2689-6859; Jie Chen 0000-0001-8113-3515; Jun Liu 0009-0002-7502-451X; Su-Zhen Zhang 0000-0002-0158-1420.

S-Editor: Qu XL
L-Editor: Filipodia
P-Editor: Yu HG

REFERENCES

1 **Fang C**, Wang W, Zhang Y, Feng X, Sun J, Zeng Y, Chen Y, Li Y, Chen M, Zhou Z, Chen J. Clinicopathologic characteristics and prognosis of gastroenteropancreatic neuroendocrine neoplasms: a multicenter study in South China. *Chin J Cancer* 2017; **36**: 51 [PMID: 28637502 DOI: 10.1186/s40880-017-0218-3]
2 **Andreasi V**, Partelli S, Muffatti F, Manzoni MF, Capurso G, Falconi M. Update on gastroenteropancreatic neuroendocrine tumors. *Dig Liver Dis* 2021; **53**: 171-182 [PMID: 32912771 DOI: 10.1016/j.dld.2020.08.031]
3 **AlDallal S**. Acromegaly: a challenging condition to diagnose. *Int J Gen Med* 2018; **11**: 337-343 [PMID: 30197531 DOI: 10.2147/IJGM.S169611]
4 **Dasari A**, Shen C, Halperin D, Zhao B, Zhou S, Xu Y, Shih T, Yao JC. Trends in the Incidence, Prevalence, and Survival Outcomes in Patients With Neuroendocrine Tumors in the United States. *JAMA Oncol* 2017; **3**: 1335-1342 [PMID: 28448665 DOI: 10.1001/jamaoncol.2017.0589]
5 **Hrabe J**. Neuroendocrine Tumors of the Appendix, Colon, and Rectum. *Surg Oncol Clin N Am* 2020; **29**: 267-279 [PMID: 32151360 DOI: 10.1016/j.soc.2019.11.010]
6 **Maione F**, Chini A, Milone M, Gennarelli N, Manigrasso M, Maione R, Cassese G, Pagano G, Tropeano FP, Luglio G, De Palma GD. Diagnosis and Management of Rectal Neuroendocrine Tumors (NETs). *Diagnostics (Basel)* 2021; **11** [PMID: 33923121 DOI: 10.3390/diagnostics11050771]
7 **Li YW**, He YP, Liu FQ, Peng JJ, Cai SJ, Xu Y, Wang MH. Grade G2 Rectal Neuroendocrine Tumor Is Much More Invasive Compared With G1 Tumor. *Front Oncol* 2021; **11**: 646536 [PMID: 33777809 DOI: 10.3389/fonc.2021.646536]
8 **Phan AT**, Oberg K, Choi J, Harrison LH Jr, Hassan MM, Strosberg JR, Krenning EP, Kocha W, Woltering EA, Maples WJ; North American Neuroendocrine Tumor Society (NANETS). NANETS consensus guideline for the diagnosis and management of neuroendocrine tumors: well-differentiated neuroendocrine tumors of the thorax (includes lung and thymus). *Pancreas* 2010; **39**: 784-798 [PMID: 20664476 DOI: 10.1097/MPA.0b013e3181ec1380]
9 **Laverman P**, McBride WJ, Sharkey RM, Eek A, Joosten L, Oyen WJ, Goldenberg DM, Boerman OC. A novel facile method of labeling octreotide with (18)F-fluorine. *J Nucl Med* 2010; **51**: 454-461 [PMID: 20150268 DOI: 10.2967/jnumed.109.066902]
10 **Laverman P**, D'Souza CA, Eek A, McBride WJ, Sharkey RM, Oyen WJ, Goldenberg DM, Boerman OC. Optimized labeling of NOTA-conjugated octreotide with F-18. *Tumour Biol* 2012; **33**: 427-434 [PMID: 22009690 DOI: 10.1007/s13277-011-0250-x]
11 **Long T**, Yang N, Zhou M, Chen D, Li Y, Li J, Tang Y, Liu Z, Li Z, Hu S. Clinical Application of 18F-AlF-NOTA-Octreotide PET/CT in Combination With 18F-FDG PET/CT for Imaging Neuroendocrine Neoplasms. *Clin Nucl Med* 2019; **44**: 452-458 [PMID: 30985413 DOI: 10.1097/RLU.0000000000002578]
12 **Dolecek TA**, Propp JM, Stroup NE, Kruchko C. CBTRUS statistical report: primary brain and central nervous system tumors diagnosed in the United States in 2005-2009. *Neuro Oncol* 2012; **14** Suppl 5: v1-49 [PMID: 23095881 DOI: 10.1093/neuonc/nos218]
13 **Mehta GU**, Lonser RR. Management of hormone-secreting pituitary adenomas. *Neuro Oncol* 2017; **19**: 762-773 [PMID: 27543627 DOI: 10.1093/neuonc/now130]

14 **Shih RY**, Schroeder JW, Koeller KK. Primary Tumors of the Pituitary Gland: Radiologic-Pathologic Correlation. *Radiographics* 2021; **41**: 2029-2046 [PMID: 34597177 DOI: 10.1148/rg.2021200203]

15 **Tjörnstrand A**, Gunnarsson K, Evert M, Holmberg E, Ragnarsson O, Rosén T, Filipsson Nyström H. The incidence rate of pituitary adenomas in western Sweden for the period 2001-2011. *Eur J Endocrinol* 2014; **171**: 519-526 [PMID: 25084775 DOI: 10.1530/EJE-14-0144]

16 **Agustsson TT**, Baldvinsdottir T, Jonasson JG, Olafsdottir E, Steinthorsdottir V, Sigurdsson G, Thorsson AV, Carroll PV, Korbonits M, Benediktsson R. The epidemiology of pituitary adenomas in Iceland, 1955-2012: a nationwide population-based study. *Eur J Endocrinol* 2015; **173**: 655-664 [PMID: 26423473 DOI: 10.1530/EJE-15-0189]

17 **Daly AF**, Beckers A. The Epidemiology of Pituitary Adenomas. *Endocrinol Metab Clin North Am* 2020; **49**: 347-355 [PMID: 32741475 DOI: 10.1016/j.ecl.2020.04.002]

18 **Katznelson L**, Laws ER Jr, Melmed S, Molitch ME, Murad MH, Utz A, Wass JA; Endocrine Society. Acromegaly: an endocrine society clinical practice guideline. *J Clin Endocrinol Metab* 2014; **99**: 3933-3951 [PMID: 25356808 DOI: 10.1210/jc.2014-2700]

19 **Ritvonen E**, Löyttyniemi E, Jaatinen P, Ebeling T, Moilanen L, Nuutila P, Kauppinen-Mäkelin R, Schalin-Jäntti C. Mortality in acromegaly: a 20-year follow-up study. *Endocr Relat Cancer* 2016; **23**: 469-480 [PMID: 27185871 DOI: 10.1530/ERC-16-0106]

20 **Dekkers OM**, Biermasz NR, Pereira AM, Romijn JA, Vandenbroucke JP. Mortality in acromegaly: a metaanalysis. *J Clin Endocrinol Metab* 2008; **93**: 61-67 [PMID: 17971431 DOI: 10.1210/jc.2007-1191]

21 **Clayton RN**, Raskauskiene D, Reulen RC, Jones PW. Mortality and morbidity in Cushing's disease over 50 years in Stoke-on-Trent, UK: audit and meta-analysis of literature. *J Clin Endocrinol Metab* 2011; **96**: 632-642 [PMID: 21193542 DOI: 10.1210/jc.2010-1942]

22 **McCabe J**, Ayuk J, Sherlock M. Treatment Factors That Influence Mortality in Acromegaly. *Neuroendocrinology* 2016; **103**: 66-74 [PMID: 25661647 DOI: 10.1159/000375163]

23 **Lavrentaki A**, Paluzzi A, Wass JA, Karavitaki N. Epidemiology of acromegaly: review of population studies. *Pituitary* 2017; **20**: 4-9 [PMID: 27743174 DOI: 10.1007/s11102-016-0754-x]

24 **Crisafulli S**, Luxi N, Sultana J, Fontana A, Spagnolo F, Giuffrida G, Ferraù F, Gianfrilli D, Cozzolino A, Cristina De Martino M, Gatto F, Barone-Adesi F, Cannavò S, Trifirò G. Global epidemiology of acromegaly: a systematic review and meta-analysis. *Eur J Endocrinol* 2021; **185**: 251-263 [PMID: 34061771 DOI: 10.1530/EJE-21-0216]

25 **Krug S**, Boch M, Rexin P, Pfestroff A, Gress T, Michl P, Rinke A. Acromegaly in a patient with a pulmonary neuroendocrine tumor: case report and review of current literature. *BMC Res Notes* 2016; **9**: 326 [PMID: 27349224 DOI: 10.1186/s13104-016-2132-1]

26 **Gadelha MR**, Kasuki L, Lim DST, Fleseriu M. Systemic Complications of Acromegaly and the Impact of the Current Treatment Landscape: An Update. *Endocr Rev* 2019; **40**: 268-332 [PMID: 30184064 DOI: 10.1210/er.2018-00115]

27 **Dworakowska D**, Grossman AB. Colonic Cancer and Acromegaly. *Front Endocrinol (Lausanne)* 2019; **10**: 390 [PMID: 31293513 DOI: 10.3389/fendo.2019.00390]

28 **Kasuki L**, Maia B, Gadelha MR. Acromegaly and Colorectal Neoplasm: An Update. *Front Endocrinol (Lausanne)* 2022; **13**: 924952 [PMID: 35795151 DOI: 10.3389/fendo.2022.924952]

29 **Patel GS**, Grossmann I, Rodriguez K, Soni M, Joshi PK, Patel SC, Shreya D, Zamora DI, Sange I. Acromegaly and the Colon: Scoping Beyond the Pituitary. *Cureus* 2021; **13**: e20018 [PMID: 34987906 DOI: 10.7759/cureus.20018]

30 **Terzolo M**, Puglisi S, Reimondo G, Dimopoulou C, Stalla GK. Thyroid and colorectal cancer screening in acromegaly patients: should it be different from that in the general population? *Eur J Endocrinol* 2020; **183**: D1-D13 [PMID: 32698136 DOI: 10.1530/EJE-19-1009]

31 **Uchoa HB**, Lima GA, Corrêa LL, Vidal AP, Cavallieri SA, Vaisman M, Buescu A, Gadelha MR. Prevalence of thyroid diseases in patients with acromegaly: experience of a Brazilian center. *Arq Bras Endocrinol Metabol* 2013; **57**: 685-690 [PMID: 24402013 DOI: 10.1590/s0004-27302013000900003]

32 **Werner H**, Laron Z. Role of the GH-IGF1 system in progression of cancer. *Mol Cell Endocrinol* 2020; **518**: 111003 [PMID: 32919021 DOI: 10.1016/j.mce.2020.111003]

World Journal of Gastroenterology

Submit a Manuscript: https://www.f6publishing.com

World J Gastroenterol 2023 September 14; 29(34): 5091-5093

DOI: 10.3748/wjg.v29.i34.5091

ISSN 1007-9327 (print) ISSN 2219-2840 (online)

LETTER TO THE EDITOR

Gastrointestinal microbiome and cholelithiasis: Prospect in the nervous system

Mirella Mancha Chahuara, Leidhy Dhy Maruja Lopez Tufino, Carlos Andrés Mugruza-Vassallo

Specialty type: Gastroenterology and hepatology

Provenance and peer review: Unsolicited article; Externally peer reviewed.

Peer-review model: Single blind

Peer-review report's scientific quality classification

Grade A (Excellent): 0
Grade B (Very good): B
Grade C (Good): C
Grade D (Fair): 0
Grade E (Poor): 0

P-Reviewer: Shi W, China; Sun X, China

Received: June 9, 2023
Peer-review started: June 9, 2023
First decision: July 23, 2023
Revised: July 25, 2023
Accepted: August 29, 2023
Article in press: August 29, 2023
Published online: September 14, 2023

Mirella Mancha Chahuara, Leidhy Dhy Maruja Lopez Tufino, Carlos Andrés Mugruza-Vassallo, Escuela Profesional de Medicina Humana, Universidad Privada San Juan Bautista, Lima Chorrillos 15067, Lima, Peru

Corresponding author: Carlos Andrés Mugruza-Vassallo, PhD, Senior Lecturer, Escuela Profesional de Medicina Humana, Universidad Privada San Juan Bautista, Ex Hacienda Villa, Av José Antonio Lavalle N° 302, Lima Chorrillos 15067, Lima, Peru. cmugruza@yahoo.com

Abstract

Dan and colleagues recently published research suggesting that the gastrointestinal microbiome (microorganisms and metabolites) in cholelithiasis. They reviewed gallbladder stones, choledocholithiasis, and asymptomatic gallstones. Finally, their discussion was on the gastrointestinal. We focused on complementing the effect of the S1 protein and neuroinflammatory changes caused by severe acute respiratory syndrome coronavirus 2. Our contribution was about to involve the microbiota and the nervous system. They can have similar functions because they have similar pathways and advantages, bearing in mind γ-aminobutyric acid in schizophrenia and serotonin in Parkinson's disease. Therefore in the next few years, more research should be encouraged on the microbiota consequences for development, and mobility.

Key Words: Gastrointestinal microbiome; γ-aminobutyric acid; Serotonin; Letter

Core Tip: The microbiota and the nervous system can have similar functions because they have similar advantages. Bearing in mindγ-aminobutyric acid (GABA) in schizophrenia and serotonin in Parkinson's disease and GABA and serotonin management, we expect in the next few years, more research should be encouraged on the microbiota consequences for development, and mobility.

Citation: Mancha Chahuara M, Lopez Tufino LDM, Mugruza-Vassallo CA. Gastrointestinal microbiome and cholelithiasis: Prospect in the nervous system. *World J Gastroenterol* 2023; 29(34): 5091-5093
URL: https://www.wjgnet.com/1007-9327/full/v29/i34/5091.htm
DOI: https://dx.doi.org/10.3748/wjg.v29.i34.5091

TO THE EDITOR

Dan and colleagues recently published research suggesting that the gastrointestinal microbiome (microorganisms and metabolites) in cholelithiasis. They reviewed gallbladder stones, choledocholithiasis, and asymptomatic gallstones. Finally, their discussion was on the gastrointestinal microbiome changes and influences on cholelithogenesis[1]. This letter focuses on complementing the effect of the S1 protein and neuroinflammatory changes caused by severe acute respiratory syndrome coronavirus 2.

In the article by Garza-Velasco *et al*[2] molecular techniques were used for sequence and nucleic acids. The polymerase chain reaction in real time provided information on the importance of the microbiota in the proper functioning of the human body, *i.e.* the treatment programs associated with the administration of antibiotics affect the normal microbiota. This treatment causes the loss of sensitive members to the antimicrobial agent. Therefore, this can open the door for pathogens, which sometimes face serious competition for nutrients and oxygen. Also, both the microbiota and the nervous system may have similar functions because they have similar advantages. They argued that the microbiota may be important for the development, mobility, learning, and memory of the human brain by influencing different neurotransmitters such as serotonin and acid γ-aminobutyric acid (GABA), certain amounts of serotonin are also produced by bacteria such as Clostridium sporogenes and Ruminococcus. In addition, the microbiota synthesizes vitamins that contribute to the formation of important compounds in the metabolism of intestinal cells, including vitamin B and niacin, which are necessary for the tissues to produce Nicotinamide Adenine Dinucleotide. On the other hand, a significant part of the primary barrier prevents the free colonization of pathogens, regulates the proliferation of pathogens, and the productivity of antimicrobial agents that harm other species and/or different clones of the same species. Research on Escherichia coli colicins, with variants of the same species causing diarrhea. The protection of the intestinal microbiota also includes SCFA, for example, the acetate synthesized by Bifidobacterium longum prevents the development of Pseudomonas aeruginosa. Therefore together with propionate and butyrate, it prevents the growth of EHEC O157 and Proteus mirabilis[2]. Bearing in mind other studies with neurotransmitters involved in brain impairments GABA and serotonin. For example in the brain GABA in schizophrenic patients (modeling in brain areas by Ferrarelli and Tononi[3]; auditory cognitive properties by Mugruza-Vassallo and Potter[4]) as well as the linear association reported for the greater serotonin the lower nigral iron in Parkinson's disease patients (Jellen *et al*[5]).

Moreover, Swidsinki and Loening-Baucke[6] have shown that intestinal bacterial monocultures are resistant. They can avoid the host's immunological responses that are persistent in harsh environments and have a coordinated response to environmental stressors. The intestine is never completely sterile, and the host never has complete control over bacterial growth. The appearance, composition, and organization of the gut microbiota in each gut segment depended on whether inhibition or segregation predominates. In areas of the intestine where the microbiota was suppressed, the bacteria were sporadically present with variable composition and low concentrations. Complete separation of bacteria from the mucosa and low levels of inhibition leads to the formation of intestinal reservoirs where bacteria can grow and reach high concentrations[3]. Intestinal reservoirs where bacteria can grow and accumulate in high concentrations are formed as a result of complete separation of bacteria from the mucosa and low levels of inhibition[3]. These bacteria are native to these regions of the intestine as well as for development and mobility.

Our contribution to the types of microbiome, the locations and how the microbiome affects or favors humans. Above all, the microbiota and the nervous system can have similar functions because they have similar advantages and pathways, bearing in mind GABA in schizophrenia and serotonin in Parkinson's disease. Therefore in the next few years, more research should be encouraged on the microbiota consequences for development, and mobility.

Our objective in this work was to make a contribution to the types of microbiome, the locations and how the microbiome affects or favors us. Above all, the microbiota and the nervous system can have similar functions because they have similar advantages, it is argued that the microbiota can be important for development and mobility. All authors are in complete agreement with the information stated. The content of this manuscript is our original work and has not been published, in whole or in part, before or simultaneously with this submission.

FOOTNOTES

Author contributions: Lopez Tufino LDM drafted a study on gastrointestinal microbiome and cholelithiasis, reviewed literature, and wrote an initial version of the paper; Mancha Chahuara M drafted study on gastrointestinal microbiome and cholelithiasis, reviewed literature, and wrote initial version of the paper; Mugruza-Vassallo CA reviewed and criticized gastrointestinal microbiome and cholelithiasis, he added the prospect in the nervous systems and corrected the paper.

Conflict-of-interest statement: The authors declare no conflict of interest.

Country/Territory of origin: Peru

ORCID number: Mirella Mancha Chahuara 0009-0006-7399-2030; Leidhy Dhy Maruja Lopez Tufino 0009-0002-6190-3441; Carlos Andrés Mugruza-Vassallo 0000-0002-9262-7198.

S-Editor: Fan JR
L-Editor: A
P-Editor: Fan JR

REFERENCES

1 **Dan WY**, Yang YS, Peng LH, Sun G, Wang ZK. Gastrointestinal microbiome and cholelithiasis: Current status and perspectives. *World J Gastroenterol* 2023; **29**: 1589-1601 [PMID: 36970590 DOI: 10.3748/wjg.v29.i10.1589]

2 **Garza-Velasco R**, Garza-Manero SP, Perea-Mejía LM. Microbiota intestinal: aliada fundamental del organismo humano. Gut microbiota: our fundamental allied. *Educación Química* 2021; **32(1)**: 10 [DOI: 10.22201/fq.18708404e.2021.1.75734]

3 **Ferrarelli F**, Tononi G. Reduced sleep spindle activity point to a TRN-MD thalamus-PFC circuit dysfunction in schizophrenia. *Schizophr Res* 2017; **180**: 36-43 [PMID: 27269670 DOI: 10.1016/j.schres.2016.05.023]

4 **Mugruza-Vassallo C**, Potter D. Context Dependence Signature, Stimulus Properties and Stimulus Probability as Predictors of ERP Amplitude Variability. *Front Hum Neurosci* 2019; **13**: 39 [PMID: 30863293 DOI: 10.3389/fnhum.2019.00039]

5 **Jellen LC**, Lewis MM, Du G, Wang X, Galvis MLE, Krzyzanowski S, Capan CD, Snyder AM, Connor JR, Kong L, Mailman RB, Brundin P, Brundin L, Huang X. Low plasma serotonin linked to higher nigral iron in Parkinson's disease. *Sci Rep* 2021; **11**: 24384 [PMID: 34934078 DOI: 10.1038/s41598-021-03700-2]

6 **Swidsinski A**, Loening-Baucke V. Spatial organization of intestinal microbiota in health and disease. *UpToDate on line* 2020; **18**: 214-254 [DOI: 10.1002/9781118409855.ch9]

Published by **Baishideng Publishing Group Inc**
7041 Koll Center Parkway, Suite 160, Pleasanton, CA 94566, USA
Telephone: +1-925-3991568
E-mail: bpgoffice@wjgnet.com
Help Desk: https://www.f6publishing.com/helpdesk
https://www.wjgnet.com